MAKERERE UNIVERSITY

INVESTIGATING THE IMPACTS OF FUTURE CLIMATE AND LAND USE/LAND COVER CHANGE ON RIVER DISCHARGE IN THE MANAFWA RIVER BASIN

BY

MUSOKE ISA

Bsc.SLIS (KYU)

2021/HD08/0092U

A DISSERTATION SUBMITTED TO THE DIRECTORATE OF RESEARCH AND GRADUATE TRAINING AS A FULFILLMENT OF THE REQUIREMENTS FOR THE AWARD OF THE DEGREE OF MASTER OF SCIENCE IN GIST OF MAKERERE UNIVERSITY

MARCH, 2026

Declaration

I, Musoke Isa, declare that this research titled "**INVESTIGATING THE IMPACTS OF FUTURE CLIMATE AND LAND USE/LAND COVER CHANGE ON RIVER DISCHARGE IN THE MANAFWA RIVER BASIN.**" is my original work and has never been submitted for an award in any higher institution of learning.

Signed..... Date..19/03/2026.....

Musoke Isa

Approval

This research dissertation has been submitted for examinations with the consent and approval of the undersigned supervisors:

Dr. Mazimwe Allan (PhD)
Department of Geomatics and Land Management, School of the Built Environment,
College of Engineering, Design Art and
Technology, Makerere University

Signed..... Date..... 30/3/2026

Prof. Musinguzi Moses (PhD)
Department of Geomatics and Land Management, School of the Built Environment,
College of Engineering, Design Art and
Technology, Makerere University

Signed..... Date..... 31-3-2026

Abstract

Land use/land cover (LULC) and climate are the most crucial drivers that shape the hydrological cycle, influencing infiltration, evapotranspiration, runoff generation, and groundwater recharge. While previous studies have provided valuable literature about the impacts of these drivers on river discharge, most assessments remain limited to historical and present conditions, leaving the future impacts of climate and LULC underexplored. Consequently, the lack of understanding of future river discharge behaviour hinders informed decision-making in water resource management and disaster preparedness. Guided by the main objective of investigating the impacts of future climate and land use/land cover on river discharge, this study applied the Soil and Water Assessment Tool (SWAT), which integrates historical analysis and future scenario assessment. Specifically, the study sought to determine LULC change in the Manafwa River Basin from 2000 to 2040 and to examine how projected climate and LULC conditions influence river discharge under different future scenarios. Historical LULC maps for 2000, 2010, and 2020 were generated using Random Forest classifier and projected to 2030 and 2040 using TerrSet's Land Change Modeler based on historical LULC maps and drivers of change. Climate data was obtained from the NEX-GDDP-CMIP6 dataset and three Global Circulation Models (GCMs) were used to create an ensemble of three models, from which past and future climate were obtained. The SWAT model was then parameterized/calibrated and validated with observed stream flow data. Thereafter, scenario simulations were carried out using the separation method. Results indicate that LULC changes alone substantially modify basin hydrology, with mean discharge projected to increase by 4.49% (from 12.70 m^3/s to 13.275 m^3/s) between 2000 and 2040, alongside rising peak flows and reduced minimum flows due to vegetation loss and agricultural expansion. However, climate change scenarios greatly amplify hydrological extremes, with mean discharge projected to 14.01 m^3/s (10.31%) by 2030 and 14.45 m^3/s (13.78%) by 2040 under high emission pathways SSP2 and SSP5 respectively, peak flows were exceeding 20 m^3/s, and minimum flows increasing to 6.507 m^3/s. These findings indicate that, while climate change emerges as the dominant driver of future river discharge variability, LULC transformations are exerting an influence that has doubled significantly over time. This study therefore recommends integrated watershed management strategies that jointly consider climate and LULC changes to strengthen resilience in flood prone areas and agriculturally dependent tropical basins.

Acknowledgement

Great thanks are extended to the following personalities for their tireless contributions and continuous guidance towards production of this research dissertation.

My great and sincere appreciation goes to the Almighty ALLAH for all the providence that enabled me to emerge from a hard beginning to the completion of this research work.

I would like to acknowledge my supervisors Prof. Musinguzi Moses and Dr. Mazimwe Allan for their cooperation and continuous guidance throughout the various stages of this research work whenever I approached them.

I am also grateful to the contributions of all my lecturers, at the department of geomatics, Dr. Ssegujja Julian from the school of environmental sciences, the Deputy Principal College of Engineering, Design, Art and Technology - Prof. Kizito Maria Kasule, and Dr Wadembere Ismail, the head of department geo-informatics, school of built environment at Kyambogo University. Their advice in this study enabled me to produce the dissertation.

I thank Madhvani foundation for supporting me financially during my study period through the Madhvani scholarship, their support enabled me to go on with my studies despite the financial constraints I was going through, may your businesses prosper.

I also extend great appreciation to my parents, and entire family, who supported me morally, emotionally, financially and I acknowledge all their support offered to me during this period of my academic journey.

I deeply acknowledge the contribution of all the above mentioned as well as those I have not mentioned, and it is my sincere prayer that the Almighty ALLAH blesses them.

Dedication

This work is dedicated to all those who have lost loved ones to natural disasters, especially floods and droughts. May their memories inspire efforts toward building safer and more resilient communities to natural disasters like floods and droughts.

Table of Contents

List of Tables

List of Figures

List of Equations

List of Acronyms

CC	:	Climate Change
CMIP6	:	Coupled Model Intercomparison Project Phase 6
$CMS/m^3/s$	:	Cubic meters per second
DJF	:	December, January and February
DM	:	Distribution mapping
GCM	:	General circulation model
GEE	:	Google earth engine
JJA	:	June, July and August
LULC	:	Land use land cover
LOCI	:	Local intensity scaling
LS	:	Linear scaling
MAM	:	March, April and May
NEX-GDDP-CMIP6	:	NASA Earth Exchange Global Daily Downscaled Projections, Coupled Model Intercomparison Project Phase
NSCE	:	Nash Sutcliffe efficiency
PBIAS	:	Percentage bias
PT	:	Power transformation
R^2	:	Coefficient of determination
RMB	:	River Manafwa Basin
RMSE	:	Root mean square error
SON	:	September, October and November
SSA	:	Sub Saharan Africa
SWAT	:	Soil and water assessment tool
VS	:	Variance scaling

CHAPTER ONE: INTRODUCTION

1.1 Background

Rivers are crucial in sustaining ecosystems, agriculture, energy production, and human livelihoods by regulating the spatial and temporal availability of freshwater. River discharge, which represents the integrated response of a catchment to atmospheric and surface processes, is mainly controlled by climate variability and land use/land cover (LULC) conditions that are increasingly stressed by human activities such as farming, hydropower generation, and urbanisation (Haider et al., 2023; Wudineh et al., 2022). Climate governs the amount, intensity, and seasonality of precipitation and evapotranspiration, while LULC regulates how incoming rainfall is partitioned into runoff, infiltration, groundwater recharge, and evapotranspiration (Mishra & Lilhare, 2016; L. Müller & Döll, 2024). Therefore, alterations in climate and LULC directly influence river discharge, with far-reaching implications for water availability and flood risk (IPCC, 2021). Investigating how these drivers interact is therefore essential for water resource management and disaster preparedness, especially for the future time frame in tropical regions where the vulnerability levels are high.

Climate change has reshaped global hydrological systems worldwide by modifying rainfall intensity, frequency, and seasonal distribution, alongside rising temperatures that enhance evapotranspiration and atmospheric moisture demand (Haider et al., 2023; Zhai et al., 2021). These changes destabilise river flow regimes, leading to shifts in peak discharge timing, increased flood magnitudes, and prolonged low flow conditions (Trenberth et al., 2015). (Escobar & Carvalho-Santos, 2022; Trenberth et al., 2015). In Sub-Saharan Africa, such changes are particularly critical because river systems are highly sensitive to climatic forcing and often support rain fed agriculture and densely populated floodplains, thereby amplifying socio-hydrological vulnerability(WBG, 2021).

On the other side, LULC change modifies catchment hydrology by altering vegetation cover, soil structure, and surface permeability. Natural vegetation such as forests and wetlands enhances rainfall interception, soil infiltration, and groundwater recharge, thereby regulating streamflow variability (Abbas et al., 2022; Guzha et al., 2018). However, agricultural expansion, deforestation, and urbanisation reduce infiltration capacity and increase surface runoff through

soil compaction and the creation of impervious surfaces (Abbas et al., 2022). These transformations amplify peak flows while diminishing baseflow contributions, ultimately increasing both flood risk and dry-season water stress, particularly in tropical and sub-Saharan African basins (Williams et al., 2020).

Well as considerable research has examined river discharge variations, most studies have focused on either climate change or land use/land cover (LULC), this has been largely driven by data limitations, computational constraints, and the assumption that land use conditions remain relatively static over short time scales. For example, Ayele et al. (2016); Jin & Sridhar. (2012); Legesse Gebre. (2015); Melese. (2016) investigated the impacts of climate change on historical and present-day stream flow in different areas of Sub-Saharan Africa, highlighting increased variability and more frequent extreme flow events. Similarly, Admas et al., (2024); Bihonegn & Awoke, (2023); Erima et al., (2024); Gashaw et al., (2018); Hermassi et al., (2025); Idowu & Zhou, (2021); Kayitesi et al., (2022); Leta et al., (2021); Liu et al.,(2022); Tanksali & Soraganvi,(2021); Turyahabwe, (2019) assessed the effects of LULC changes such as deforestation, agricultural expansion, and urbanization on catchment hydrology, and found that such changes significantly increased surface runoff, reduced infiltration, and increased river discharge variations. Most existing assessments remain confined to historical or present conditions, with limited attention on future projections, particularly in tropical basins where rapid land transformation and climate variability coexist. This gap constrains the ability of water managers and planners to anticipate future river discharge behaviour under combined climate and LULC changes, thereby limiting proactive flood risk management, water allocation planning, and ecosystem protection. Addressing this gap requires an integrated assessment framework that explicitly evaluates future climate and LULC impacts on river discharge within vulnerable tropical watersheds.

1.2 Problem Statement

Land use and land cover (LULC), along with climate, are crucial factors in the hydrological cycle. They significantly influence key components, including infiltration, evaporation, evapotranspiration, runoff, and groundwater recharge. Numerous studies (Abbas et al., 2015; Atharinafi & Wijaya, 2021; Costa et al., 2003; Mahmoud & Alazba, 2015) have examined how

changes in land use and land cover affect river discharge, only a few have focused on the impacts of climate change. Additionally, some research (Arnell & Gosling, 2013; Gelete et al., 2020; Han et al., 2024; Mango, 2010; Omondi & Angel, 2023) has looked into the combined effects of both factors, providing valuable insights into hydrological responses under historical and current conditions.

While previous studies have provided valuable literature about the impacts of these drivers on river discharge, most assessments remain limited to historical and present conditions, leaving the future impacts of climate and LULC underexplored. Consequently, the lack of understanding of future river discharge behaviour hinders informed decision-making in water resource management and disaster preparedness.

1.2 Main Objective

The aim of the study was to investigate the impacts of future climate and land use/land cover on river discharge.

1.3 Specific Objectives

The following objectives were used to address the main objective;

I. To determine land use/land cover change for the Manafwa river basin for 2000 to 2040.
II. To examine the influence of both land use/land cover changes and climate change on river Manafwa's discharge under different scenarios.

1.5 Research Questions

I. How has land cover changed from 2000 to 2040?
II. How does climate and land use/land cover changes influence river discharge in the Manafwa River Basin under different scenarios?

1.6 Justification of the Study

Changes in climate and land use/land cover significantly affect river discharge, exposing communities to disasters such as floods and droughts. These hydrological extremes threaten livelihoods, agriculture, infrastructure, and ecosystem stability by reducing water availability and increasing disaster risks especially in tropical basins like the Manafwa. Most existing planning

frameworks rely on historical hydrological conditions, which are increasingly inadequate under rapidly changing climate and land-use dynamics. Therefore, a reliable understanding of how future climate and LULC affect river discharge is imperative for effective decision-making, as sustainable water resource management and disaster preparedness require reliable projections of future river discharge. By investigating the separate impacts of climate and land use/land cover on river discharge, this study generates evidence required to support proactive and risk-informed water resource management. Specifically, separating and quantifying the individual effects of climate and LULC change enables identification of dominant drivers of hydrological change, thereby informing targeted land-use planning, effective flood and drought mitigation strategies, and sustainable watershed management interventions. Such knowledge is essential for anticipating future hydrological risks rather than responding to them after they occur. In doing so, the study contributes to Uganda's National Development Plan IV by enabling higher household incomes for wealth creation through sustainable resource use and disaster preparedness. It further supports global priorities under the Sustainable Development Goals, particularly SDG 6.6.1 (protecting water-related ecosystems), SDG 13.2 (integrating climate action into national policy), and SDG 15.3 (sustainable land use and land degradation neutrality).

1.7 Study Area

The Manafwa river catchment was chosen as the study area because it is one of the few rivers with relatively high-quality discharge data. In addition, its topography creates frequent flooding in the lowland areas of Butaleja and Bududa districts, as well as water scarcity during the dry seasons. The basin has also undergone intensive agricultural expansion due to the Doho rice scheme, as well as deforestation and population growth over the last two decades.

It covers a total area of 502 km^2 in the Mt Elgon region of eastern Uganda (Figure 1.1). The river is the sole source of irrigation water for the Doho rice scheme, located on the river floodplain in the low-lying areas of the neighbouring Butaleja district to the west of the watershed (Wamala et al., 2023).

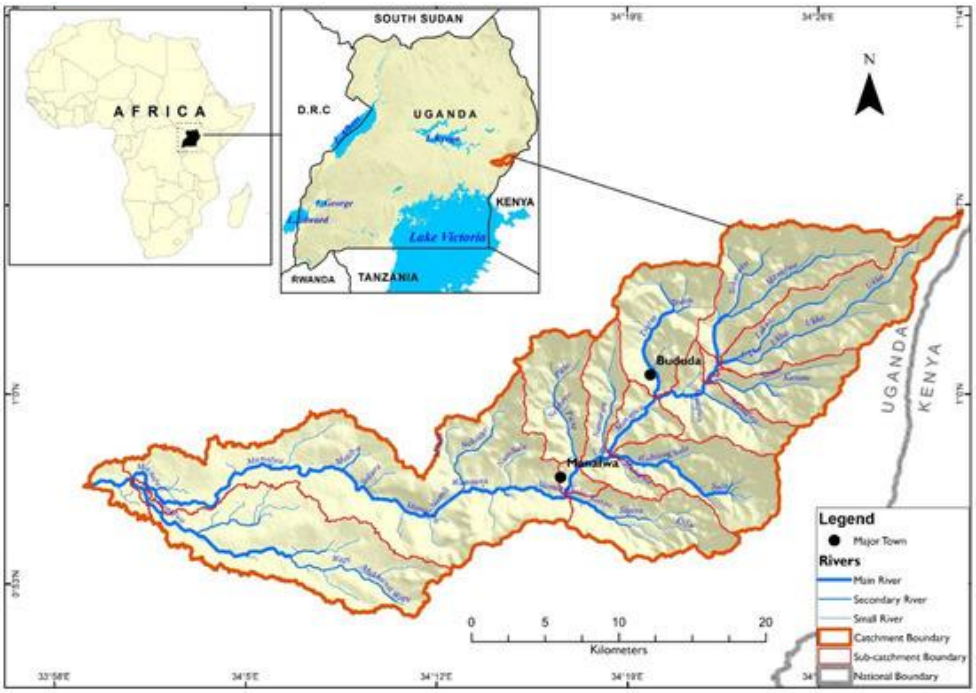

Figure 1. 1: Manafwa river basin (adopted from Erima et al., 2022)

The catchment is characterised by high relief in the East, with altitudes ranging from 1041 to 4301 m above sea level, and its main stream drains from Mt Elgon to Lake Kyoga. The annual mean temperature is 23°C, and the mean annual rainfall is 1500 mm. The annual rainfall in the area follows a bimodal pattern, with the dry season spanning June to August (JJA) and December to February (DJF). The rainy season occurs from March to May (MAM), and short rains occur from September to November (SON).

The geology in the Mt. Elgon region comprises mainly Pre-Cambrian and Cainozoic rock formations, including volcanics, granites, and sediments. As per Erima et al. (2022), the predominant soil type in the basin is Vertisols, also known as "black cotton soils" regionally. Generally, the soils in the highlands are clays, while those in the midlands and the lowlands are clay loams or sandy (Erima et al., 2022). River discharge in the Manafwa watershed is measured at the Manafwa river gauge along the Tororo-Mbale highway, with station ID. 82212. However, it is worth noting that there is only one stream gauge in the watershed (Nakkazi et al., 2022).

1.8 Conceptual Framework

The conceptual framework below in figure 1.2 recognizes river discharge as a function that interacts with various biophysical and socio-economic drivers operating within the watershed

system. River discharge responds directly to changes in land use/land cover (LULC) and climate, which jointly regulate key hydrological processes including runoff generation, infiltration, evapotranspiration, and groundwater recharge.

Land use and land cover change is influenced not only by biophysical conditions but also socio-economic drivers such as population growth, agricultural expansion, settlement development, and land-use policy enforcement. These socio-economic forces determine the conversion of natural vegetation into farmland or built-up areas, thereby modifying surface characteristics such as vegetation cover, soil structure, and imperviousness, which in turn affect hydrological responses within the basin (Belay et al., 2022).

In contrast, Climate change acts as an external forcing that alters atmospheric inputs including rainfall magnitude and intensity, temperature regimes, humidity, and solar radiation, influencing hydrological processes across broader spatial and temporal scales(Change, 2021). The impacts of climate variability on river discharge are further mediated by land surface conditions shaped by socio-economic activities, indicating strong feedbacks between human systems and hydrological processes.

Overall, the framework highlights that river discharge variability in the basin is not solely a product of climatic or biophysical processes, but also a consequence of socio-economic decision-making that drives land use transformation and exposure to hydrological extremes. This integrated perspective provides the basis for assessing how future climate and land use/ land cover changes collectively influence river discharge.

Figure 1.2 below summarizes the conceptual framework for the study.

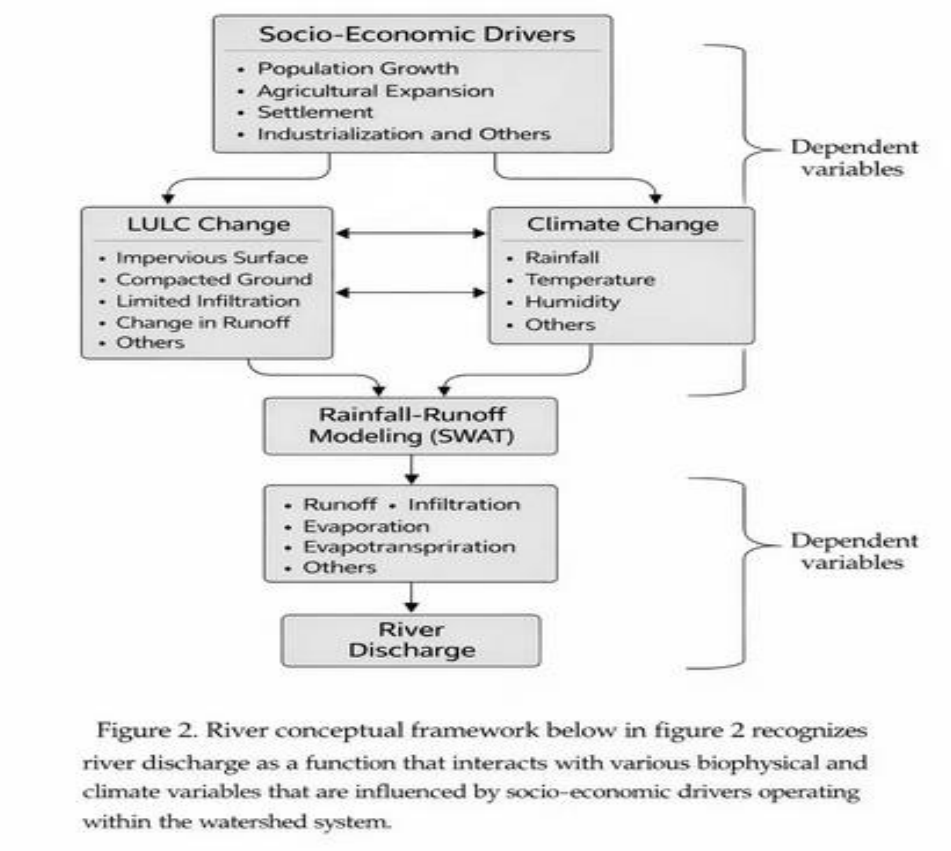

Figure 1. 2: Conceptual Framework

1.9 Organization of the Thesis

This thesis is structured into six chapters. Chapter One introduces the study by presenting the background, problem statement, research objectives, research questions, justification, and the study area. Chapter Two reviews relevant literature on river discharge, land use/land cover change, climate change impacts, hydrological modelling using SWAT, bias correction and downscaling techniques, and, finally, the separation method. Chapter Three describes the methodology used, including data sources, land cover classification, development of future scenarios, SWAT model setup, calibration, validation, and separation analysis. Chapter Four presents the results section, including land use/land cover maps (both classified and projected), change analysis, scenario analysis under climate and land use/land cover changes, and the impacts of climate and LULC changes on stream flow. Chapter Five is the discussion section that

interprets the findings, relates them to existing literature, and discusses the strengths, limitations and implications of the study. Chapter Six is the conclusion and recommendation section that summarises the main findings and provides recommendations for future research and practical implications. The thesis concludes with a list of references and appendices containing reports, additional data and graphs that support the main findings.

CHAPTER TWO: LITERATURE REVIEW

2.1 Introduction

This section reviews the existing literature on hydrology, the effects of climate change and LULC changes, their combined impacts on hydrological systems, and the separation method used to assess these impacts. It also focuses on the use of hydrological models, such as SWAT, to simulate river discharge under changing conditions.

2.2 Introduction to hydrology and River Discharge

River discharge is the volume of water passing a given point over a given time period (Rhoads, 2020). Discharge is measured in rivers and streams and reported as cubic feet per second (cfs) or cubic meters per second (cms) (Lohani, 2018). River discharge is the primary parameter that characterises the runoff formation process in hydrology and determines the characteristics and stability of natural rivers (Lohani, 2018). In addition, river discharge is a fundamental physical parameter in various environmental assessment and engineering design processes, including ecosystem conservation, climate change studies, watershed management, water resource scheduling, river hydrodynamics, and water quality modelling.

2.2.1 Hydrology

Hydrology is the study of the hydrologic cycle, which involves the endless circulation of water between the Earth and its atmosphere (Nandi, 2018). This knowledge is applied to the use, management and control of water resources on the earth's surface, especially for areas that are near water bodies.

2.2.2 Historical development of the hydrological cycle concept

The concept of the hydrological cycle can be traced back to the ancient Greeks, who recognised the role of evaporation and precipitation in the water cycle (Koutsoyiannis & Mamassis, 2021). Earlier research by scientists such as Bernard Palissy, Edme Mariotte, and Edmund Halley laid the foundation for the concept of the hydrological cycle in the 19th and 20th centuries. However, the development of new technologies and methods, such as isotopes, remote sensing, and GIS, has led to significant advances in understanding the hydrological cycle (Jasechko, 2019).

The earth contains enormous amounts of water in the form of ocean water, fresh water and saline water. It should be noted that water exists in different layers of the Earth, including the

atmosphere, lithosphere, hydrosphere, and biosphere. Among all these layers of the Earth, water masses are continuously circulating, hence forming the hydrologic cycle. This is as well-known as the World's Great Water Cycle, since it is the driving wheel for all the movements of available water resources on planet earth (Anderson et al., 2024). The hydrologic cycle serves as the central focus of hydrology, with no beginning or end (Koutsoyiannis., 2020). Therefore, all its processes occur continuously as summarised in Figure 2.1.

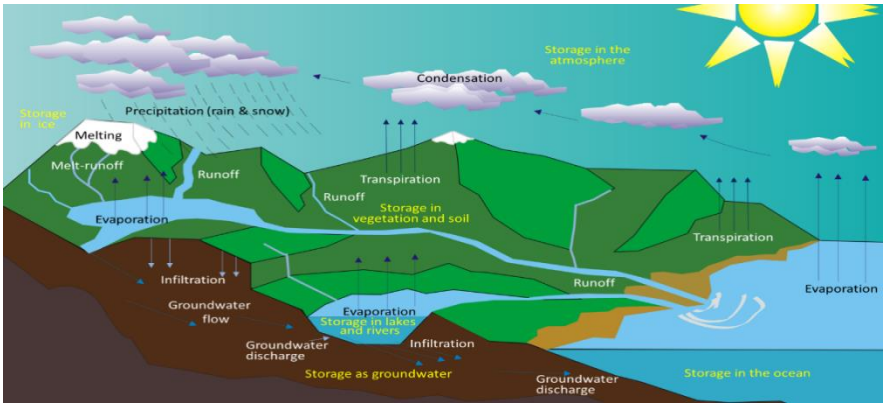

Figure 2. 1: The hydrologic cycle (source: The Hydrological Cycle. (2018))

2.2.3 Components of the Hydrologic Cycle

The hydrologic cycle consists of three fundamental systems: the oceans, which serve as the primary reservoir and source of water; the atmosphere, which functions as the carrier and distributor of water; and the land, which utilises this water. The availability of water at any given location varies over time, influenced by the changes in the primary processes of the cycle. According to Yang et al. (2021), While water movement operates as a closed system on a global scale indicating that the total amount of water on Earth remains constant it behaves as an open system at the local level. This variability means that water availability in specific regions can fluctuate significantly, affected by the interplay of the cycle's components.

The major components (or) elements of the hydrologic cycle are: Precipitation, evaporation, transpiration, evapotranspiration, Surface Runoff, condensation, infiltration, groundwater base flow, sublimation and interception (Davie, 2019).

Precipitation is defined as water in liquid or solid form falling on the Earth's surface (Wang et al., 2018). Precipitation is a common term for various forms of water, including mist, rain, hail, sleet, and snow. For precipitation to form, a sequence of four processes must occur: the

atmosphere must have sufficient water vapour present; it must be cooled to the dewpoint; water vapour condenses; water droplets grow; and water vapour is imported.

Whenever water vapour in the air is cooled below the temperature corresponding to the saturated vapour pressure, condensation occurs on dust particles, water droplets, grass, or other foreign objects (Hodnebrog et al., 2019). Condensation of moisture from the atmosphere above the Earth's immediate surface occurs on dust particles or suspended water droplets and forms fog, clouds, rain, snow, or hail (Easton Z & Bock E, 2015). During warm weather, cyclonic areas are usually accompanied by thunderstorms, lightning, thunder and usually precipitation. According to Mukrimaa et al. (2016), the condensed water vapour floats through the air in the form of clouds, cooled adiabatically, from which extensive air masses fall below the dew point. Thereafter, water particles grow in size until they are too heavy to float, then fall as rain, snow, or other forms of precipitation. These conditions are fulfilled in the atmosphere every time during the monsoons. Even though several atmospheric mechanisms cool the air, only adiabatic cooling from vertical uplift can produce precipitation of any significance.

Evaporation is the process of converting a liquid or solid into a gas by transferring heat energy (Hanks, 2015). It occurs when water is converted to water vapour at the evaporating surface the interface between the water body and the surrounding air (Zhang et al., 2017). The author further elaborates that two main factors influence evaporation from an open water surface: the supply of energy to provide the latent heat of vaporisation, and the ability to transport the vapour away from the evaporative surface. Evaporation occurs more rapidly with increased temperature and wind speed, as well as higher boiling point and vapour pressure (Gao et al., 2018). The greater a substance’s vapour pressure, the more rapidly the substance evaporates and escapes into the air.

Under constant temperature, humidity, and wind conditions, evaporation from the Earth's large water surfaces must remain constant; therefore, any temporary increase in temperature results in increased evaporation and, in turn, increased precipitation, as water evaporates more rapidly in dry air. Figure 2.2 presents the process of evaporation. Adopted from (Questions, n.d.)

Figure 2. 2: Evaporation (source: Questions, n.d.)

According to Koehler et al. (2023), transpiration is the movement of liquid water into, through, and out of the plant, as illustrated in Figure 2.2. Vegetation, including numerous growing plants, plays a significant role in the hydrologic cycle, as water drawn into the plant's rootlets from soil moisture moves up through the plant's stems and leaves (Boursiac et al., 2022). Through stomatal openings, water is released as water vapour, and the amount of transpiration depends on the density and size of the vegetation present.

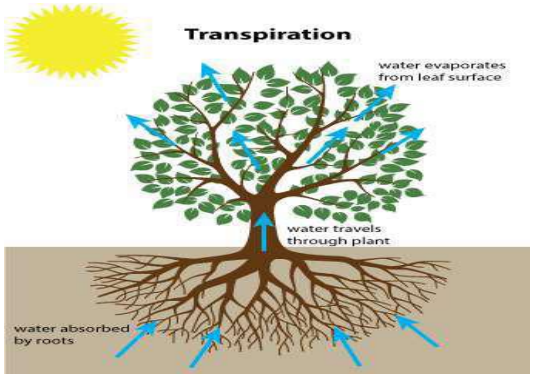

Figure 2. 3: Transpiration (source: Sc et al., n.d.)

Evapotranspiration refers to the loss of water from a vegetated surface through the combined processes of soil evaporation and plant transpiration (Yang et al., 2023). Evapotranspiration is the combined effect of evaporation from soil, surface water bodies, snow, and ice, and transpiration from vegetation. Furthermore, the majority of water loss due to evapotranspiration occurs during summer months and the growing seasons, clearly indicating that there will be no or little loss expected during winter months/period.

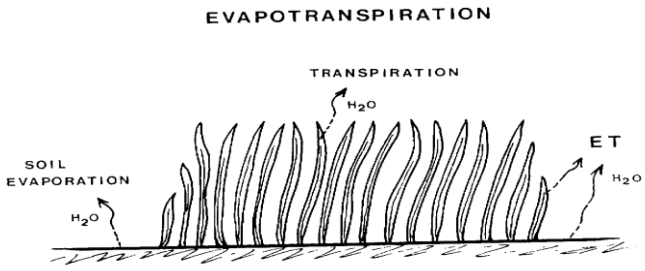

Figure 2. 4: Evapotranspiration (source: Cuxart & Boone, 2020).

Balasubramanian, (2017) defines surface water runoff as the quantity of water discharged from a drainage basin during a given time period. He further elaborates that "Runoff data may be presented as volumes in acre-feet, as mean discharges per unit of drainage area in cubic feet per second per square mile, or as depths of water on the drainage basin in inches". Discharge data are measured by installing stream gauges at selected locations along the river course (Cuxart & Boone, 2020). In the Manafwa river basin, there is only one discharge station, which is located along the Mbale Tororo road, and it is located in the lower sections of the basin.

Overland flow begins when the rainfall rate exceeds the soil infiltration rate and the slope increases.

As the rain continues, water reaching the ground surface infiltrates into the soil until the rate of rainfall (intensity) exceeds the soil's infiltration capacity. At this point, surface puddles, ditches, and other depressions are filled with water (depression storage), and afterwards, overland flow (runoff) is generated. The process of runoff generation continues as long as rainfall intensity exceeds the soil's infiltration capacity, but it stops once rainfall intensity drops below the infiltration rate (Balasubramanian, 2017).

Two major groups of factors determine the flow of any stream. The first set consists of geomorphological factors of the drainage basin and meteorological variables. Meteorological variables include Rainfall Intensity and type, rainfall duration, rainfall distribution, storm direction, and soil moisture conditions (Turner, 2022). The geomorphological factors include land use and land cover, soil type, area, shape, elevation, slope, drainage network, and indirect influences on runoff (Rezaei et al., 2019).

Infiltration is the process by which water enters the soil (Rocha et al., 2024). Water movement downward occurs in the topsoil layer, primarily through smaller pore spaces. According to

Rocha et al., (2024), infiltration is governed by two forces: gravity and capillary action. Infiltration begins when precipitation reaches the land surface, while runoff begins when the precipitation rate exceeds the infiltration rate, and retention and surface storage are filled. The relationship between rainfall, infiltration, and runoff is illustrated in Figure 2.5.

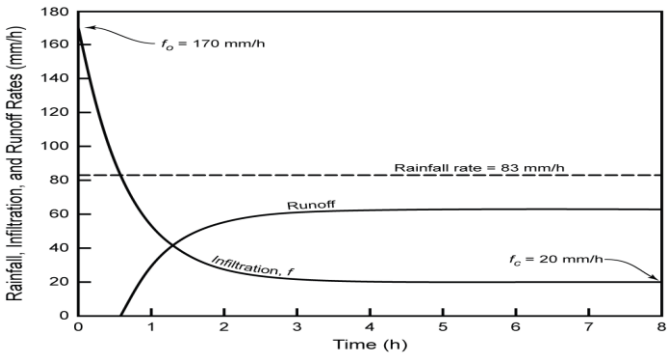

Figure 2. 5: Relationship between rainfall, infiltration and runoff (source: Rodney et al., (2013))

From the figure 2.5 above, at a rainfall rate of 83mm/h, the infiltration rate is high (170mm/h) and the runoff is absent (0mm/h). With continuous rainfall, the soils become saturated, thereby reducing infiltration until the rate becomes constant. As that happens, runoff will begin, and after some time, it will become constant. The rate of infiltration varies from soil to soil and is therefore highly dependent on the soil's hydrologic properties, such as porosity and permeability. Infiltration occurs only when there is space for water to enter the soil surface (Thiemig et al., 2011). This depends on the soil's porosity and the rate at which previously infiltrated water can move away from the surface. The maximum rate at which water can enter a soil layer under a given subsurface condition is known as the infiltration capacity, a measure of the rate at which a soil can absorb rainfall or irrigation water. This is measured in inches per hour or millimetres per hour.

2.3 River discharge in the global context

River discharge, as a dynamic outcome of the hydrological cycle, is key to global water resource availability, energy production, ecological stability, disaster preparedness, and regulation. Meles et al. (2024) describe how watershed outflow hydrographs reflect the combined effects of rainfall properties, surface conditions, and subsurface flow dynamics, demonstrating the integrated catchment response to diverse inputs. Turner (2022) analysed Mississippi River discharge data

and found that average discharge increased by approximately 4.5% per decade, and maximum discharge increased by ~2.3% per decade. He attributed the increase to both climatic change and land-use and land-cover alterations. River discharge over time changes from a static nature; however, it increasingly shows a nonlinear response to both climate and land use/land cover changes, later on indicating a shift in baseline hydrological behaviour.

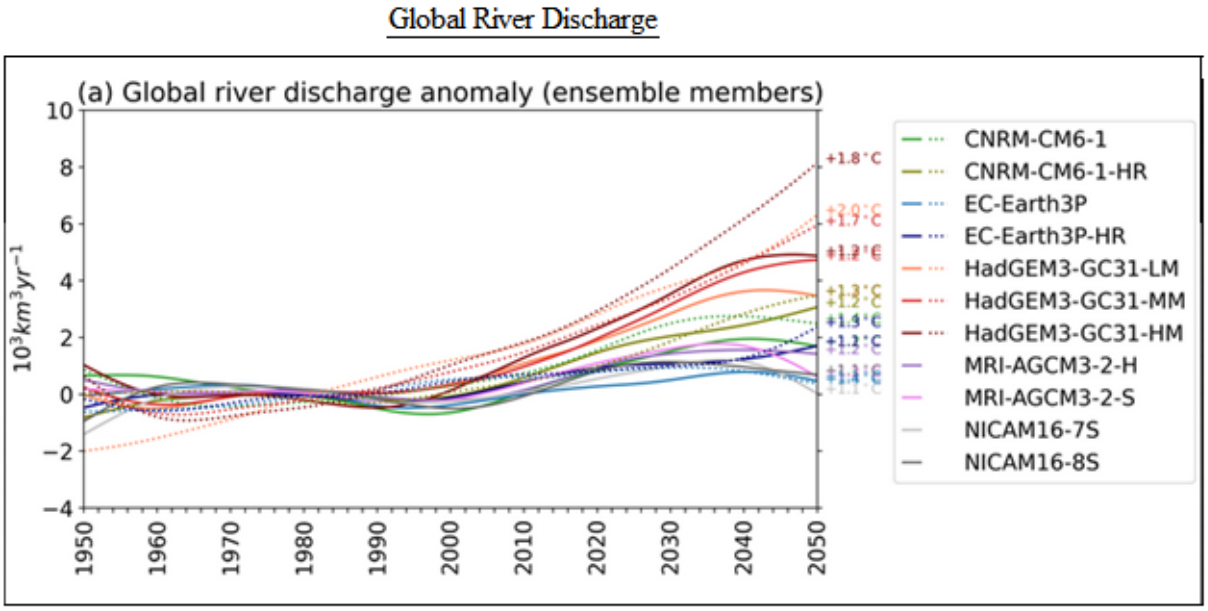

Figure 2. 6: Global River discharge (source: Müller et al., (2024))

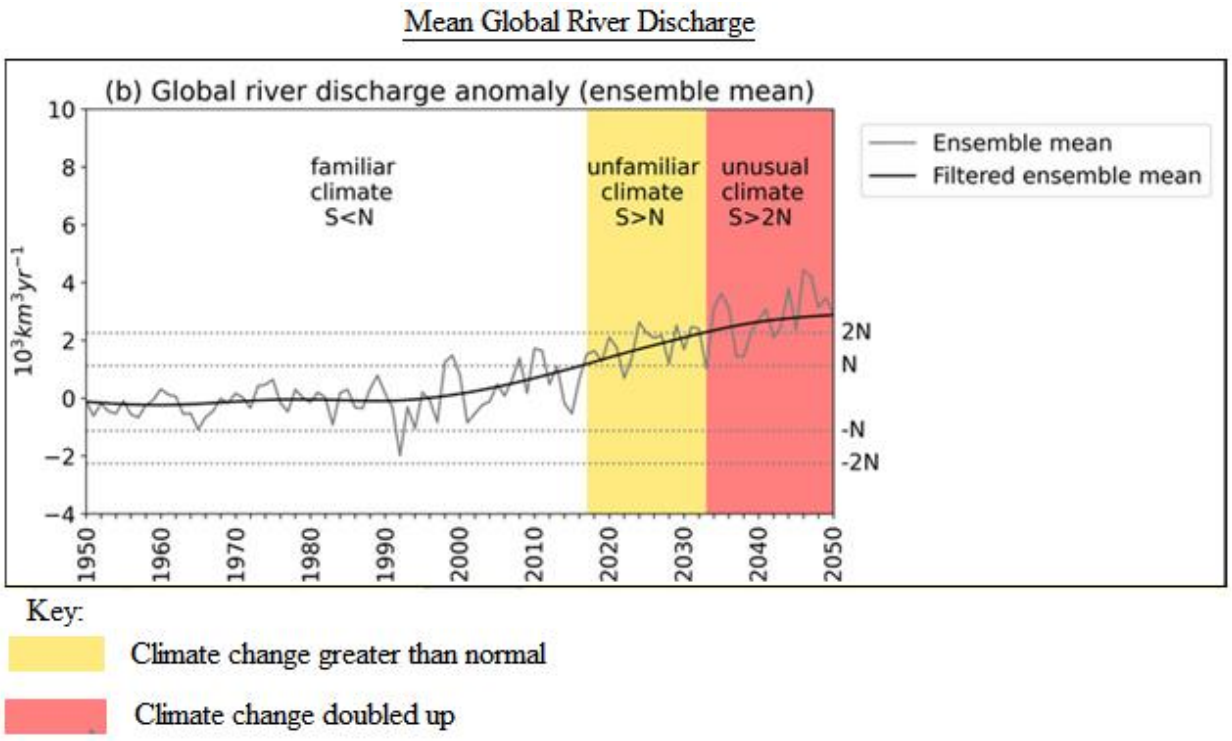

Figure 2. 7: Global mean river discharge (source: Müller et al., (2024))

Figures 2.6 and 2.7 above display simulations of river discharge variations over a century. The hydrographs above display a simulated global river discharge anomaly over a century. Figure 2.7 is a compilation of 11 global circulation models that indicate a vivid increase in river discharge patterns globally. This demonstrates an increase in future disasters driven by rising river discharge. Figure 9 shows abnormal climate changes (S>N) foreseen within timelines of (2020-2030). However, (S>2N) indicates a doubling of the rate of climatic change. This calls for doubling efforts in strategic disaster planning in the future. The river discharge S/N ratio and ToE are calculated following the approach proposed by (Müller et al., 2024). The goal of the method is to decouple the climate change signal (S) from the natural variability (the noise N). Müller et al. (2024) analysed river discharge globally in the context of climate change.

Global scientific research highlights an increased pattern in terms of discharge variability, shaped by spatial heterogeneity (Castino et al., 2017; Cohen et al., 2014; Déry et al., 2016; Guerrero et al., 2012; Hansford et al., 2020; Harrigan et al., 2020; Sperna Weiland et al., 2012; Willems et al., 2016). Regarding earlier research, increased flows are projected in high-latitude basins, such as the Manafwa River basin, whose latitude ranges from 1041 to 4301m (Robert & Brown, 2004). Furthermore, this region remains prone to variations in river discharge. However,

significant reductions are also anticipated in subtropical dry regions, such as the Mediterranean and the southwestern United States, due to declines in precipitation and increases in evapotranspiration (IPCC, 2021; Milly et al., 2005). Recent literature shows that in flood-prone areas such as Southeast Asia and parts of South America, discharge peaks are intensifying in both frequency and magnitude, overwhelming existing infrastructure and heightening socio-economic vulnerability (Turksezer et al., 2017). The shift towards more extreme discharge profiles underlines the inadequacy of historical hydrological baselines in predicting future water scenarios.

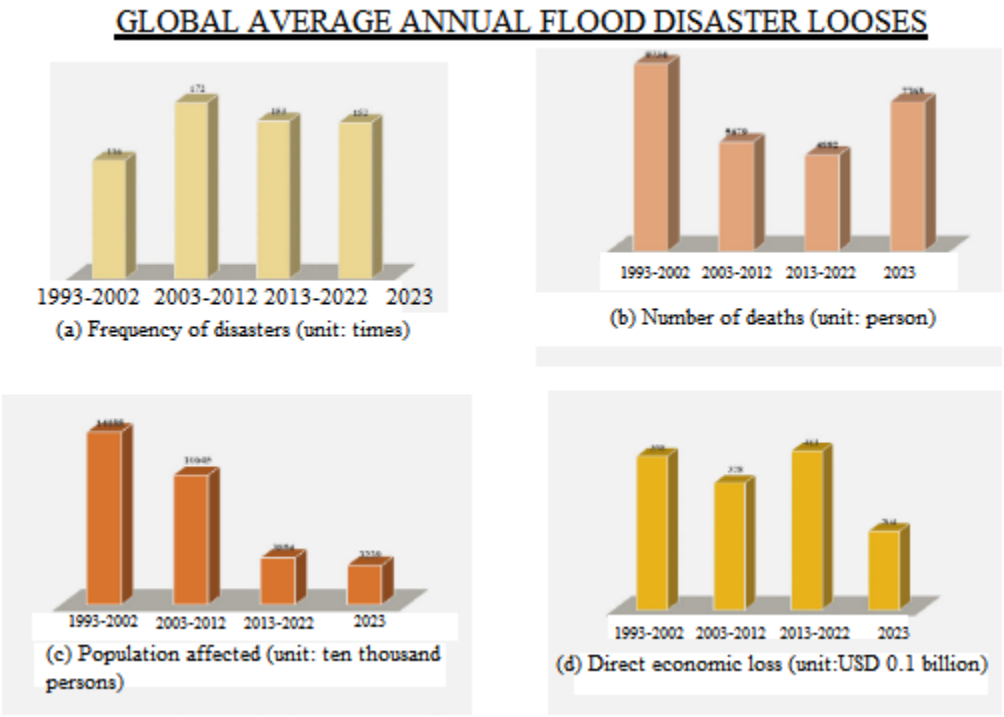

Figure 2. 8: Global average annual flood disaster loses (source: Müller et al., (2024))

As seen in figure 2.8 above, (**a**), flood disasters are increasing globally, even though the population affected is reducing (**c**), the number of deaths reported are high (**b**), this implies that those affected are reducing but those that die are many, this is evident in developing countries that have adopted and improved their flood warning and adaptation mechanisms compared to developing countries, this therefore leads to more deaths, reduced economic loss and reduced population affected in terms of disasters. A 1983–2022 observational study in the Kathmandu Valley (Nepal) showed that ENSO, as measured by the Niño 3.4 index, significantly influences

total and extreme precipitation patterns. These changes in precipitation directly translate into variability in river discharge regimes and flood risks in the region (Fernández-Castillo et al., 2025). These complexities necessitate hydrological models that incorporate both climate variables and land surface conditions. Therefore, understanding global discharge patterns requires not only climatological insights but also a systemic view of land-atmosphere-water interactions under human influence.

2.4 River discharge in developing countries

In developing countries, river discharge variability creates multidimensional challenges, including technical, institutional, and socio-environmental issues. These regions, many of which lie within the tropics and subtropics, are highly exposed to the risks associated with changing hydrological regimes.

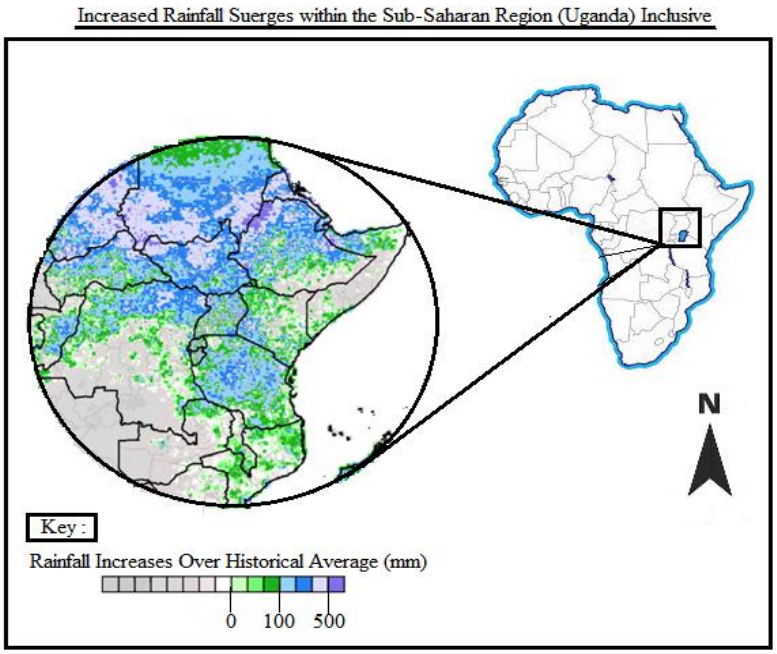

Figure 2. 9: Rainfall surges in SSR (source: Müller et al., (2024))

Figure 2.9 above shows countries that have experienced a pronounced increase in precipitation patterns within Africa. It should be noted that these are the same countries most affected by variations in river discharge, as shown by the risk index.

Table 2. 1: Flood disaster risk index

Governance Factors Closely Linked to Greater Population Impacts From Flooding

Country	Percentage of People Affected by Flooding	Lack of Disaster Coping Capacity (0-1-)	Corruption Perceptions Ranking (0-180)	Global Freedom Score (0-100)	Experiencing Armed Conflict	Riverene Flood Vulnerability (0-10)
Chad	9.95	8.6	167	15	✓	8.1
South Sudan	9.15	9.3	178	1	✓	7.8
Niger	5.70	7.4	123	21	✓	6.6
Burundi	2.22	6.7	171	14	✓	2.6
Cameroon	1.68	5.8	142	15	✓	6.7
Mali	1.55	6.4	137	26	✓	7.9
Somalia	1.32	8.5	180	8	✓	7.8
Guinea	1.26	6.9	147	30	ø	5.5
Sudan	1.24	6.7	162	33	✓	8.6
DRC	0.95	8	166	19	✓	7
Liberia	0.93	7.7	142	64	ø	7.4
Kenya	0.80	5.7	123	52	ø	5.1
Nigeria	0.57	6	150	44	✓	8.2
Senegal	0.56	5.3	72	67	ø	6.3
CAR	0.55	8.8	150	5	✓	6
Gambia	0.32	5.4	110	50	ø	4.6
Tanzania	0.31	5.8	94	36	ø	4.2
Sierra Leone	0.30	6.3	110	60	ø	5.8
Ethiopia	0.27	6.7	94	20	✓	5.1
Mauritania	0.27	6	130	39	ø	6.1
Uganda	0.23	6.9	142	34	ø	3.9
Congo, Republic	0.21	7.4	164	17	ø	7.6
Togo	0.15	7.4	130	42	ø	3
Benin	0.08	6.4	72	61	ø	6.6
Burkina Faso	0.07	6.4	77	6	✓	2.2
Côte d'Ivoire	0.05	6.5	99	49	ø	4.8
Guinea-Bissau	n/a	7.7	164	43	ø	2.8

Note: Red, Orange and Yellow shading reflect the rankings (most, moderate, least) among the flood affected countries on the disaster risk index. Adopted from United Nations Office for the Coordination of Humanitarian Affairs (UNOCHA, 2024)

(Source: Rainfall & Across, (2024))

According to the disaster risk index above (*Table 2.1*), the percentage of the Ugandan population affected by floods is 0.23%. According to the *MIDRC Data Commons*, (2017), 0.23% translates to 110400 people, this indicates that even though our country is within the least affected countries, with changes in climate and land use/land cover, there might be an upward movement from the least to moderately or even most affected countries since it is one of the countries that are to face heavy rainfall surges as reported by Rainfall & Across, (2024).

The situation is exacerbated by limited hydrometeorological monitoring infrastructure, outdated land use planning, and weak institutional capacity to implement integrated watershed management approaches (United Nations Environment Programme, 2020). Consequently, variations in river discharge in these settings often result in catastrophic socio-economic outcomes, including loss of life, disruption of livelihoods, and destruction of infrastructure. As

depicted from the graphs below, the frequency of disasters is on the rise specifically in Africa, this, without doubt translates into increased number of deaths, economic loses, displacement and destruction of infrastructures, therefore with anticipations that global warming would amount to 2.7°C by the end of the century (Scafetta, 2024), the number of deaths, economic loses and displacement will triple the current ones.

Several case studies from the Mekong Delta (Vietnam), Indus Basin (Pakistan), and the Limpopo Basin (Southern Africa) illustrate how climate variability, deforestation, and urban expansion have significantly altered discharge regimes, triggering both floods and droughts (Ahmad et al., 2012; Chuenchum et al., 2020; Legesse Gebre & Getahun, 2016). In the absence of predictive models, early warning systems, and adaptive infrastructure, such events cause repeated cycles of vulnerability (Cantoni et al., 2022; Erima et al., 2022). According to Jain et al. (2018),traditional flood management measures have proven inadequate, mainly due to climate change, land-use/land-cover change, urbanisation, population growth, and the complexity of flood dynamics, among other factors.

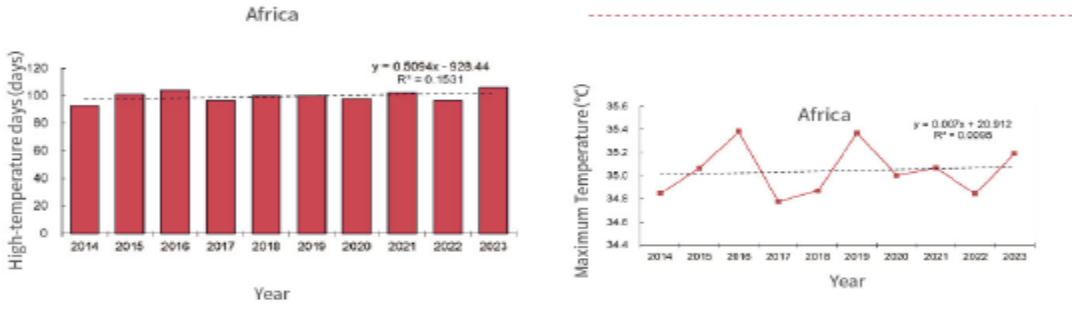

Figure 2. 10: Increment in temperature (source: (Global-Natural-Disaster-Assessment-Report.2023))

According to the *Global-Natural-Disaster-Assessment-Report*.(2023), days with high temperatures are increasing across our continent, accompanied by a gradual increase in maximum temperatures, which will lead to higher evaporation and evapotranspiration, resulting in reduced river discharges. While there is a debate over whether climate action is a lost cause, others report that Earth is on track to reach 2.7°C of warming this century (Yun et al., 2020). This, without doubt, will lead to chaotic river discharge patterns.

Besides that, the ecological degradation of upstream catchments has reduced the natural buffering capacity, deforestation and land degradation have reduced the ability of natural systems to absorb rainfall, leading to increased runoff and flood risk. Institutional fragmentation, lack of coordination, conflicting goals, and limited data sharing across agencies hinder the development of water resource strategies (Erima et al., 2022). The absence of long-term hydrological datasets in developing countries limits trend analysis, model calibration, and policy design (Borzì, 2025). The over-reliance on donor-funded technical interventions, particularly in water, sanitation, and irrigation sectors, results in weak sustainability. This is because such initiatives lack deep contextual alignment. Such interventions may be less effective in local conditions and poorly maintained once external support ends (Gedamu et al., 2025; Matsa et al., 2023). Thus, the challenge of managing river discharge in developing countries is not merely technical, but deeply embedded in systemic governance, capacity, and ecological resilience constraints.

2.5 River Discharge

2.5.1 Sub Saharan Africa

River discharge variations in the sub-Saharan Africa has also been reported to be erratic because of a number of reasons, among them are; The rugged terrain: Sub Saharan Africa is characterized by complex and rugged terrain, this is evident in eastern and central regions, these rugged terrains play a crucial role in shaping hydrological responses of watersheds. The presence of steep slopes, escarpments, and hill slopes accelerates surface runoff generation and decreases infiltration leading to higher peak river discharges and shorter lag times during rainfall events (Lei et al., 2020). Ethiopian highlands in Ethiopia, Rwenzori mountains in Uganda and the Aberdare ranges in Kenya, receive intense rainfall events, with slope induced flow acceleration, these have been greatly linked to floods, rapid sediment transport and increased downstream erosion (Gebremichael et al., 2025), these effects are further magnified when natural vegetation cover is moved, this is often the case due to deforestation or agricultural expansion.

Complex terrains complicate development of infrastructures and limit spatial coverage of hydrological monitoring networks, this results into high spatial variability in the different hydrological processes that are difficult to capture using low resolution models (Martini et al., 2021). In rugged landscapes of Sub Saharan Africa, watershed scale hydrological modeling

should integrate high-resolution elevation data (30 m DEMs), slope sensitive runoff algorithms, and careful sub basin delineation to capture critical topographic variability and improve the reliability of discharge simulations (Sciuto et al., 2025). The Manafwa river basin in eastern Uganda, characterized by rugged terrain and intense rainfall, highlights how topography driven hydrological extremes can result into severe social and environmental impacts if not adequately modeled. Therefore, incorporating terrain complexity into hydrological models is not only methodologically necessary but also essential for understanding and managing discharge variability in Sub Saharan watersheds.

2.5.2 Tropical climate

Tropical climate is characterized by high temperatures, intense solar radiation, seasonally concentrated rainfall that profoundly influences watershed hydrology. In tropical regions, rainfall is characterized by abundant, delivered in short but of high intensity that often exceeds soil infiltration capacities leading to rapid surface runoff and sharp discharge peaks (Rech et al., 2022). The combination of intense precipitation and high evapotranspiration rates contribute to pronounced wet and dry seasonal contrasts in river flow regimes. Seasonal extremes are further accelerated by the intra annual variability in rainfall distribution, often driven by climatic drivers such as the Indian Ocean Dipole and ENSO, increase rainfall variability and contribute to shifting discharge regimes in major basins like the Nile, Zambezi, and Niger (Mahmoud et al., 2022)**.**

2.6 Land use/land cover changes

Anthropogenic factors including deforestation, catchment degradation, and unregulated urbanization alter natural hydrological responses, reducing infiltration, increasing runoff, and destabilizing base flows (Babaremu et al., 2024; Kayitesi et al., 2022; Kimbi et al., 2024). This is particularly evident in highland systems where steep gradients increase runoff peaks, leading to flash floods and rapid sedimentation in downstream areas of the rivers.

Despite the intensifying impacts of river discharge variations, many SSA countries suffer from sparse and fragmented hydrological data networks, limiting their ability to monitor trends or model discharge accurately (Akpoti et al., 2024; Koch et al., 2025). Investment in integrated, transboundary water governance remains weak, while national level water resource policies often

fail to reflect the realities of localized hydrological behavior. These constraints hinder not only disaster preparedness but also sustainable development planning. As a result, improving discharge forecasting in SSA demands both technological advances in modeling and institutional innovations in data coordination and land water governance.

2.7 River Discharge in Uganda

Uganda's river systems, particularly in the eastern highlands, are increasingly characterized by discharge variations both in terms of magnitude and timing posing direct threats to communities and ecosystems. The Manafwa River Basin serves as the best example, with increased vulnerability, frequently experiencing flood events that result in fatalities, displacements, and infrastructural loss. According to Erima et al., (2022), floods in December 2019 led to four deaths, displaced over 2,000 people, and destroyed more than 20 homes. These events are not isolated but part of a growing pattern linked to both climate variability and unsustainable land management practices. Topographically, Manafwa's steep slopes, as illustrated in Figure 2.11 below, together with it's high rainfall intensity, make it highly responsive to runoff generation. At the same time, deforestation and land degradation have diminished its capacity for natural regulation.

Figure 2. 11: Manafwa steep slopes

Agricultural expansion into wetlands and floodplains has further limited the river's ability to accommodate excess flows. Concurrently, rainfall patterns have become more erratic, with increasingly intense storms and shifting seasons, this is consistent with climate projections of East Africa (Zhai et al., 2021). This is also consistent with the findings of our study where it has revealed that extreme weather events are intensifying. However, despite these known drivers,

most local level studies have focused narrowly on descriptive assessments or uncalibrated statistical models that do not integrate land use dynamics or future climate scenarios.

Moreover, policy shareholders remain largely inactive, early warning systems are limited, while spatial planning rarely considers hydrological risk zoning. Previous modeling efforts in Uganda have often lacked model calibration, downscaled climate inputs, or dynamic LULC integration, limiting their predictive utility (Haider et al., 2023). Consequently, a knowledge gap exists in understanding the future trajectory of discharge in the Manafwa River Basin, putting into use the dual focus approach that merges land use/land cover and climate modeling through physically based tools like SWAT.

2.8 Land Use and Land Cover Change and River Discharge

Land use and land cover (LULC) changes lead to profound effects on catchment hydrology, with measurable impacts on discharge volume, timing, and peak intensity (Erima et al., 2024; Chen & Chang, 2021; Abbas et al., 2015), The conversion of forests, wetlands and grasslands into croplands, settlements, and bare lands alters the land surface's ability to absorb, store, and release water (Erima et al., 2024). These alterations reduce infiltration capacity, accelerate surface runoff, and reduce evapotranspiration buffering, collectively increasing flood potential and modifying flow seasonality (Idowu & Zhou, 2021). In tropical regions, where rainfall events are often of high intensity, these effects are particularly pronounced.

Multiple studies across Africa have linked LULC change to altered hydrological behavior. For instance, deforestation in the upper Tana Basin (Kenya) has been associated with a 30% increment in peak discharge and a 20% decline in base flows over two decades (Engdaw et al., 2024). In Ethiopia's highlands, rapid cropland expansion has led to an increase in sediment yield and flash flood (Berihun et al., 2022; Taye et al., 2019). However, these studies often treat LULC as a static variable, failing to simulate future land cover dynamics under policy or demographic scenarios, this limits their utility for long-term planning.

Within Uganda, LULC changes are evident in the eastern region, where rising population pressure has driven extensive cultivation on steep slopes, and informal urban sprawl has reduced vegetation cover (Erima et al., 2022, 2024). Despite this, there is limited use of projected LULC

data in discharge modeling. Integrating LULC changes and climate changes with hydrological models is critical for capturing future discharge variability. Without this, hydrological forecasts risk underestimating climate and land-induced flood risks, particularly in vulnerable basins like Manafwa.

2.9 Land use/land cover classification

Land use/land cover classification is a fundamental step in environmental monitoring and watershed management, it provides spatial information on landscape patterns and human activities. Accurate LULC maps are key for hydrological modelling as different land use/land cover types influence surface runoff, infiltration, evaporation, evapotranspiration, and sediment yield differently (Dibaba et al., 2020; Haider et al., 2023; Hwang, 2017; Lamichhane & Shakya, 2019; Shrestha, 2019; Woldesenbet et al., 2017; Zope et al., 2017). Earlier research shows that remote sensing combined with geographical information system (GIS) offers efficient means to produce up to date LULC classifications over large areas with varying spatial and temporal resolutions (Kamusoko, 2022).

LULC classification techniques generally are categorized into supervised and unsupervised classification. Unsupervised classification algorithms automatically group pixels into clusters based on spectral similarity. Methods such as K-means and ISODATA are commonly applied to explore spectral patterns in the data (Kucuk Matci & Avdan, 2020), it should as well be noted that unsupervised classification methods require substantial post classification labelling and interpretation, which may introduce user bias and reduce accuracy more so in complex landscapes (Talukdar et al., 2020). In contrast, supervised classification relies on user defined training data where land use/land cover types are known prior to guide the classification process (Sharma Banjade et al., 2024). This approach often yields higher accuracy because the algorithm learns to discriminate classes based on representative spectral signatures. Several supervised classifiers have been developed and are widely applied, these include decision trees(DT), support vector machines(SVM), artificial neural networks(ANN), and random forest (RF) (Simarmata et al., 2025). Among the supervised classifiers, decision trees (DT) have gained prominence due to their interpretability, computational efficiency, and ability to handle nonlinear relationships and mixed data types (Simarmata et al., 2025). These split the dataset recursively based on spectral

feature threshold, resulting in an intuitive tree structure which classifies pixels through a series of decision rules (Zhou et al., 2021), it should however be noted that single decision trees have a limitation of overfitting training data which leads to reduced performance (Maxwell et al., 2018). To overcome the above, ensemble methods such as random forests, which build multiple decision trees and aggregate their predictions, provide more robust and accurate classifications, especially in heterogeneous and complex environment (Mutale et al., 2024). According to Mutale et al., (2024) algorithms like support vector machines utilize hyperplanes to maximize class separability in high dimensional feature space and are well suited for handling limited training data. Artificial neural networks mimic human brain function to model complex relationships but require extensive training data and computational resources that are often lacking especially in developing countries (Alshari et al., 2023).

Based on the reviewed literature (Alshari et al., 2023; Ibrahim, 2023; Khan et al., 2024; Talukdar et al., 2020), supervised classification approaches offer greater flexibility and accuracy for land use and land cover mapping, particularly when supported by machine learning algorithms. Among these, the Random Forest classifier consistently demonstrates superior performance due to its robustness, ability to handle high dimensional data, and resistance to overfitting. Given its proven effectiveness in complex landscapes and its suitability for remote sensing applications, this study adopted the Random Forest algorithm with 50 decision trees to perform supervised classification of satellite imagery. This choice ensures a reliable and replicable framework for generating accurate LULC maps necessary for subsequent hydrological modeling.

2.10 Climate change and river discharge

Climate change is increasingly acknowledged as a very crucial driver of hydrological change, influencing rainfall amount, intensity, distribution, and temperature influenced evapotranspiration (Nahib et al., 2021; Nakkazi et al., 2022; Trenberth, 2011). These alterations in turn, affect the magnitude and frequency of river discharge events (Anand & Oinam, 2020; Gelete et al., 2020). According to the IPCC, (2021), the association projects that tropical regions, including East Africa, will experience more intense rainfall events, accompanied by longer dry spells conditions that exacerbate both flooding and droughts. Discharge behavior is thus shifting not only in quantity but also in hydrological seasonality. Numerous global and regional studies

have acknowledged the implications of climate change on discharge regimes. In West Africa's Niger and Blue Nile Basins, climate simulations suggest a 25-35% reduction in mean annual discharge under RCP4.5 by mid-century (Krysanova et al., 2017). In the Nile Basin, rainfall variability and temperature increases are expected to disrupt seasonal flow, affecting agriculture and hydropower reliability. These examples underline the need for climate-informed water planning.

In the context of East Africa, several studies have documented similar climate driven hydrological disruptions, though with basin specific variability. Nsubuga et al. (2014) highlighted that Uganda's river basins are increasingly experiencing altered flow regimes, with rising flood frequencies linked to intensified rainfall events. Ayugi et al. (2021) further noted that East African highlands are projected to face both wet seasons and drier dry seasons, amplifying extremes in discharge behavior. Despite these advances, most of the existing research in Uganda, including studies on the Lake Victoria and Nile sub-basins (Mubialiwo et al., 2020), has predominantly emphasized climate change as the sole driver of flow variability. Limited attention has been given to the future influence of climate and land use/land cover changes. This gap is particularly critical for tropical basins like the Manafwa Basin, a flood-prone mountainous catchment that supports both agriculture and economic development. Investigating the impacts of future climate and LULC scenarios on discharge is therefore vital for understanding compounded risks, improving water resource planning, and safeguarding community resilience.

2.11 The SWAT Model in Hydrological Applications

Hydrological modeling has evolved as a powerful approach for understanding water dynamics and supporting watershed management, especially under changing environmental conditions (Erima et al., 2022, 2024). Among the leading tools is the Soil and Water Assessment Tool (SWAT), a semi distributed, process based model developed to simulate the long-term effects of land use, land management, and climate on water, sediment, and agricultural chemical yields in complex watersheds (Hermassi et al., 2025; Regasa & Nones, 2023). Its modular structure and integration with GIS make SWAT highly adaptable for simulating discharge under diverse biophysical and socio environmental conditions.

The model divides the watershed into hydrological response units (HRUs) based on unique combinations of land use, soil, and slope, enabling it to capture spatial variability in runoff generation and evapotranspiration (Erima et al., 2024). Notably, SWAT accommodates future scenario modeling, making it ideal for simulating climate and land use changes using projected data (Brighenti et al., 2023). Studies in regions such as the Upper Blue Nile in Ethiopia and the Limpopo Basin have demonstrated SWAT's capacity to model both water quantity and quality under future climate and LULC scenarios (Chawanda et al., 2024). However, the predictive accuracy of SWAT depends heavily on rigorous model calibration and validation using observed discharge data (Gasirabo et al., 2023; Mengistu et al., 2019). Haider et al., (2023) emphasized that uncalibrated applications of SWAT often lead to poor performance metrics and misleading policy recommendations.

Furthermore, the use of static LULC data and raw GCM outputs has been a critical shortfall in many African studies, without incorporating temporally dynamic land use/land cover and downscaled climate data, SWAT simulations cannot fully capture the complex hydrological responses to anthropogenic and climatic shifts. Previous SWAT modeling studies in the Manafwa Basin, failed to incorporate future climate and land use changes (Erima et al., 2024), resulting in methodological gaps that undermine predictive reliability highlighting the need for a more robust modeling framework as proposed in this study.

Table 2.2 below summarizes the crucial parameters that were considered during calibration, highlighting parameters and their hydrological roles

Table 2. 2: Sensitive parameters

No.	parameter	What it does	Effect on river discharge/hydrology
1	R__CN2.mgt	Adjusts the SCS runoff curve number, which controls surface runoff	↓ CN → more infiltration, less runoff; ↑ CN → more surface runoff.
2	V__ALPHA_BF.gw	Controls the baseflow recession rate (days).	Larger values = slower baseflow decrease, sustaining discharge longer after rain.
3	V__GW_DELAY.gw	Time lag between recharge and baseflow (days).	Longer delay = slower groundwater response; affects timing of low flows.
4	V__GWQMN.gw	Minimum aquifer water depth required to generate baseflow.	Higher threshold = less frequent baseflow contribution.
5	R__LAT_SED.hru	Controls sediment concentration in lateral and groundwater flow.	Affects water quality and sediment yield; minor effect on discharge volume.
6	R__SOL_AWC(..).sol	Soil's available water capacity (mm/mm).	Higher AWC = more soil water storage → less runoff, more infiltration.
7	R__CH_K2.rte	Effective hydraulic conductivity of the riverbed (mm/h).	Controls seepage loss from river to aquifer. Higher values = more infiltration from stream.
8	R__CH_N2.rte	Manning's roughness coefficient for main channel.	Higher values = slower flow, more channel storage.

9	R__ESCO.hru	Soil evaporation compensation factor.	Higher values = more evaporation → less water available for runoff.
10	R__OV_N.hru	Manning's "n" for overland flow (surface roughness).	Higher = slower surface runoff → increased infiltration time.
11	R__SURLAG.bsn	Surface runoff lag time coefficient.	Controls delay of surface runoff; higher = smoother hydrograph.
12	R__RCHRG_DP.gw	Deep aquifer percolation factor.	Higher = more percolation to deep aquifer → less shallow aquifer baseflow.
13	R__GW_REVAP.gw	Governs groundwater to root zone movement ("revap").	Affects evapotranspiration; higher = more loss from groundwater to plants.
14	R__SOL_K(..).sol	Saturated hydraulic conductivity of the soil (mm/h).	Higher = more infiltration and percolation hence reduced surface runoff, increased groundwater flow.

2.12 Downscaling climate data for hydrological modeling

Downscaling is a vital pre-processing step for using climate projections in local and regional hydrological modeling. General circulation models (GCMs), though indispensable for assessing global climate change trends, operate at spatial resolutions (100-250 km) that are too coarse for watershed level applications (Bjarke et al., 2024; Keller et al., 2022).

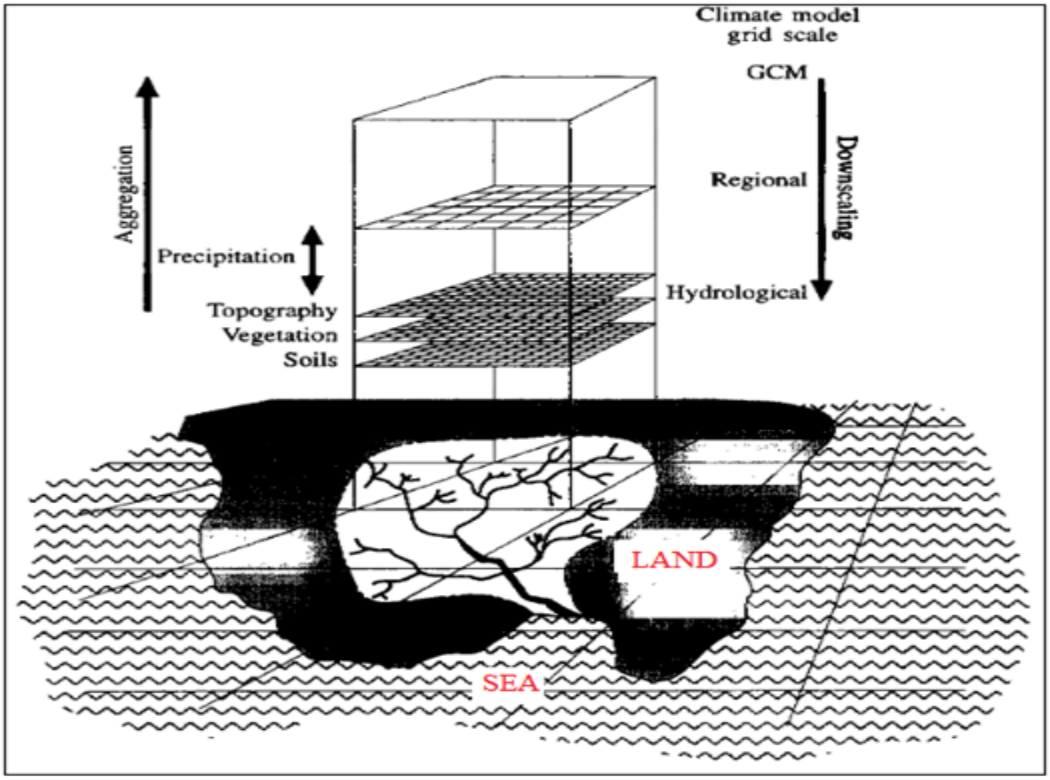

Figure 2. 12: Downscaling concept

Figure 2.12 above summarizes downscaling of GCM data to a basin scale level, due to the coarse resolutions accompanied by GCMs, the applicability at a basin is minimal without downscaling. It should be noted that GCM outputs cannot accurately represent local rainfall regimes, temperature variations, or extreme weather events critical inputs for discharge modeling.

Two main approaches to downscaling exist: dynamical downscaling, which involves running a high-resolution Regional Climate Model (RCM), and statistical downscaling, which derives empirical relationships between large scale predictors and local climate observations (Attique et al., 2023; Reder et al., 2025). While dynamical downscaling provides more physically consistent outputs, it is computationally expensive and data-intensive. Statistical methods, such as those used in CDO tool, are more accessible and have been effectively applied in East African basins, including the Awash and Mara Rivers (Ongoma et al., 2018). Many hydrological studies in Uganda and broader Sub-Saharan Africa rely on raw GCM outputs or skip downscaling altogether which introduces significant uncertainties in their model outcomes due to coarse spatial resolutions and bias in GCM projections (Banda et al., 2022; Onyutha, 2024).

This oversight results in under or overestimation of discharge extremes and misinforms water planning. To address this, the present study integrates bias corrected and statistically downscaled NEX-GDDP-CMIP6 data into SWAT, ensuring that the simulated discharge reflects possible future climate variability for the Manafwa River Basin. This step directly responds to methodological gaps in prior studies and enhances the reliability of future discharge projections under climate change conditions.

2.12.1 Bias Correction Methods

The bias correction methods used to correct the mean, variance, and distribution of the modeled variable, are explained below by using a function h (Londhe et al., 2023; Piani, Haerter, et al., 2010; Piani, Weedon, et al., 2010).

$$P_{observed} = h(P_{modeled}) \quad \text{.....Equation 1}$$

The aim of bias correcting is to make sure that the corrected outputs match the observed data, the different methods are explained in detail below:

Linear Scaling (LS) is a simple bias correction method that is widely used to adjust precipitation and temperature from GCM (Londhe et al., 2023; Maraun et al., 2010). This method reduces the biases by comparing the mean of the bias-corrected values with the observed values (Lenderink et al., 2007; Londhe et al., 2023). The LS function is used to calculate the corrected values based on the differences of the observed and GCM-simulated data. Precipitation data is rectified using a multiplier term where the simulated precipitation data are multiplied by the scaling factor While temperature is corrected using an additive term, where the simulated temperature data are added to the scaling factor (Londhe et al., 2023). LS equations of precipitation and temperature are given below;

$$P_{cor,m,d} = P_{raw,m,d} \times (\mu(P_{raw,m}) / \mu(P_{obs,m})) \quad \text{.....Equation 2}$$

For tempreture:

$$T_{cor,m,d} = T_{raw,m,d} + (\mu(T_{obs,m}) - \mu(T_{raw,m})) \quad \text{.....Equation 3}$$

where $P_{cor,\ m,d}$ and $T_{cor,m,d}$ are corrected precipitation and temperature on the dth day of mth month, respectively; $P_{raw,m,d}$ and $T_{raw,m,d}$ are raw precipitation and temperature on the dth day of mth month, respectively; $\mu(P_{obs},m)$ and μ $(T_{obs,m})$ are mean values of observed precipitation and

temperature at month m, respectively; and μ ($P_{raw,m}$) and μ ($T_{raw,m}$) are mean values of raw precipitation and temperature at month m, respectively (Londhe et al., 2023).

Local Intensity Scaling method (LOCI) of Precipitation, adjusts the biases in the frequency and intensity of precipitation which prevents the model-simulated raw data having an excessively large number of drizzle days (Londhe et al., 2023). This method involves two-step; first, a threshold for a wet day for a month, m Pthreshold, m is determined from the time series of model-simulated raw precipitation data (Praw,m,d), so that the threshold should match the observed (Pobs,m,d) wet day frequency, (Londhe et al., 2023) and in the second step, scaling factor (Sm), is calculated using

$$Sm = \frac{\mu(Pobs,m,d|Pobs,m,d>0)}{\mu(Praw,m,d|Praw,m,d>Pthreshold,m)} \quad \text{..... Equation 4}$$

The above equation is used to verify that the corrected model precipitation mean is equal to that of the observed precipitation data and calculated using the equation below;

$$Pcor,m,d = \begin{pmatrix} 0, & \\ Praw,m,d \times Sm & if\ Praw,m,d < Pthreshold,m \\ & otherwise \end{pmatrix} \quad \text{.....Equation 5}$$

The Power Transformation (PT) method for Precipitation removes biases in the precipitation taking into account the variance, the PT method adjusts the standard deviation of the data using an exponential form. In the PT method, initially, we have to estimate bm, which can be minimized using the formula below:

$$f(bm) = \begin{pmatrix} \delta(Pobs,m)/ \\ \mu(Pobs,m) \end{pmatrix} - \begin{pmatrix} \delta(PLOCI,m)/ \\ \mu(PLOCI,m) \end{pmatrix} \text{.....Equation 6}$$

where bm is the exponent for the mth month; σ represents the standard deviation operator; and $P_{LOCI,m}$ is the LOCI corrected precipitation in the mth month (Londhe et al., 2023).

If bm > 1, the LOCI-corrected precipitation data underestimate the coefficient of variance in month, m. Once the optimum value of bm is found, the scaling factor is determined using the formula below (Londhe et al., 2023):

$$Sm = \left(\frac{\mu(Pobs,m)}{\mu(PLOCI,m)}\right) \text{..... Equation 7}$$

The calculated scaling factor, Sm, should match the mean of the corrected values and observed values. Then, the corrected precipitation data are calculated using the LOCI corrected precipitation data, $P_{LOCI,m,d}$, using the equation below (Londhe et al., 2023):

$$Pcor, m, d = Sm \times PLOCI, m, d \quad \textbf{Equation 8}$$

Variance Scaling method (VARI) of Temperature, this method is used for bias correction and downscaling of temperature because, temperature is known to have an approximately normal distribution (Londhe et al., 2023; Terink et al., 2010). This method was developed to correct both the mean and variance of normally distributed variables such as temperature (Londhe et al., 2023; Terink et al., 2010; Teutschbein & Seibert, 2010b). Therefore, temperature data is corrected using the VARI method below:

$$Tcor, m, d = [Traw, m, d - \mu(Traw, m)] \times \left(\frac{\partial(Tobs,m)}{\partial(raw,m)}\right) + \mu(Tobs, m \quad \textbf{Equation 9}$$

The delta change method is one of the earliest and most widely applied approaches for adjusting climate model outputs for use in impact studies. This method operates on the assumption that future climate will differ from the baseline by a fixed "delta" (change) factor, which is typically calculated as the difference (for temperature) or ratio (for precipitation) between future and historical model simulations (Navarro-Racines et al., 2020; Sharma et al., 2023). The delta is then applied to observed baseline data, creating a corrected dataset that maintains the observed temporal pattern while incorporating future climate shifts.

The strength of the DC method lies in its simplicity, transparency, and minimal data requirement, making it particularly suitable for regions with limited observational records (Rica, 2020). In this method, the temporal structure of observed data such as seasonal cycles is preserved, which can be advantageous for hydrological models that require daily or sub daily inputs. The delta change method assumes stationarity in variability, in other words, it does not account for changes in variability, extremes, or distribution shape makes it less suitable for modeling future hydrological extremes or convective rainfall regimes, which are common in tropical regions like Uganda.

In literature, the DC method is increasingly being replaced or combined with distribution based or quantile mapping methods to better capture changes in frequency and intensity of events

(Lehner et al., 2023; Mendoza Paz & Willems, 2023). Its ease of use keeps it popular in large scale or data scarce studies. For the Manafwa river basin, while the DC method can provide a first approximation of climate driven discharge changes, it should ideally be complemented with methods like distribution mapping or local intensity scaling to better capture extremes relevant for discharge variation forecasting and water security planning.

The Distribution Mapping method (DM) for Precipitation and Temperature is based on the distribution function of the simulated GCM model data is corrected with that of the distribution function of the observed data. The DM method adjusts the mean, standard deviation, and quantiles. In addition, it retains the extreme data values (Londhe et al., 2023; Themeßl et al., 2012). This method assumes that the observed data and model-simulated raw data of variables follow the same distribution function, which leads to the addition of new unnecessary biases (Londhe et al., 2023). For precipitation, the gamma distribution function with shape parameter α and scale parameter β is used for distribution and has been verified to be effective (Turco et al., 2017):

$$f\gamma(x|\alpha,\beta) = x(\alpha-1) \times \left(\frac{1}{\beta\alpha\times\alpha}\right) \times \varepsilon\beta; x \geq 0, \alpha, \beta > 0 \ldots\ldots\ldots\ldots\ldots\ldots \textbf{Equation 10}$$

where x is the observed variable; fγ is Gamma function; is form parameter; and b is scale parameter. As previously discussed regarding the LOCI method, a precise threshold value is used to define a wet day as a large number of drizzle days are recorded in the raw GCM-simulated precipitation data, causing distortion in the distribution of raw data (Londhe et al., 2023). The bias correction is performed like LOCI-corrected precipitation data, $P_{LOCI,m,d}$ using:

$$Pcor, m, d = F\gamma(F\gamma(PLOCI, m, d|\alpha LOCI, m, \beta LOCI, m)|\alpha obs, m, \beta obs, m) \ldots\ldots. \textbf{Equation 11}$$

where F_γ ( ) and F_γ^{-1} are the gamma CDF (cumulative distribution function) and its inverse; a LOCI,m and b LOCI,m are the fitted gamma parameters for the LOCI-corrected precipitation in a given month m; and $\alpha_{obs,m}$ and $\beta_{obs,m}$ are the fitted gamma parameters for observed data (Londhe et al., 2023).

For temperature, the Gaussian cumulative distribution function shown below, or normal distribution with mean μ and standard deviation σ, is assumed to fit temperature best (Londhe et al., 2023; Teutschbein & Seibert, 2010a):

$$fN(x|\mu,\sigma) = (1/(\sigma \times \sqrt{2\pi})) \times e(-(x-\mu)2/2\sigma 2); x \epsilon R \ldots\ldots\ldots\ldots\ldots\ldots\ldots\ldots\ldots\ldots$$ **Equation 12**

Similarly, the corrected temperature can be estimated using the formula below:

$$Tcor, m, d = FN - 1(FN(Traw, m, d|\mu raw, m, \sigma raw, m)|\mu obs, m, \sigma obs, m \ldots\ldots$$ **Equation 13**

where F_N ( ) and F_N^{-1}( ) are the Gaussian CDF and its inverse; $\mu_{raw,m}$ and $\mu_{obs,m}$ are fitted and observed means for the raw and observed temperature data at a given month, m; and $\sigma_{raw,m}$ and $\sigma_{obs,m}$ are fitted and observed standard variation for the raw and observed temperature time series at a given month, m.

The NEX-GDDP-CMIP6 dataset developed by NASA, employs the Bias-Correction Spatial Disaggregation (BCSD) method. This combines distribution based bias correction with spatial downscaling (Lehner et al., 2023). The BCSD technique corrects model biases by adjusting the cumulative distribution functions (CDFs) of simulated climate variables to match those of observed data, thereby ensuring that the corrected data's statistical properties closely match those of the reference observations (D. Gao et al., 2024; Velasquez et al., 2020). This approach aligns conceptually with the Distribution Mapping or Quantile Mapping method, which also modifies the model output to reproduce the observed probability distribution(Lehner et al., 2023). Consequently, BCSD can be considered a specialised form of distribution mapping that includes an additional spatial disaggregation step to enhance the resolution of global climate projections. Therefore, it ensures that downscaled datasets such as NEX-GDDP-CMIP6 maintain both statistical fidelity and spatial detail suitable for regional hydrological and climate impact studies.

Table 2.3 below summarizes the advantages and disadvantages of the different bias correction methods.

Table 2.1: Bias correction methods

Bias correction method	**Advantages**	**Disadvantages**
Linear scaling (LS)	• Simple and computationally efficient • Corrects mean bias effectively	• Fails to adjust variance and distribution • Poor performance in simulating extremes and rainfall frequency
Local intensity scaling (LOCI)	• Adjusts both precipitation frequency and intensity • Reduces overestimation of light precipitation (drizzle)	• Ineffective in correcting variability and extremes • Limited to wet-dry threshold-based adjustment
Power transformation (PT)	• Corrects skewness and variance in precipitation • Improves coefficient of variation in highly skewed rainfall distributions	• Requires prior frequency correction using LOCI • More complex than LS • Not applicable to temperature data
Variance scaling (VS)	• Suitable for temperature correction • Adjusts both mean and variance • Works well with normally distributed variables	• Not suitable for precipitation • Assumes normal distribution which may not always hold
Distribution mapping or Quantile mapping (DM)	• Corrects mean, variance and quantiles • Best for preserving observed statistical properties • Suitable for extremes	• Computationally intensive • Sensitive to distribution selection • Risk of overfitting in poorly observed regions
Delta Change (DC)	• Easy to apply and interpret • Requires minimal data • Preserves observed temporal patterns	• Assumes stationary variability • Cannot represent future changes in extremes, frequency, or variance.

2.13 Separation method

In hydrological impact assessments, one methodological challenge is separating the individual contributions of climate change and land-use/land-cover change to observed or simulated changes in stream flow. This is essential for understanding attribution, informing targeted mitigation strategies, and supporting evidence-based watershed management. The separation method involves scenario-based model simulations under four distinct configurations: baseline LULC and climate, future climate only, future LULC only, and both future LULC and climate. The Scenario framework for separating climate and LULC effects on river discharge is summarised in equations 16 and 17 below.

$$contribution\ of\ climate\ change(CC) = \frac{Q2-Q1}{Q4-Q1} \times 100 \text{.....} \textbf{Equation 14}$$

$$contribution\ of\ LULC\ change\ (LULCC) = \frac{Q3-Q1}{Q4-Q1} \times 100 \text{ .....} \textbf{Equation 15,}$$

where;

Table 2. 4: Separation method

Scenario	LULC condition	Climate condition	Purpose
Q1	Baseline (2000)	Baseline (2000)	Reference scenario (status quo)
Q2	baseline	Future	Isolates climate change effect
Q3	future	Baseline	Isolates LULC change effect
Q4	future	future	Captures combined effect of LULC and climate change

This enables the quantification of isolated and combined impacts through comparative analysis of model outputs across scenarios (Guo et al., 2016; Wudineh et al., 2022). To quantify the relative contributions, researchers use additive decomposition methods, in which the total change in river discharge is partitioned into components due to LULC and climate, along with a residual interaction term. Alternatively, sensitivity-based methods use derivatives or elasticity indices to quantify how stream flow responds to incremental changes in climatic or land-use variables (B.

J. Anderson et al., 2024; Awasthi et al., 2024). While effective, these techniques assume linearity or independence; however, this assumption cannot hold in every catchment due to variations in terrain, climate, and hydrological behaviour.

In Uganda, the separation method remains underutilised; most hydrological studies in the region have focused on single-driver assessments, either modelling LULC change under static climate conditions or applying future climate scenarios under constant land-use/land-cover changes.

2.14 Pearson's Correlation Coefficient

Correlation analysis is widely used in hydrological and environmental studies to evaluate relationships among climatic variables, land-surface characteristics, and stream flow behaviour. According to literature (Bati et al., 2023; Nakkazi et al., 2022; Ngoma et al., 2021; Omay et al., 2023), there are various correlation measures and the Pearson's correlation coefficient has been one of the most commonly applied due to its ability to quantify the strength and direction of linear relationships between continuous variables. In catchment-scale studies, Pearson correlation has been used to explore how changes in land use/land cover influence runoff responses, as well as to examine the association between rainfall inputs and resulting discharge patterns (Woldetsadik et al., 2021). Establishing such relationships provides critical insight into interpreting hydrological model outputs, particularly in basins experiencing both climate variability and land-use change, such as the Manafwa catchment.

2.15 Synthesis of Literature

The reviewed literature demonstrates that river discharge is an outcome of interacting climatic, land surface, and subsurface processes operating within a catchment system. The catchment hydrology theory conceptualizes river discharge as the integrated response of precipitation inputs, evapotranspiration losses, soil moisture dynamics, surface runoff, and groundwater contributions. These processes are governed by both atmospheric forcing and land surface characteristics, implying that neither climate nor land use/land cover can be examined in isolation when assessing discharge behaviour.

Hydrological processes controlling river discharge include rainfall interception, infiltration, surface runoff generation, evapotranspiration, percolation, and groundwater recharge. The balance among these processes determines flow magnitude, timing, and variability. In tropical catchments, these processes are highly sensitive due to intense rainfall events, steep topography especially in the upper reaches, shallow soils, and strong dependence on vegetation cover. Consequently, relatively small changes in climate or land use/land cover can trigger large hydrological responses, particularly in terms of floods and drought.

Existing studies across tropical and sub-Saharan African basins consistently report increasing rainfall variability, rising temperatures, and altered streamflow regimes characterized by higher peak flows and more pronounced low-flow conditions. These trends reflect both climatic forcing and land use/ land cover transformations and underscore the non-stationarity of hydrological systems. Projections from climate models further suggest that future changes in precipitation intensity and temperature will amplify hydrological extremes, reinforcing concerns over water security and flood risk (Intergovernmental Panel on Climate Change, 2021).

However, much of the existing literature has adopted reductionist approaches, assessing either climate change impacts under fixed land use conditions or land use change impacts under stationary climate assumptions. Climate studies capture shifts in rainfall and temperature but overlook how land surface alterations influence runoff generation and storage. On the other side, LULC only highlights changes in infiltration and runoff but fail to account for evolving climatic drivers. These approaches, while informative, are limited in their ability to represent future hydrological behaviour in rapidly changing tropical basins.

Integrated climate and LULC studies provide a more realistic representation of catchment dynamics by accounting for the interaction between atmospheric forcing and land surface changes. Evidence from such studies indicates that combined impacts on river discharge are frequently non-linear and more pronounced than the effects of individual drivers. This highlights the necessity of integrated assessments for reliable future projections, particularly in basins experiencing concurrent climate change and rapid land cover transformations.

Reliable future hydrological assessment also depends on robust land use/land cover projection techniques. Approaches such as cellular automata, Markov chain models, and hybrid methods have been widely applied to simulate future LULC dynamics based on observed transition probabilities and driving factors. When coupled with hydrological models, these techniques enable scenario-based evaluation of how evolving land systems interact with projected climate conditions to influence river discharge.

Overall, the literature converges on the understanding that future river discharge behaviour in tropical catchments can only be adequately assessed through integrated modelling frameworks that combine climate projections with realistic land use change scenarios. This synthesis therefore provides the conceptual and theoretical foundation for the present study, which adopts an integrated climate, LULC approach to assess future river discharge variations in the Manafwa River Basin.

CHAPTER THREE: METHODOLOGY

3.1 Introduction

This chapter presents the research methodology, aligning it with the study's objectives and research questions. It discusses the research design; including data collection, Landsat image preparation and classification, accuracy assessment, land-use/land-cover prediction, SWAT model setup and simulation, calibration and validation, and analysis of future LULC and climate impacts on river discharge. The chapter also elaborates on data collection tools and analysis methods, their reliability and validity, and presents a step-by-step illustration of the research process, as shown in Figure 3.1.

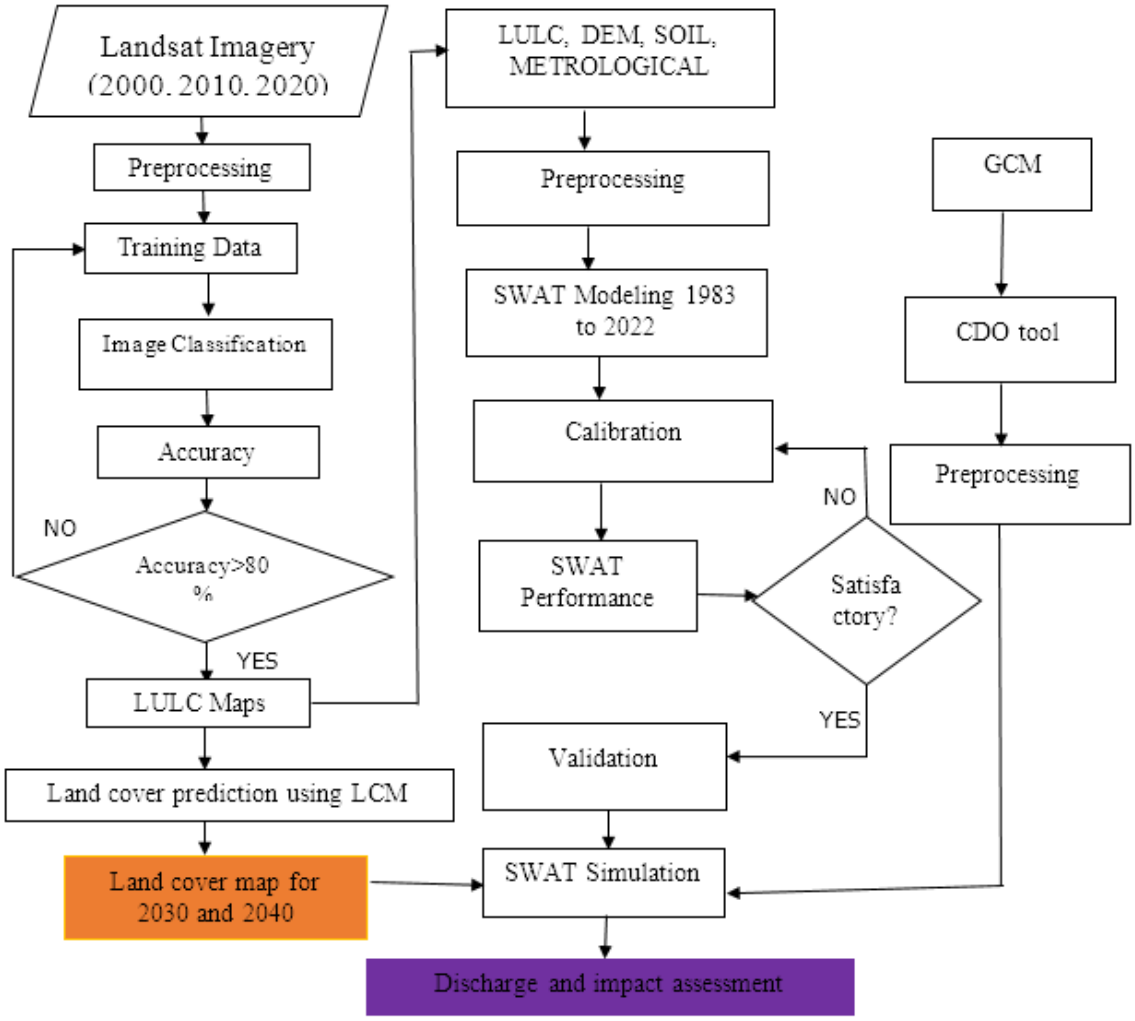

Figure 3. 1: Methodology flow

3.2 Research Design

This study adopted a quantitative, process-based modelling research design, to generate an objective, replicable, and system level understanding of how future climate and land-use/land-cover (LULC) changes will influence river discharge in the Manafwa River Basin. Unlike qualitative approaches that emphasise subjective interpretation, this design prioritises numerical precision, controlled experimentation, and predictive simulation, allowing the researcher to evaluate hydrological responses under clearly defined, scientifically defensible scenarios.

3.3 Data Sources

Spatial data needed for hydrological modelling using the ArcSWAT interface include a Digital Elevation Model (DEM), Land Use/Land Cover (LULC), Soil, Weather data (precipitation, temperature, solar radiation, wind velocity, relative humidity), and Stream flow (discharge). This data was collected from various sources, as shown in Table 3.1 below.

Table 3. 1: Spatial data

Data Type	**Scale/ Period (s)**	**Source (s)**	**Description**
Digital Elevation Model (DEM)	30 m × 30 m	United States Geological Surveys (USGS) website	Shuttle Radar Topography Mission (SRTM) (.tiff)
Landsat 4 TM and Landsat 7 ETM+	2000, 2010 and 2020	open-source U.S. Geological Survey Web site (http://glovis.usgs.gov/),	Classified LULC maps for 2000, 2010 and 2020.
Soil map	1:5,000,000	Food Agricultural Organization (FAO) http://www.fao.org/soils-portal/soil-survey/soil-maps-and-databases-FAO UNESCO-soil-map of the world/en/	Clipped Soil map for Manafwa river basin showing Soil types, classification and physical properties
Daily observed stream discharge of Station ID 82212	1983 - 2022	Directorate of Water Resources Management-Entebbe (DWRM)	Discharge (cms)

Daily observed rainfall data	1983-2024	NEX-GDDP-CMIP6	kilograms per square meter per second (kg/m2/sk g / m squared / s $kg/m2/s$)
Daily observed temperature (min and max)	1983-2024	NEX-GDDP-CMIP6	Temperature (kelvin)
Solar radiation	1983-2024	NEX-GDDP-CMIP6	W/m² (watts per square meter)
Relative humidity	1983-2024	NEX-GDDP-CMIP6	Percentage (%)
wind speed	1983-2024	NEX-GDDP-CMIP6	meters per second (m/s)
Future daily climate (Tempreture, solar radiation, relative humidity, wind speed and rainfall)	2025 to 2040	NEX-GDDP-CMIP6	

Historical Climate Data were obtained from the mean ensemble of 3 GCMs, namely; UKESM1-0-LL, GFDL-ESM4, and GFDL-CM4 from the NEX-GDDP-CMIP6. This was for meteorological data: precipitation, humidity, wind speed, solar radiation, and minimum and maximum temperature. These 3 GCM models were used because they had shown good representation of different seasons in previous studies (Omay et al., 2023), making it appropriate for use in the Manafwa River Basin, where ground measurements are of limited quality and future data is not available. Furthermore, Erima et al. (2022, 2024) successfully applied CHIRPS data in studies conducted within the same basin, since its spatial resolution is 5 km. The mean ensemble was also downscaled to 5 km.

3.4 Data Preprocessing

3.4.1 Past and Present

Given that hydrological models are sensitive to the quality, consistency, and precision of climatic inputs, this study adopted a multi-stage preprocessing framework to transform regional climate projections into locally representative, SWAT-compatible forcing data. Daily maximum and minimum temperature, precipitation, relative humidity, wind speed, and solar radiation were obtained from the ensemble mean of three CMIP6 Global Climate Models (GCMs) under the NEX-GDDP framework for the period 1983–2040. This dataset was deliberately selected

because its statistical bias correction and 0.25° (25km) spatial resolution reduce systematic model errors and provide a closer representation of local climate patterns compared to raw GCM outputs a critical requirement for distributed hydrological modelling in tropical basins.
However, because GCM outputs are generated at a global scale, several scientific and practical transformations are necessary before they can be used in SWAT. The datasets were clipped to the eastern region of Uganda, which covers the Manafwa basin boundary.

Units of the climate variable that were not consistent with SWAT's internal parameterisation were converted. For the NEX-GDDP dataset, precipitation is provided in $kg \cdot m^{-2} \cdot s^{-1}$ and must be converted to daily totals in millimetres; temperature is provided in Kelvin and must be converted to degrees Celsius. Solar radiation provided in $W \cdot m^{-2}$ was converted into daily $MJ \cdot m^{-2}$, and wind speed was converted into $m \cdot s^{-1}$. These conversions were essential not only for consistency but also because incorrect units propagate substantial structural errors within SWAT, distorting evapotranspiration estimates, surface runoff generation, and water-balance ratios.

The datasets underwent refinement and quality assurance, including checks for missing values, removal of extra days in February, and removal of duplicate entries. While NEX-GDDP is statistically bias-corrected, internal consistency checks were conducted to verify that the historical climate trends align with known regional climatology, such as the bimodal rainfall distribution. This step is critical because hydrological outputs are extremely sensitive to temperature-based evapotranspiration drivers and precipitation intensity distributions.
The cleaned and standardised climate data were restructured into a SWAT-acceptable format, with each climate variable supplied as a separate station file (*.pcp, *.tmp, *.slr, *.wnd,* *.hmd*). This process required assigning station IDs, geographic coordinates and date formatting conventions consistent with SWAT's input parser. This reorganisation ensures that the model correctly interprets the spatial and temporal dynamics of the climate drivers, a necessity for accurately simulating water balance components across hydrological response units.

3.4.2 Future Climate Projections

Future climate projections for the Manafwa River Basin were obtained from the NASA Earth Exchange Global Daily Downscaled Projections (NEX-GDDP) dataset under the CMIP6 framework for both SSP2 and SSP5 pathways**.** Three General Circulation Models (GCMs) were

selected: UKESM1-0-LL, GFDL-ESM4, and GFDL-CM4. The choice of these models was based on their robust performance in representing East African climate dynamics, specifically Uganda, the availability of all climate variables needed to perform SWAT modelling, and prior validation in regional climate assessments (Ayugi et al., 2021; Dinku et al., 2018; Ngoma et al., 2021; Omay et al., 2023, 2025). Each model provides projections under various Shared Socioeconomic Pathways (SSPs). It should be noted that this study focused on the SSP2 (middle-of-the-road) and SSP5 (extreme events) scenarios, which represent a moderate emissions pathway consistent with current global trends.

The selected NEX-GDDP-CMIP6 models included the following key variables required by the SWAT model: daily precipitation (pr), maximum temperature (tasmax), and minimum temperature (tasmin), solar radiation (slr), wind speed (sfc wind) and relative humidity (hmd). Since NEX-GDDP-CMIP6 models are already bias-corrected against observational and reanalysis data, specifically the Global meteorological forcing dataset (GMFD), no additional bias correction was applied. However, using the CDO software, the netcdf files were merged and clipped to the eastern region, from which the mean ensembles were computed. To ensure consistency with previous research carried out in the basin, downscaling to 5km resolution using chirps as the reference data in the CDO tool was performed using bilinear interpolation, the reference data had initially performed well in the basin (Erima et al., 2022, 2024). The data was then extracted at intervals of not more than 5 km, since it was downscaled to the exact resolution. This ensured that differences in climate data were well captured during the hydrological simulations, as emulated in the research of Song & Yan (2022). Therefore, 11 stations were used in the study, some within the basin, others near, and others virtual stations established as a result of the buffer analysis, especially in the upper zones of the basin. These datasets provided the necessary historical and future climatic forcing inputs for simulating the potential impacts of climate change on river discharge while keeping land use and land cover constant. The results from these simulations are presented and discussed in Chapter 4.

3.4.3 Preparation of Soil Lookup Table

The soil map from the Food and Agriculture Organisation of the United Nations (FAO-UNESCO) at a scale of 1:5,000,000 was downloaded from http://www.fao.org/soils-portal/soil-survey/soil-maps-and-databases-FAO UNESCO-soil-map of the world/en/. The data's default

coordinate system was WGS1984, which was used throughout the study. The soil data was resampled to 30-meter resolution and geo-processed to a dataset format compatible with Arc SWAT. A specific soil lookup table was created, and the map was clipped to the AOI to create a soil GIS layer for the Manafwa river basin. This soil map provides information on soil type, soil classification, and physical properties, including texture, soil depth, and soil drainage attributes, needed by the SWAT model. Using the Arc SWAT soil database provided by the US Department of Agriculture (USDA), soil properties such as clay content, sand content, loam content and hydrological group were analysed, from which an assessment was then conducted to identify SWAT user-defined soils that closely correspond to the characteristics of the soils within the study area.

3.4.4 Terrain Analysis

The SRTM DEM of 30 m resolution for the study area was downloaded from the United States Geological Survey (USGS) website https://lta.cr.usgs.gov in the WGS 1984 datum. This was preferred because of its high spatial resolution and because it does not require reprojecting from one coordinate system to another. The DEM was used to delineate the watershed by filling sinks and removing spikes, thereby enabling the computation of flow direction and accumulation in ArcSwat. Thereafter, watershed delineation was performed, yielding sub-basins, HRUs, the stream network, the longest reaches, and drainage surfaces.

3.4.5 Preprocessing of River Discharge (flow).

The daily river discharge/flow data were obtained from the Directorate of Water Resources Management (DWRM), Entebbe, for River Gauging Station (ID) No. 82212. It is worth noting that the Manafwa River has only one discharge gauge station. The observed daily stream flow data were aggregated to average monthly stream flow, as the model's performance in simulating monthly scenarios was satisfactory in previous research carried out within the same basin (Pouyan Nejadhashemi A, 2011). Besides that, most daily river discharge data have been reported to be noisy (Navarro-Racines et al., 2020). The discharge data were then arranged in the SWAT CUP acceptable format, as required for calibration inputs. This data was used to calibrate and validate the SWAT model.

3.5 Land Use Land Cover Mapping in the Manafwa Catchment

3.5.1 Past Land Cover Mapping

Landsat imagery (Landsat 4, 7, and 8) from the Collection 2, Tier 1 Surface Reflectance (SR) dataset was utilised for land-use/land-cover (LULC) mapping in the Manafwa catchment. The data were accessed and processed within the Google Earth Engine (GEE) cloud platform. The SR product was preferred because it provides atmospherically corrected surface reflectance values generated by the LaSRC algorithm, which accounts for aerosol scattering and water vapour absorption. This ensures radiometric consistency and minimises sensor-related and atmospheric distortions, thereby improving the reliability of subsequent classification results.

Prior to classification, the imagery was filtered by date and cloud cover (10%) to ensure optimal visibility of surface features. Additional preprocessing steps, such as cloud and shadow masking were applied to enhance image quality. The images were then composited to generate annual median reflectance mosaics representing each study year (2000, 2010, and 2020). These composites provided consistent and cloud-free datasets suitable for time-series LULC analysis.

Supervised classification was conducted in GEE using the Random Forest (RF) machine learning algorithm with 50 decision trees. Training data were obtained through visual interpretation of high-resolution imagery and expert knowledge of the catchment. A minimum of 60 representative training samples were collected for each LULC category: Built-up areas, Farmland, Grassland, Tropical Forest, Wetland, and Woodland. The Natural Colour (RGB) composite was primarily used for identifying land cover types during training data collection. The Random Forest algorithm was selected due to its robustness, resistance to overfitting, and superior classification accuracy in complex landscapes (Belgiu & Drăguţ, 2016).

Accuracy assessment was performed using a stratified random sampling approach, with 20% of the training data reserved for validation. The assessment metrics included overall accuracy, producer's accuracy, and user's accuracy, ensuring a comprehensive evaluation of classification performance. An acceptable minimum accuracy threshold of 80% was adopted, following the recommendations of Wang & Mountrakis (2023).

The classified maps for 2000, 2010, and 2020 were subsequently exported from GEE for post-classification analysis and cartographic visualisation in ArcGIS 10.2.2. These maps form a

consistent spatial dataset that supports further temporal change detection and hydrological modelling within the Manafwa basin.

3.5.2 Future Land Use/Land Cover

Future land use/land cover (LULC) maps were generated using TerrSet's Land Change Modeler (LCM), following procedures outlined by Haider et al. (2023). Historical LULC maps for 2000, 2010, and 2020, along with spatial driver variables such as distance from road networks, distance from the river network, population density, distance from urban centres, elevation (DEM), and aspect and slope, were used as inputs to inform the projections (Li et al., 2020; Lukas et al., 2023). LULC maps for 2010 and 2020, along with the spatial variables, were used to project the 2030 LULC map, maintaining a 10-year temporal interval. For the 2040 projection, LULC maps from 2000 and 2020 were combined with the spatial drivers to ensure a consistent 20-year temporal interval. This approach allowed the incorporation of both historical trends and spatial determinants into projections of future land use/land cover.

3.6 Calibration and Validation

3.6.1 Swat Model Setup and Input

The processes used to set up a SWAT model are summarised in Figure 3.2 below. These include automatic watershed delineation, HRU analysis, creation of input tables and SWAT simulation.

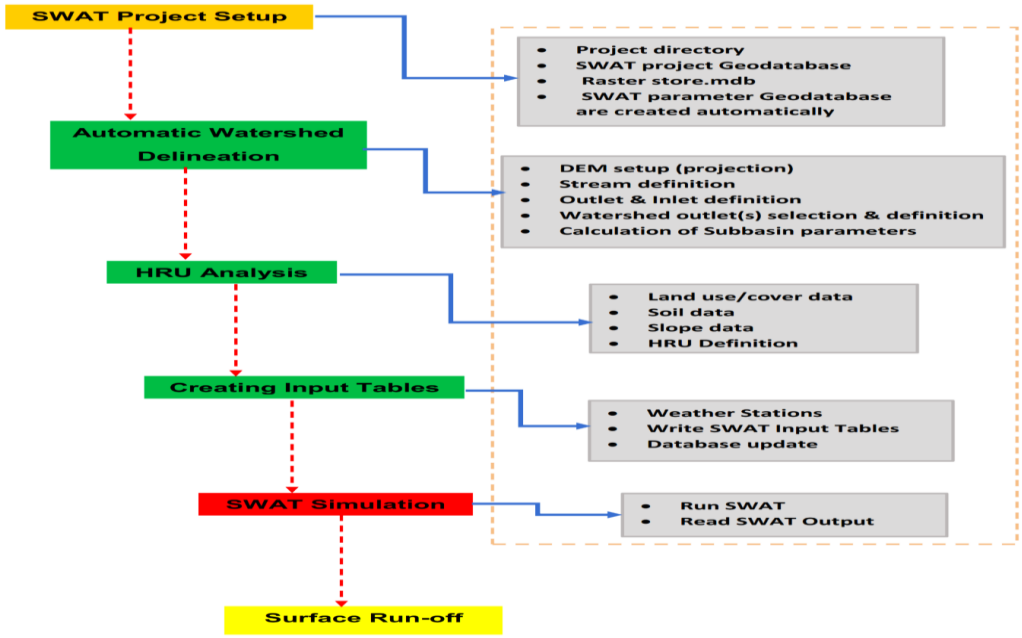

Figure 3. 2: SWAT hydrological model setup (source: Arnold et al., 2013; Turyahabwe, 2019)

In hydrological modelling, the watershed delineation process involved five steps: setting up the DEM, stream definition, outlet and inlet definition, watershed outlets selection and calculation of sub-basin parameters. The automated watershed delineation interface in Arc SWAT was used to delineate the Manafwa watershed. A 30-meter-resolution DEM was used for the DEM setup, from which stream definition based on DEM conditions was performed to obtain flow accumulation and direction. The watershed outlet was added manually because I had the gauge station's coordinates within the basin.

Having delineated the watershed, the hydrologic response unit creation process was then executed. In the HRU Analysis section, under the land use/soils/slope definition subsection, the land use/cover, soil, and slope data, along with their respective lookup attribute tables, were also imported and defined as required by SWAT. The LULC and Soils were reclassified, overlapped, and connected to the SWAT catalogues, therefore ready for HRU definition. The LULC maps lookup table was prepared into five classes in the "SWAT Land Use Classification Table", namely: FRST – Tropical Forest, AGRL – Farmland, WATR – Water bodies, URBN –Built-up, WETL – Wetland and PAST – Grassland and RNGE - Woodland.

For the SWAT Slope Classification, five slope classes were defined, each with lower- and upper-class limits expressed as percentages (%). Slope elevation bands of 0–2, 2–4, 4-8, 8-16 and 16-99.9 and above were provided to the model. For the HRU definition, thresholds of 1% for land use, 10% for soil class, and 10% for slope were set. These thresholds were chosen to capture LULC transformation effects well during the simulations. Having executed the overlay option, the HRU feature class and Overlay reports were created.

Weather data files were prepared using the WXGEN weather database, and the resulting files were imported into Arc-SWAT. The files contained data with the same start and end dates as the SWAT simulation. The WXGEN user option for generating weather data was used, and only the files containing the coordinate locations of the weather data (precipitation (pcp), temperature (tmp), relative humidity (rh), wind speed (wind), and solar radiation (solar) were imported into SWAT. The SWAT model was finally set up for simulation by selecting and defining the simulation period from 1983 to 2022, with the first 7 years used as a warm-up period to allow the simulated processes to reach dynamic equilibrium. After running, the model creates output files that were used for subsequent hydrological modelling, calibration, and validation.

3.6.2 SWAT CUP Project Setup

To prepare the model for calibration, the output files generated from SWAT were organized in a separate folder dedicated to SWAT-CUP processing. SWAT-CUP was then launched, and the SWAT output folder was linked to the software so that it could read the required simulation files. The appropriate SWAT version and calibration method were selected based on the model configuration, after which a new project was created and saved in the designated working directory.

3.6.3 Sensitivity Analysis

Sensitivity analysis is used to estimate the rate of change in model outputs in relation to changes in the model inputs (Turyahabwe, 2019). It helps to determine which parameters are important for accurate results (Atkinson et al., 2010; Turyahabwe, 2019). Sensitive parameters for the basin were obtained from a study by Erima et al. (2024), who conducted hydrological modelling in the Manafwa basin. His findings highlighted key parameters associated with surface runoff (CN2, SOL_K, SOL_AWC), groundwater response (ALPHA_BF, GW_DELAY, GWQMN, RCHRG_DP), evapotranspiration and vegetation processes (ESCO, EPCO, CANMX), and channel routing (CH_N2, CH_K2), along with flow timing factors such as SURLAG and HRU_SLP. These parameters were therefore prioritized in the sensitivity analysis for the basin.

3.6.4 Calibration of the Model

The SWAT model was calibrated using observed daily data from the Directorate of Water Resources Management (DWRM) for the Manafwa River gauge station (82212), which were converted to monthly discharge. The calibration timeframe was from 1983 to 2015, with a seven-year warm-up period incorporated to initialise the model state. The calibration involved using the Sequential Uncertainty Fitting (SUFI-2) algorithm within the SWAT-CUP tool, following the procedures outlined by G. Arnold et al. (2012). Below is Figure 3.3, which summarises the calibration procedure.

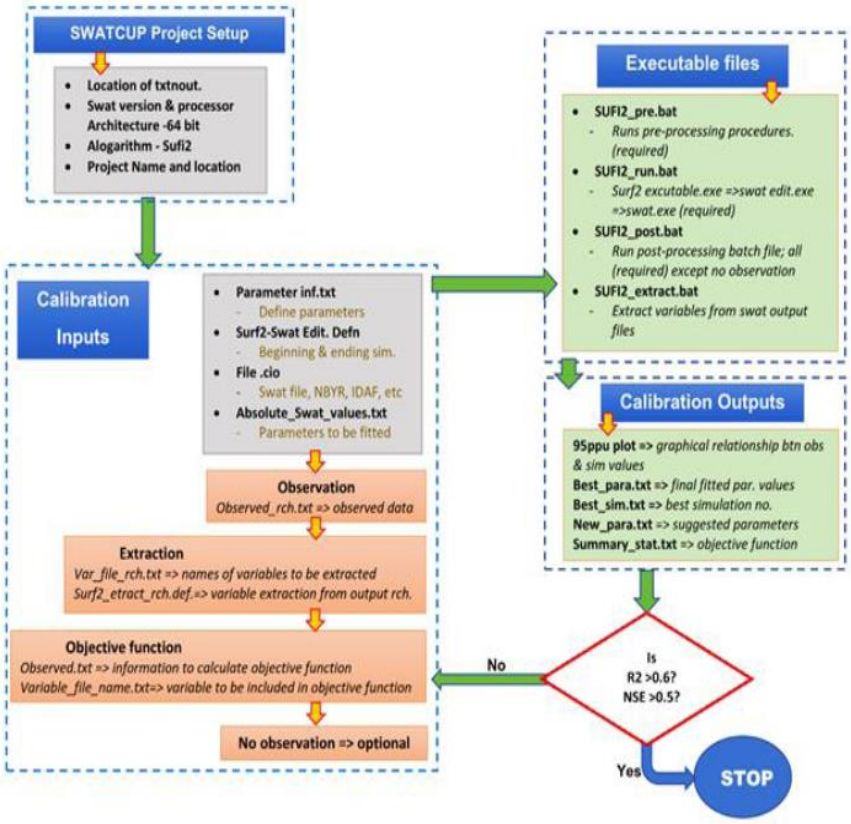

Figure 3. 3: Calibration process (source: ((Turyahabwe, 2019))

Calibration was carried out using the Sequential Uncertainty Fitting Algorithm (SUFI-2) implemented in the SWAT-CUP software. This approach follows the procedures recommended by Arnold et al. (2012) and has been widely applied in similar catchments. The process involved defining the project, selecting the observation data, and specifying the model parameters to be adjusted during calibration. Based on previous work in the Manafwa basin (Erima et al., 2024; Turyahabwe, 2019), fourteen key hydrological parameters were selected, including those controlling surface runoff (CN2, SOL_K, SOL_AWC), groundwater response (ALPHA_BF, GW_DELAY, GWQMN, RCHRG_DP), evapotranspiration (ESCO, EPCO, CANMX), channel routing (CH_N2, CH_K2), and flow timing (SURLAG, HRU_SLP). These parameters were assigned initial ranges and used as inputs for SUFI-2 iterations.

The observation dataset, the simulation period, and the objective function were then specified within SWAT-CUP. The Nash–Sutcliffe Efficiency (NSE) and coefficient of determination (R^2) were used to assess the agreement between simulated and observed discharge. The calibration

process involved running multiple simulations, comparing the results with observed data, and updating parameter ranges until an acceptable level of model performance was achieved.

SWAT-CUP produced several outputs summarising calibration performance, including the 95% prediction uncertainty (95PPU) plot, the set of best-fitted parameters, suggested parameter ranges for subsequent iterations, and summary statistics for NSE and R^2. Model uncertainty was evaluated using the P-factor, which measures the percentage of observed data captured within the 95PPU band, and the R-factor, which represents the width of that uncertainty band. Parameter sets yielding high P-factor and low R-factor were considered satisfactory and selected for use in subsequent model evaluation. All these steps followed are summarized in figure 3.4 below.

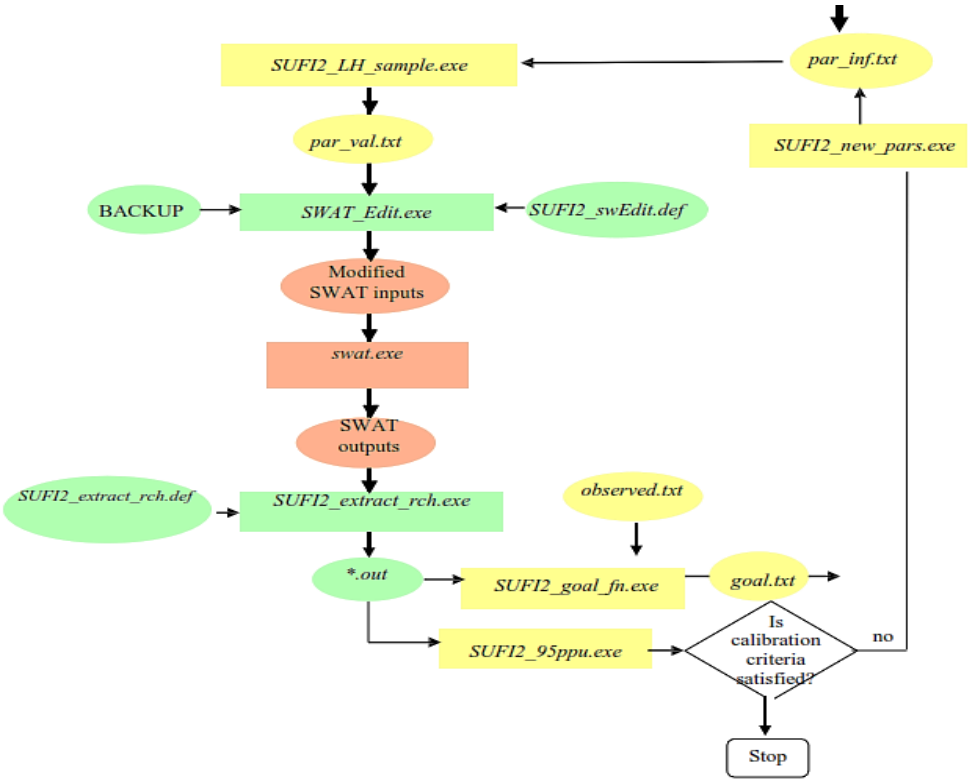

Figure 3. 4: SUFI2 algorithm operation (source: (Turyahabwe, 2019)

3.6.5 Model Validation

Model validation is the process of determining the extent to which a model or simulation accurately represents observed behaviour from the perspective of its intended uses (Turyahabwe, 2019). This process was conducted in SWAT-CUP using observed discharge data from 2016 to 2022.

The model's accuracy was evaluated using statistical metrics as those recommended by N. Moriasi et al. (2007). Statistical metrics include: Nash-Sutcliffe Efficiency (NSE), Coefficient of Determination (R^2), Root Mean Square Error (RMSE), and Per cent Bias (PBIAS). Turyahabwe. (2019) recommended performance rating for SWAT model simulations as presented in the table 3.2 below, and these were used as a basis in this study.

Performance ratings recommended for stream flow simulation

Table 3. 2: Performance ratings.

Performance rating	**NSE**	**R^2**
Unsatisfactory	NSE ≤ 0.5	R^2<0.6
satisfactory	0.5<NSE ≤ 0.65	0.5<R^2 ≤ 0.65
Good	0.65 < NSE ≤ 0.75	0.65 < R^2 ≤ 0.75
Very good	0.75< NSE ≤ 1	0.75< R^2 ≤ 1

Source: (Turyahabwe, 2019)

3.7 Modelling River Discharge for Different Climate and Land Use/Land Cover Scenarios

3.7.1 Land Use/Land Cover Change with Constant Climate

Following Turyahabwe. (2019)'s methodology, investigating the isolated impacts of land use/land cover (LULC) change on river discharge involves keeping climate inputs constant while changing LULC data. Specifically, historical climate variables from the period (1983–2022) were employed across all scenarios to ensure consistency. Projected and historical LULC datasets for 2010, 2020, 2030, and 2040 were introduced into the model, one at a time. This approach enabled the influence of LULC change on river discharge to be evaluated independently of the climate variables. In the SWAT model setup, LULC maps for 2010, 2020, 2030, and 2040 were introduced, one at a time, while keeping the climate variables, soil, and topographic datasets fixed. For each scenario, the model was run and generated results like the topographic reports, HRU reports, elevation and discharge reports which reflected hydrological responses to the changing LULC. The newly generated TxtInOut file which contains all the essential SWAT input and output files, including model configuration, parameter files was then imported into SWAT-CUP, and the minimum and maximum parameter values were set to the

fitted values that were obtained during calibration. This ensured that the model adjusts to the fitted parameters, thereby maintaining consistent model performance. SWAT-CUP simulations were subsequently executed, and the output tables were extracted for each LULC scenario. The results from the simulations provided the basis for analysing the impacts of land cover change on river discharge under constant climate conditions.

3.7.2 Climate Change with Constant Land Use/Land Cover

For the climate change scenarios, land use/land cover (LULC) was held constant at the year 2000, which corresponds to the baseline period used during model calibration. This approach, also known as the separation method, was adopted to isolate the influence of climate change on river discharge without the effects of LULC change.

Within the SWAT model setup, future climate projections were introduced while all other input datasets (soils, topography, and land cover) remained fixed. The model was then run to generate new model files, reflecting different simulation outputs under the altered climatic conditions. The new model files were then imported into SWAT-CUP, where parameter values were maintained at the obtained fitted calibrated values. This ensured consistency between the baseline model setup and the subsequent climate change simulations. Thereafter, SWAT-CUP was executed, and corresponding output tables were generated for the new climate scenarios. These outputs provided the basis for evaluating the impacts of climate change on river discharge under fixed LULC conditions.

3.8 Quantifying the Individual Contributions of Land Use/Land Cover Changes and Climate Changes on River Discharge.

The separation method was used to quantify or attribute discharge changes to either climate change or land-use/land-cover change. By differencing discharge from baseline discharge values, one can quantify the individual contributions of LULC and climate change. The separation method has been extensively applied in hydrological studies to quantify the impacts of specific drivers on stream flow variability (Guo et al., 2016; Wudineh et al., 2022). The method, therefore, enables the evaluation of the distinct and combined impacts of two domino factors, thereby facilitating hydrological evaluations.

CHAPTER FOUR: RESULTS

4.1 Introduction

This chapter presents research findings for each specific objective and begins with past classified land-use/land-cover maps, followed by those for the future. The chapter further presents sensitivity analysis, calibration, validation, and hydrological simulation outcomes under future LULC and climatic scenarios.

4.2 Land Use/Land Cover Changes for Manafwa River Basin from 2000 to 2040.

4.2.1 Land Use/Land Cover Maps

Figure 4.1 below shows the spatial distribution of LULC for 2000, 2010, 2020, 2030, and 2040. From the maps, six land cover classes; Wetland, Forest, Farmland, Built-up, Grassland, and Woodland were identified. Visually, Farmland, Forest, Woodland, Grassland, and Wetland were the most dominant LULC classes in the watershed. It should be noted that, despite their earlier coverage, this changed significantly over time.

The dominance of farmland and the decline in forest, woodland, and wetland areas clearly indicate a transition from a watershed predominantly covered by natural vegetation in 2000 to a human-modified watershed by 2040. These transitions point to increasing agricultural and urban expansion as major drivers of land cover change.

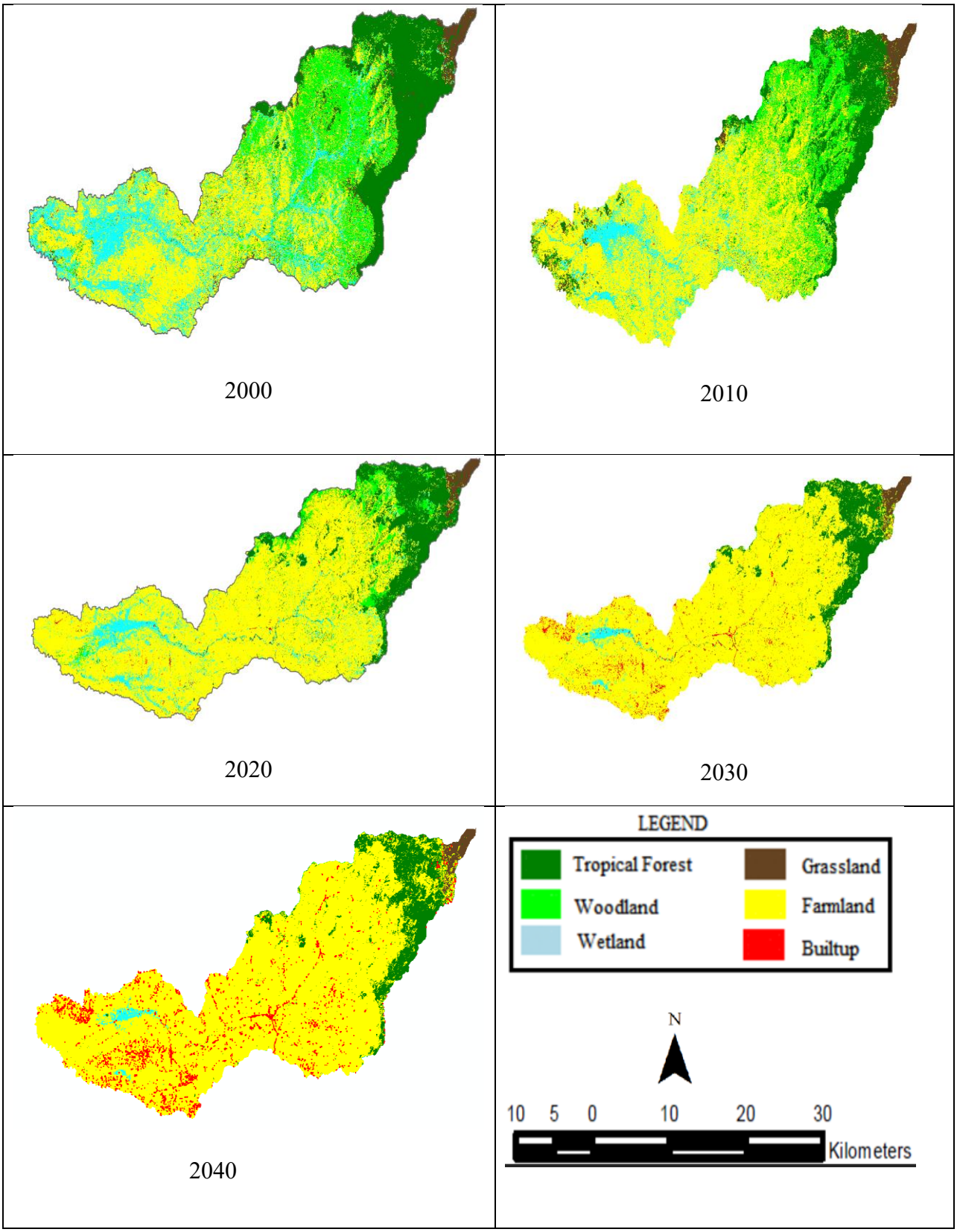

Figure 4. 1: LULC maps for 2000, 2010 2020, 2030 and 2040

Table 4. 1: Area Statistics

LULC class	2000 (km2)	2000 (%)	2010 (km2)	2010 (%)	2020 (km2)	2020 (%)	2030 (km2	2030 (%)	2040 (km2	2040 (%)
Built-up	0.3	0.1	1.0	0.2	2.8	0.42	16.8	2.6	40.9	6.2
Wetland	128.5	19.6	66.4	10.1	49.4	7.53	11.7	1.8	5.3	0.8
Farmland	263.6	40.2	351.6	53.6	461.5	70.38	538.6	82.2	533.8	81.4
Tropical forest	114.2	17.4	111.8	17.1	100.1	15.27	78.7	12.0	66.8	10.2
Woodland	118.8	18.1	102.3	15.6	32.3	4.92	0.7	0.1	0.5	0.1
Grassland	30.4	4.6	22.7	3.5	9.7	1.48	9.0	1.4	8.2	1.3
Total	655.8	100	655.8	100	655.8	100	655.8	100	655.8	100

Table 4.1 above presents area statistics for both classified and projected LULC classes in the Manafwa River Basin for 2000, 2010, 2020, 2030, and 2040. The results show the transformation of the basin's land cover over 40 years. The built-up area has increased steadily from 0.3 km² (0.1%) in 2000 to 40.9 km² (6.2%) by 2040, indicating rapid urban expansion driven by population growth, infrastructure development, and improvements in living standards.

On the other hand, natural vegetation classes specifically tropical forest, woodland, wetland, and grassland show a consistent decline across the study period. Area covered by Tropical Forest declined from 114.2 km² (17.4%) in 2000 to 66.8 km² (10.2%) in 2040, and that of woodland reduced from 118.8 km² (18.1%) to 0.1 km² (0.02%): such a trend points towards intensified deforestation and natural vegetation degradation within the Manafwa basin. In addition to the above, the wetland area also experienced significant reductions, from 128.5 km² (19.6%) in 2000 to 5.3 km² (0.8%) in 2040, reflecting increasing human pressure that has led to conversion to Farmland and urban development. Therefore, Farmland is the most dominant and expanding LULC class throughout the study period and it increased significantly from 263.6 km² (40.2%) in 2000 to 533.8 km² (81.4%) in 2040. This exponential expansion points towards intensified agricultural activity in the basin. The expansion of Farmland primarily occurred at the expense of forest, woodland, and wetland areas, demonstrating a clear trend of conversion from natural land cover to agricultural landscapes.

Therefore, the LULC maps reveal a transition from natural land cover in 2000 to a more human-modified surface cover by 2040, as demonstrated in Figure 4.2. These findings highlight the accelerating impact of human activities on land cover in the Manafwa River Basin, with potential implications on the hydrological cycle.

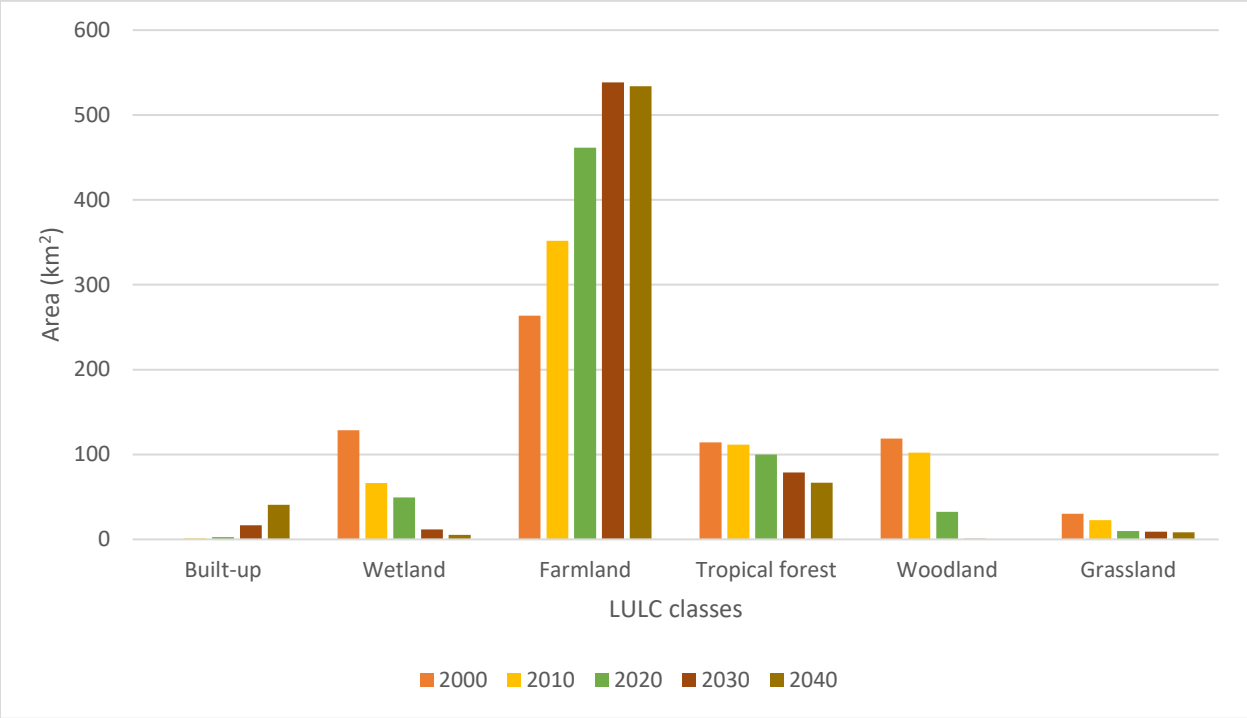

Figure 4. 2: LULC classes for different years

4.2.3 Change Detection

This was conducted to quantify and visualise spatial and temporal transitions in LULC classes between 2000 and 2040, using transition matrices and change maps to assess the direction, rate, and magnitude of these changes. The analysis revealed that wetlands and woodlands are the most dynamic classes, with high probabilities of conversion to farmland and built-up areas.

Between 2000 and 2010, approximately 13% of the basin's natural LULC classes were converted into farmland and built-up areas. However, this pattern intensified between 2000 and 2020, when about 30.6% of the basin underwent conversion. The spatial patterns of change indicate that the upper catchment retained more forest cover, while the mid and lower zones experienced extensive farmland and built-up expansion, as shown in Figure 4.3 below.

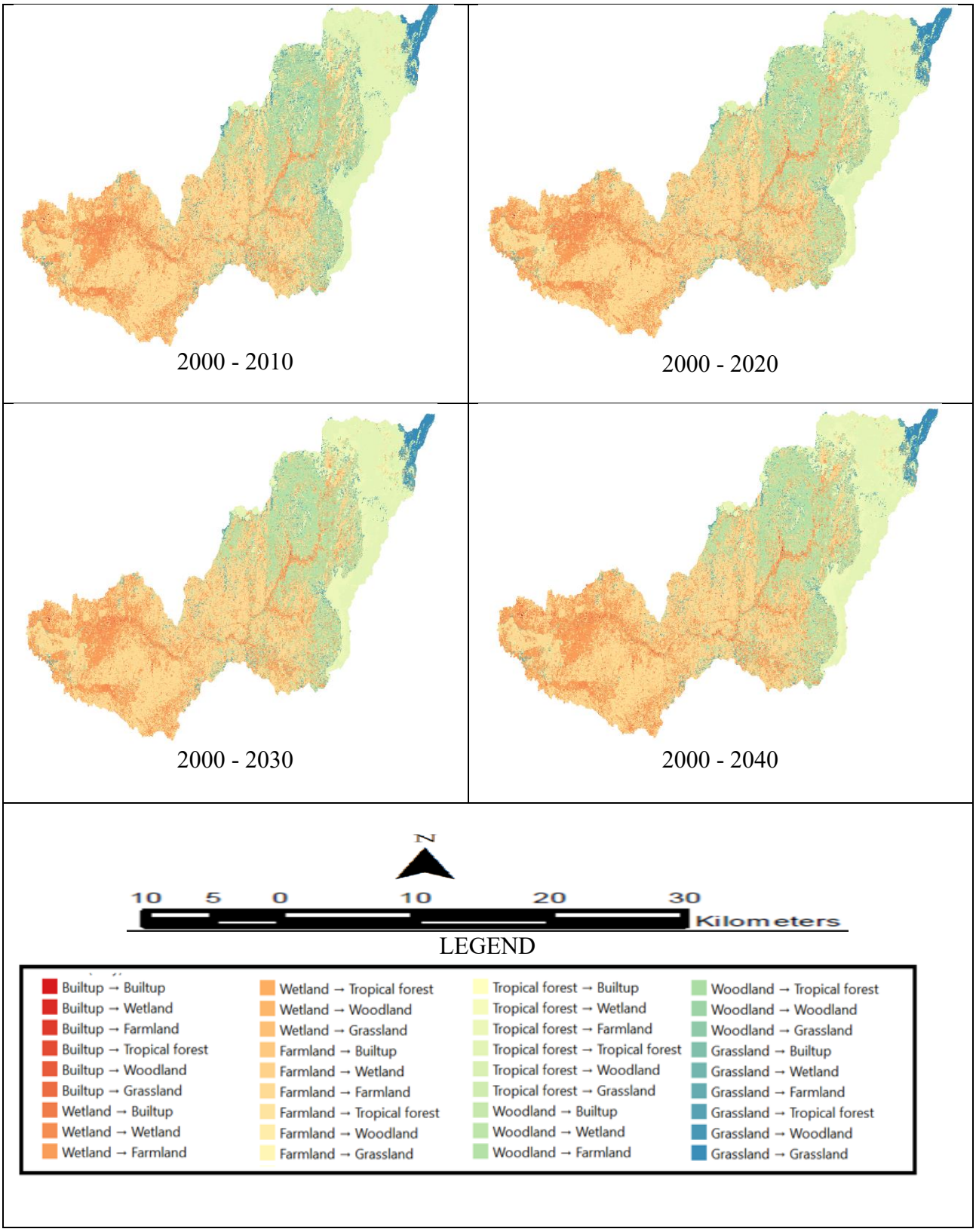

Figure 4. 3: LULC Change maps

Table 4.2 below summarises the area change statistics (in km²) for each land cover class across different intervals. Farmland shows the most significant increase, while woodland and wetland show the greatest declines. Built-up classes, though smaller in total extent, demonstrate a high rate of growth during the analysed interval; these patterns show a clear trajectory of land-use change in the Manafwa River Basin.

The continued expansion of built-up and farmland LULC classes at the expense of natural vegetation may have hydrological consequences, including reduced infiltration, increased surface runoff, and altered river discharge dynamics. These findings provide a critical input to the following sections on hydrological modelling and the assessment of river discharge responses to changing LULC and climatic conditions.

Table 4. 2: Area change statistics

AREA CHANGE STATISTICS (km^2)				
	2010	2020	2030	2040
Built-up	0.09	0.95	2.51	6.19
Wetland	-9.59	-12.05	-17.78	-18.77
Farmland	13.20	29.67	41.96	41.23
Tropical forest	-0.19	-2.43	-5.42	-7.23
woodland	-2.34	-12.98	-18.02	-18.05
Grassland	-1.16	-3.14	-3.24	-3.36

Figure 4.4 below summarises the direction of change for the different LULC classes in the Manafwa river basin over the study period of 2000-2040.

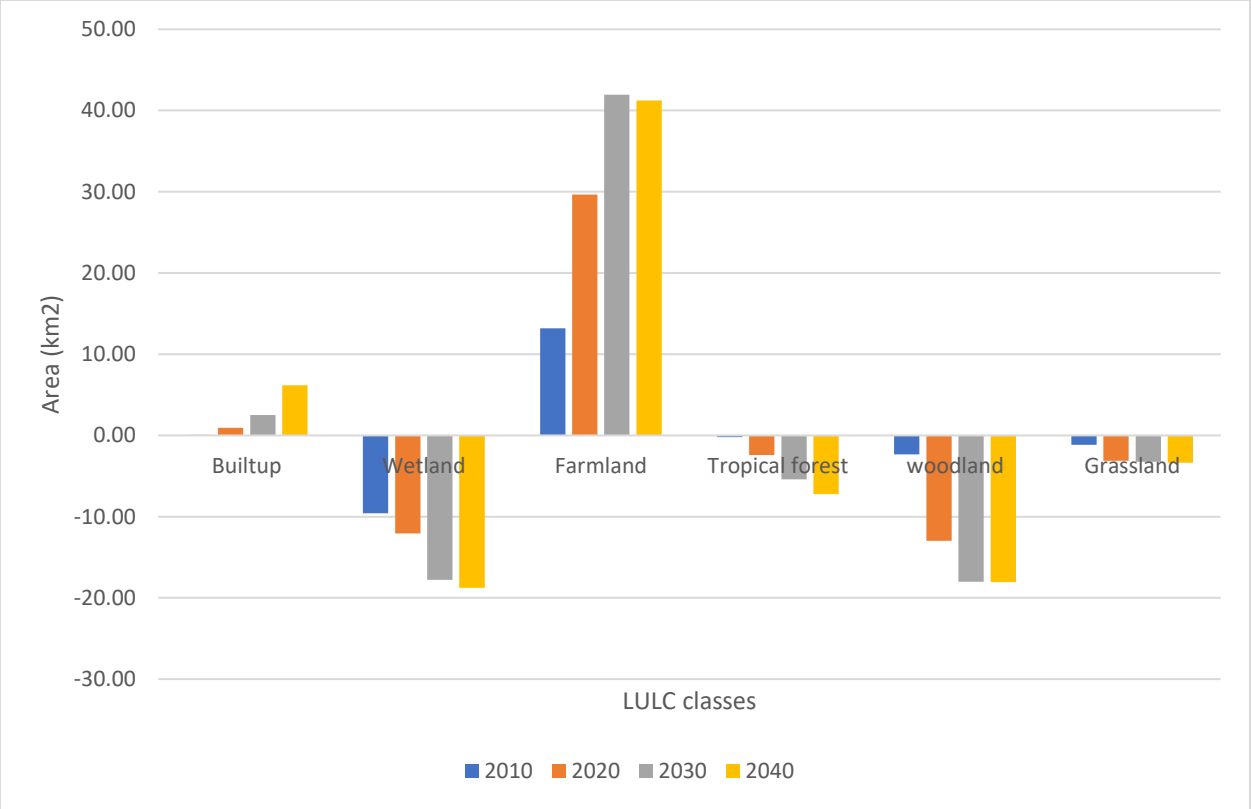

Figure 4. 4: Comparative bar graph showing direction

Tables 4.3, 4.4, 4.5, and 4.6 present the land-use/land-cover transition matrices for the years 2000**,** 2010, 2020, 2030, and 2040, respectively. The matrices show the probabilities with which the different LULC classes were converted from one class to another over time, with the most dominant transitions being from wetland and woodland to farmland, indicating the conversion of natural land cover to human-governed land cover.

During the 20-year interval, the farmland and built-up classes had high probabilities of expansion, particularly in the basin's middle and lower zones. These zones were originally wetland and woodland classes, which were later replaced. Therefore, change detection shows that conversion from LULC classes to farmland in the basin is high; however, even though built-up is not dominant at the moment, the probability of conversion to built-up is high, especially in the subsequent years.

Table 4. 3: Transition matrix 2000 to 2010

	Built-up	Wetland	Farmland	Tropical forest	woodland	Grassland
Built-up	1	0	0	0	0	0
Wetland	0.00	0.22	0.64	0.04	0.08	0.02
Farmland	0.00	0.11	0.73	0.04	0.10	0.02
Tropical forest	0.00	0.01	0.09	0.70	0.17	0.04
woodland	0.00	0.04	0.47	0.11	0.36	0.01
Grassland	0.00	0.04	0.29	0.13	0.21	0.33

During the 2000 to 2020 span, the magnitude of these conversions increased as farmland and built-up areas continued to expand relative to 2000 (base year); all these conversions occurred at the expense of natural vegetation, as depicted in the transition matrix below.

Table 4. 4: Transition matrix 2000 to 2020

	Built-up	Wetland	Farmland	Tropical forest	woodland	Grassland
Built-up	1	0	0	0	0	0
Wetland	0.01	0.18	0.77	0.02	0.02	0.003
Farmland	0.02	0.07	0.85	0.03	0.04	0.002
Tropical forest	0.00	0.02	0.18	0.66	0.13	0.010
woodland	0.00	0.03	0.85	0.07	0.05	0.002
Grassland	0.01	0.03	0.49	0.17	0.05	0.245

A considerable portion of natural vegetation cover, which was lost to farmland and built-up areas, accounted for approximately 200.51 km^2 (30.61%) of the basin, this is clearly depicted in the transition matrix below (2000-2030)

Table 4. 5: Transition matrix 2000 to 2030

		2000-2030				
	Built-up	Wetland	Farmland	Tropical forest	woodland	Grassland
Built-up	1	0	0	0	0	0
Wetland	0.01	0.18	0.77	0.02	0.02	0.00
Farmland	0.02	0.07	0.85	0.03	0.04	0.00
Tropical forest	0.00	0.02	0.18	0.66	0.13	0.01
woodland	0.00	0.03	0.85	0.07	0.05	0.00
Grassland	0.01	0.03	0.49	0.17	0.05	0.24

Table 4. 6: Transition matrix 2000 to 2040

		2000-2040				
	Built-up	Wetland	Farmland	Tropical forest	Woodland	Grassland
Built-up	1	0	0	0	0	0
Wetland	0.01	0.25	0.70	0.02	0.02	0.00
Farmland	0.01	0.07	0.86	0.03	0.02	0.00
Tropical forest	0.00	0.02	0.26	0.62	0.09	0.01
Woodland	0.00	0.04	0.71	0.11	0.14	0.00
Grassland	0.01	0.04	0.32	0.26	0.02	0.36

The transition matrices revealed that wetland and woodland are the most dynamic land cover classes, with high probabilities of conversion to farmland and built-up areas. This pattern therefore suggests that human activities, mainly urbanisation and agriculture, are the main drivers influencing future LULC distribution in the Manafwa Basin.

4.3 Examining the Influence of both Land Use/Land Cover Changes and Climate Change on River Manafwa's Discharge

4.3.1 Observed Discharge Characteristics (1983 -2022)

Discharge data for the historical period (1983–2022) was analysed, enabling the establishment of baseline hydrological behaviour, specifically the mean monthly discharge and the maximum and minimum monthly discharge within the Manafwa River basin. Figure 4.5 below shows the mean monthly discharge, reflecting the basin's characteristic flow patterns under historical climate and land cover conditions. The results indicate a pronounced bimodal flow regime, with significant peaks in April-May and September-November, corresponding to the long and short rainy seasons. The highest flows occur in May, with mean monthly discharge reaching approximately 14.09 m^3/s, while a secondary peak is observed in October at about 8.83 m^3/s. Contrary, dry season months (December – February and June – August) record significantly lower flows, with minimum discharge values dropping to 3.23 m^3/s in January. This analysis shows that the discharge of the Manafwa river basin is mainly governed by seasonal rainfall patterns, with distinct differences between wet and dry periods. Therefore, these baseline conditions provide a reference against which the impacts of land use/land cover and climate change are assessed in subsequent sections.

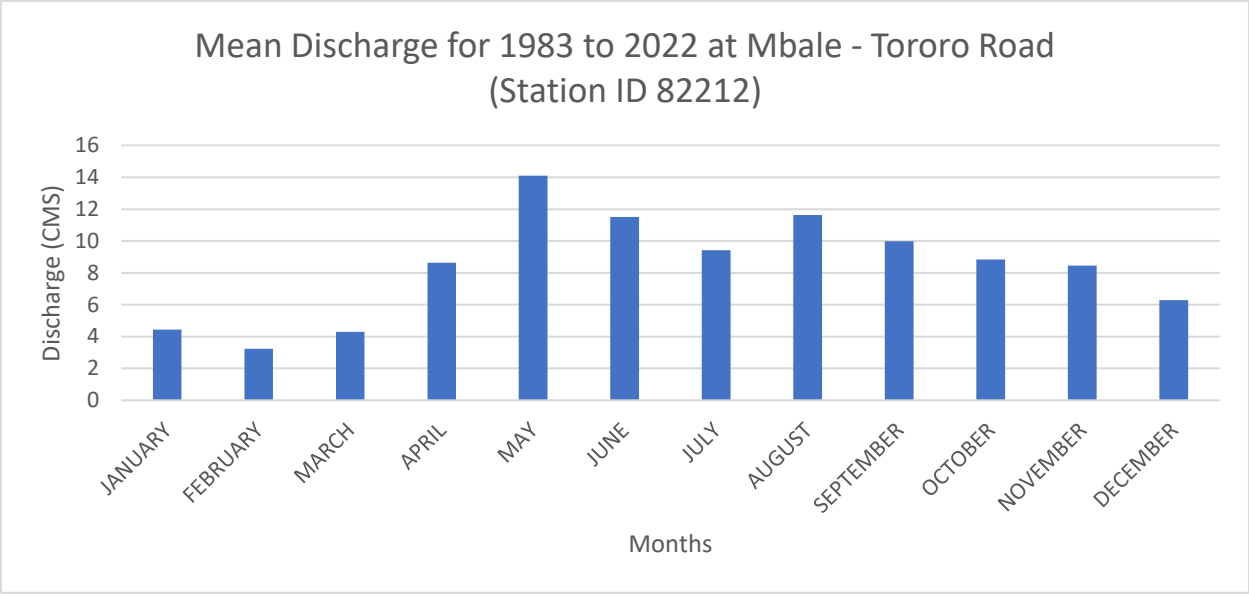

Figure 4. 5: Mean observed discharge (insitu)

4.3.2 Model Calibration Results

The model was calibrated using monthly stream flow data derived from daily data obtained from the Manafwa gauging station (ID: 82212). Model performance was evaluated using Nash-Sutcliffe Efficiency (NSE), Coefficient of Determination (R^2), and the root mean square error. Table 4.7 summarises the model calibration performance statistics.

Table 4. 7: Performance statistics of model calibration

PARAMETERS	CALIBRATION (1990-2015)
NSE	0.79
R2	0.78
RMSE	1.76

The SWAT model demonstrated a strong performance during the calibration period, with a Nash Sutcliffe Efficiency (NSE) of 0.79, a coefficient of determination (R^2) of 0.78, and a Root Mean Square Error (RMSE) of 1.76 mm/day. According to the model evaluation guidelines by Moriasi et al., (2007) & Arnold et al., (2012), NSE values above 0.75 and R^2 values exceeding 0.70 indicate good model performance for monthly stream flow simulation.

Figure 4.6 compares observed and simulated monthly discharge during calibration.

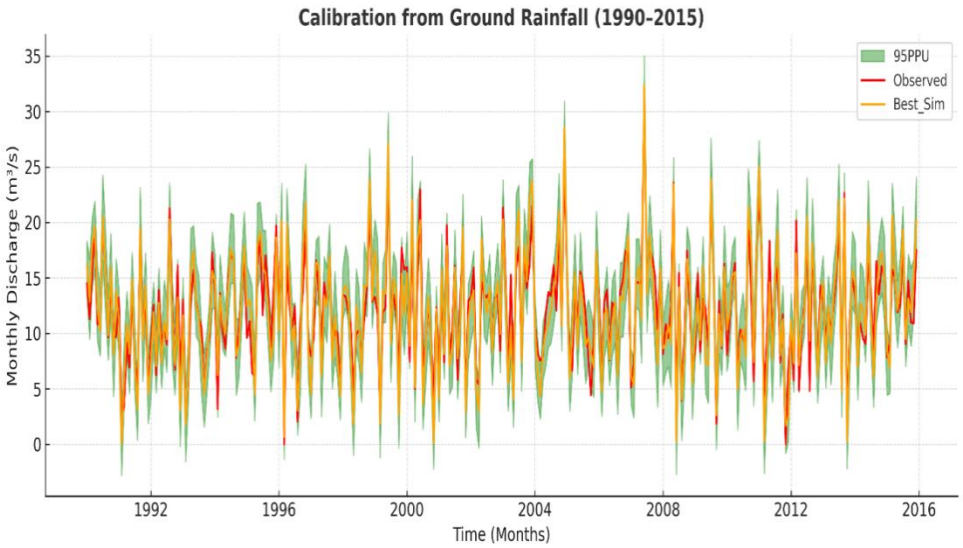

Figure 4. 6: Calibration

Figure 4.6 above presents the 95% Prediction Uncertainty plot (95PPU) for monthly discharge during the calibration period (1990–2015) at the Manafwa gauging station (ID: 82212), using the 2000 land-use scenario. The shaded region represents the uncertainty band, while the observed and simulated stream flow hydrographs are shown for comparison. The graph indicates that the majority of observed stream flow values fall within the 95PPU band, suggesting that the calibrated model captures hydrological process uncertainty reasonably well.

The Fitted parameter values of the study are summarized in the table below 4.8.

Table 4. 8: Top sensitive parameters

No.	Parameter Name	Definition	Fitted value	Min value	Max value	t-stat
1	R__CN2.mgt	Initial SCS runoff curve number for moisture condition II	-0.24	-0.4	0.2	0.53
2	V__ALPHA_BF.gw	Baseflow alpha factor (days)	1.52	1.04	1.55	0.09
3	V__GW_DELAY.gw	Groundwater delay time (days)	35.26	-50.05	98.83	17.11
4	V__GWQMN.gw	Threshold depth of water in the shallow aquifer	-0.63	-0.77	0.12	-0.54
5	R__LAT_SED.hru	Sediment concentration in lateral and groundwater flow (mg/L)	59.56	43.68	74.52	-0.96
6	R__SOL_AWC(..).sol	Available water capacity of the soil layer (mm/mm)	-0.3	-0.49	-0.06	-0.44
7	R__CH_K2.rte	Effective hydraulic conductivity in main channel alluvium (mm/h)	46.8	1.07	62.45	-1.53
8	R__CH_N2.rte	Manning's "n" value for the main channel	0.05	0.05	0.12	0.55
9	R__ESCO.hru	Soil evaporation compensation factor	-0.04	-0.05	0.5	0.15
10	R__OV_N.hru	Manning's "n" value for overland flow	16.04	6.49	16.88	0.56
11	R__SURLAG.bsn	Surface runoff lag coefficient	15.19	12.34	17.29	0.91
12	R__RCHRG_DP.gw	Deep aquifer percolation factor	1.29	0.92	1.42	0.1
13	R__GW_REVAP.gw	Groundwater "revap" coefficient	0.47	0.28	0.76	1.72
14	R__SOL_K(..).sol	Saturated hydraulic conductivity (mm/h)	3.37	3.06	5.81	-2.94

The sensitivity analysis revealed that GW_DELAY.gw is the most sensitive parameter affecting stream flow simulation in the Manafwa River Basin, followed by GW_REVAP.gw and SURLAG.bsn. Other parameters with notable sensitivity included SOL_K.sol**,** OV_N.hru**,** CH_K2.rte**,** ALPHA_BF.gw**,** SOL_AWC.sol**,** LAT_SED.hru**,** and GWQMN.gw. The results suggest that both surface runoff generation and groundwater response processes play significant roles in controlling stream flow variations in the basin.

4.3.3 Model Validation

The model was validated using monthly stream flow data (2016 to 2022) derived from daily data obtained from the Manafwa gauging station (ID: 82212). Model performance was evaluated using Nash-Sutcliffe Efficiency (NSE), Coefficient of Determination (R^2), and the root mean square error. Table 4.9 summarises the model validation performance statistics.

Table 4. 9: Performance statistics of the model validation

PARAMETERS	VALIDATION (2016-2022)
NSE	0.77
R^2	0.76
RMSE	2.41

The model validation statistics obtained were NSE of 0.77, R^2 of 0.76, and RMSE of 2.41 mm/day, indicating that the SWAT model maintained a strong performance when applied to an independent dataset for the 2016–2022 period. Even though the statistics are slightly lower than those obtained during calibration (NSE = 0.79, R^2 = 0.78), they still fall within the performance thresholds defined by Moriasi et al. (2007) for satisfactory monthly stream flow simulation. The consistency between calibration and validation outcomes confirms the model's ability to reliably simulate stream flow dynamics in the Manafwa River Basin. It therefore supports its use in further scenario-based simulations under changing land-use and climate conditions.

Figure 4.7 illustrate the comparison between observed and simulated monthly discharge during the validation.

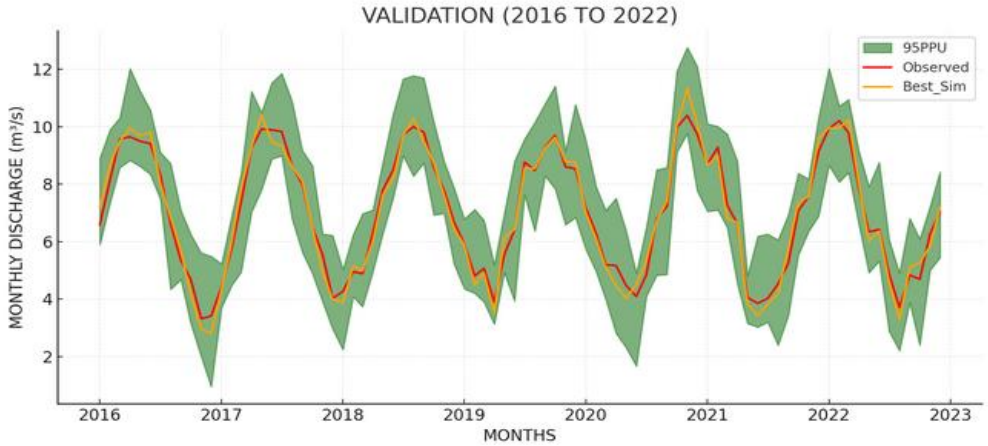

Figure 4. 7: Validation

Figure 4.7 presents the 95% Prediction Uncertainty plot (95PPU) for the monthly discharge during the validation period (2016–2022) at the Manafwa gauging station (ID: 82212). The shaded region represents the uncertainty band, while the observed and simulated stream flow hydrographs are shown in different colours, as indicated in the legend, for easy comparison. Based on sensitivity analysis and statistical evaluation after calibration and validation, the SWAT model demonstrates sufficient predictive applicability for scenario analysis. Therefore, the fitted values obtained during calibration are used in subsequent sections to simulate the impacts of LULC and climate change on river discharge in both historical and projected timeframes.

4.4 Impacts of Land Use/Land Cover Change on River Discharge with Constant Climate.

Table 4.10 presents the simulated mean discharge values under different land-use scenarios, based on fixed climate data (1983 to 2022).

Table 4. 10: Mean discharge

LULC	MEAN DISCHARGE(CMS)
LULC 2000	12.70421212
LULC 2010	12.78748485
LULC 2020	12.99675253
LULC 2030	13.04559848
LULC 2040	13.2752

The results show an upward trend in stream flow as land cover changes from mainly natural vegetation to more farmland and built-up areas. The mean discharge increased from 12.70421 m^3/s under the baseline scenario to 12.78748 m^3/s for LULC 2010, 12.99675 m3/s for LULC 2020, 13.0456 m3/s for LULC 2030 and 13.0752 m^3/s for LULC 2040 in the 2040 scenario, reflecting a consistent rise of approximately 2.92% over the 40-year land use change time. The above is illustrated in Figure 4.8 below.

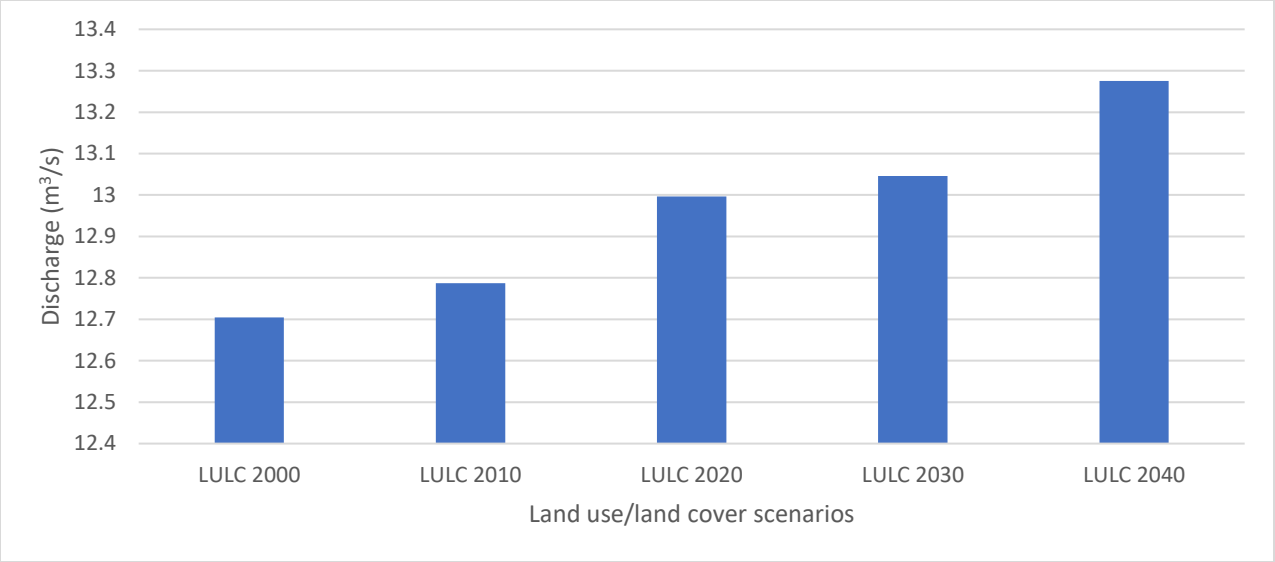

Figure 4. 8: Mean discharge under different LULC Scenarios

For maximum monthly discharge, a similar trend was observed as discharge increased from 19.48 m³/s to 20.66 m³/s when the LULC of 2040 was used, indicating a growing intensity of peak flow events under future LULC conditions. On the other hand, the minimum monthly discharge showed a decreasing trend, declining from 6.235 **m³/s** during the baseline period to 6.162 **m³/s** under the projected LULC of 2040. The above results relate directly to reduced soil water retention, low baseflow contribution, and faster depletion of catchment moisture reserves during dry months. This, therefore, means that during dry months, discharge will decrease to levels not experienced in the river basin, calling for controlled water storage by humans living in and near the watershed. These variations therefore demonstrate that land use and land cover change in the Manafwa River Basin significantly influence not only the average discharge volume but also the occurrence of hydrological extremes, clearly demonstrating the catchment's sensitivity to land use and cover changes, even under constant climatic conditions. Table 4.11 and Figure 4.9 below summarise the discharge statistics as explained above.

Table 4. 11: Discharge Results under Different LULC Scenarios

LULC Scenario	Year	Max Monthly (m^3/s)	Month (year)	Min Monthly (m^3/s)	Month (year)
LULC 2000	2000	19.48	November (1994)	6.235	August (2015)
LULC 2010	2010	19.68	November (1994)	6.229	August (2015)
LULC 2020	2020	20.34	November (1994)	6.261	August (2015)
LULC 2030	2030	20.56	November (1994)	6.227	August (2015)
LULC 2040	2040	20.66	November (1994)	6.162	August (2015)

Figure 4.9 provides a comparison of Monthly Discharge Metrics under Baseline and LULC Scenarios (2010, 2020, 2030 and 2040) with climate held constant (1983 to 2022). The figure shows increase in mean and maximum discharge and a decline in minimum discharge as land use/land cover shifts from natural vegetation to more farmland and built-up areas.

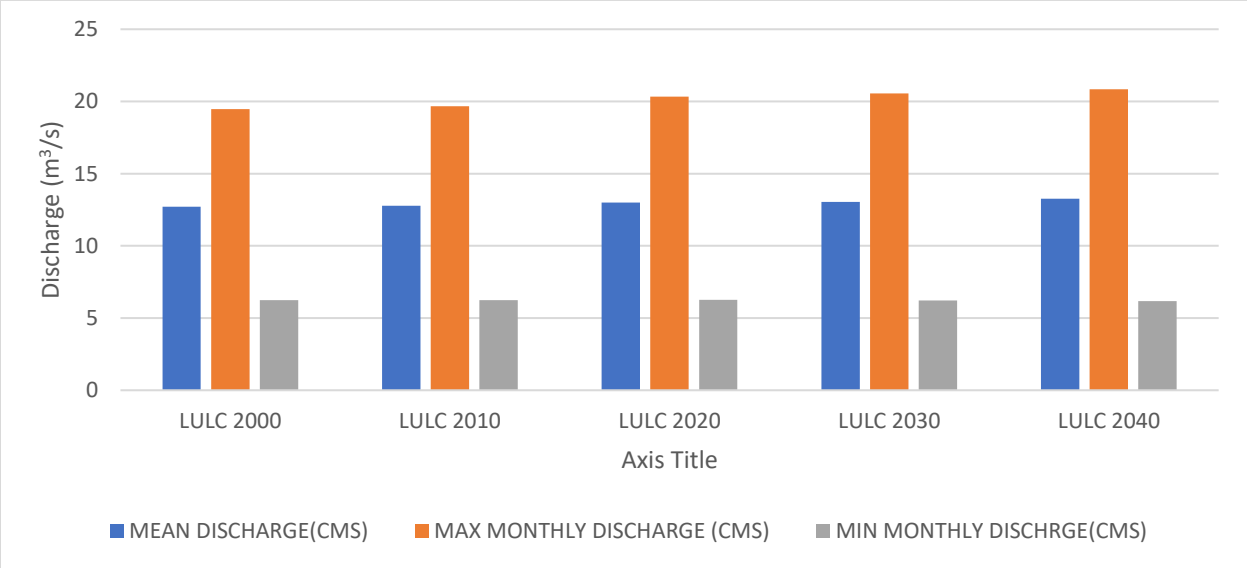

Figure 4. 9: Monthly discharge statistics under LULC change

4.5 Impact of Climate Change on River Discharge with Constant LULC.

Using the downscaled CMIP6 climate models UKESM1-0-LL, GFDL-ESM4, and GFDL-CM4, climate projection data were obtained for stations within, around, and virtual within the Manafwa

River Basin. These datasets provided future climate inputs for both SSPs, enabling the simulation of river discharge under a constant land-use/land-cover (LULC) scenario, thereby isolating the influence of climate change on river discharge variations.

4.5.2 Discharge Results under Future Climate Scenarios

Discharge outputs were evaluated in terms of mean**,** maximum monthly, and minimum monthly discharge for each period. Table 4.12 presents the simulated mean, maximum, and minimum monthly discharge values for the baseline period (1983-2022) and two future climate periods (1983-2030 and 1983-2040), using a fixed land-use/land-cover scenario for 2000. Results are shown for both SSP2-4.5 and SSP5-8.5 climate pathways. The mean discharge shows a progressive increase from 12.70 **m³/s** during the baseline to 14.01 **m³/s** and 14.45 **m³/s** for the 1983-2030 and 1983-2040 projections, respectively. Maximum monthly discharge under SSP2-4.5 increased from 19.48 **m³/s** in November 1994 to 19.78 m^3/s in October 2027 and 20.122 **m³/s** in October 2038. Under SSP5-8.5, the maximum discharge increased to 20.01 m3/s in November 2030 and 24.86 **m³/s** in September 2038. Minimum monthly discharge values also increased across future periods, under SSP2-4.5. Minimum discharge increased from 6.235 m^3/s in August 2015 to 6.64 **m³/s** in April 2026 and 6.87 m^3/s in April 2029. While under SSP5-8.5, an increment is observed from 6.31 **m³/s** in April 2028 (1983 to 2030) to 6.507 **m³/s** in April 2030 (1983 - 2040). These results reflect increasing hydrological variability under projected climate conditions.

Table 4. 12: Discharge results under future climate scenarios

			LULC 2000		
Year	Mean Monthly (m^3/s)	Max Monthly (m^3/s)-SSP2-4.5	Max Monthly (m^3/s)-SSP5-8.5	Min Monthly (m^3/s)-SSP2-4.5	Min Monthly (m^3/s)-SSP5-8.5
baseline	12.70	19.48 November 1994	-	6.235 August 2015	-
1990-2030	14.01	19.78 October 2027	20.01 November 2030	6.64 April 2026	6.31 April (2028)
1990-2040	14.45	20.122 October 2038	24.86 September 2038	6.87 April 2029	6.507 April (2030)

Figure 4.10 below compares simulated mean, maximum, and minimum monthly discharge under SSP2-4.5 and SSP5-8.5 climate scenarios, which were a result of using fixed land use/land cover from the year 2000. The Results indicate a steady increase in mean and peak discharge, and an increment in minimum flow values across future periods, reflecting enhanced hydrological extremes driven by climate change.

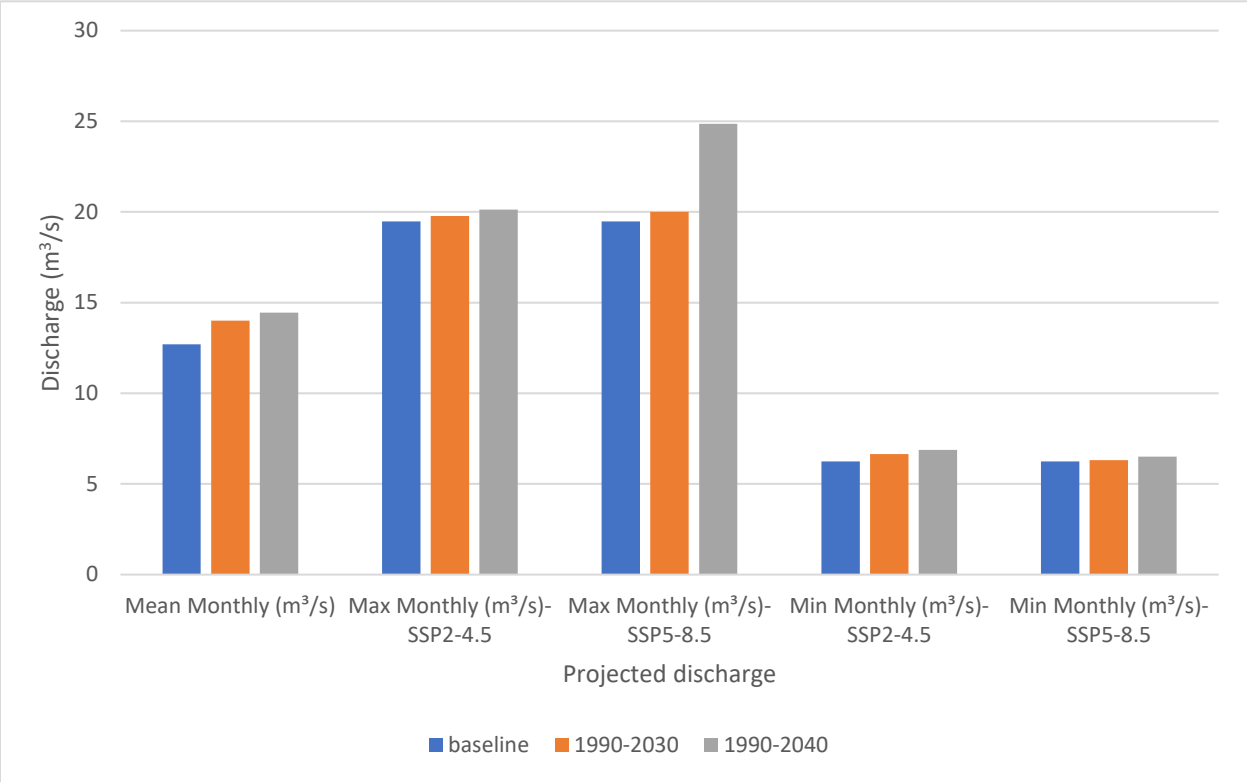

Figure 4. 10: SWAT simulated discharge trends under future climate scenarios with constant LULC

4.6 Relationship Between LULC Change, Climate Change and River Discharge

The water balance ratios presented in Table 4.13 were obtained from the SWAT model generated during scenario simulations under different land use/land cover (LULC) and climate conditions. These ratios provide an overview of how simulated changes in land cover and climate affect the hydrological components of the Manafwa River Basin. They represent the relative contribution of each hydrological component stream flow, baseflow, surface runoff, percolation, deep recharge, and evapotranspiration (ET) to the total water balance of the basin.

Table 4. 13: Water balance ratios

Climate/land use land cover scenario	Streamflow	Baseflow	Surface runoff	percolation	Deep recharge	ET
LULC2000	0.04	0.98	0.02	0.39	0.5	0.61
LULC2010	0.04	0.98	0.02	0.42	0.55	0.55
LULC2020	0.04	0.97	0.03	0.44	0.57	0.53
LULC2030	0.04	0.95	0.05	0.46	0.59	0.5
LULC2040	0.05	0.89	0.11	0.45	0.58	0.5
Future climate ssp5 (lulc2000)	0.04	0.98	0.02	0.41	0.53	0.57
Future climate ssp2 (lulc2000)	0.04	0.98	0.02	0.41	0.53	0.57

A Pearson correlation analysis was conducted to evaluate the relationship between land use/land cover (LULC) classes and river discharge characteristics, namely mean, maximum, and minimum discharge. The analysis quantifies the degree and direction of the relationship between changes in LULC classes and stream flow characteristics within the river Basin. A positive correlation coefficient (r) indicates that an increase in a given LULC class corresponds to an increase in a given characteristic. However, a negative correlation coefficient means that an increase in a given class corresponds to a reduction in a given discharge characteristic; on the other hand, a reduction in a given LULC class can also correspond to an increase in a given discharge characteristic.

Table 4. 14: Pearson correlation coefficients

LULC CLASS	(r) MEAN DISCHARGE	(r) MAX DISCHARGE	(r) MIN DISCHARGE
Built-up	0.90	0.76	-0.94
Wetland	-0.90	-0.93	0.58
Farmland	0.92	0.99	-0.50
Tropical forest	-0.95	-0.92	0.78
Woodland	-0.92	-1.00	0.49
Grassland	-0.90	-0.98	0.38

As shown in Table 4.14, built-up and farmland classes exhibit strong positive correlations with mean and maximum discharge, with correlation coefficients ranging from 0.76 to 0.99. This indicates that expansion of these land use categories increases surface runoff, thereby increasing stream flow magnitude. However, natural vegetation classes such as forest, woodland, grassland, and wetland show strong negative correlations with both mean and maximum discharge (r values ranging from –0.9 to –1). These negative correlation coefficients indicate that natural vegetated areas play a critical role in reducing surface runoff by improving infiltration, interception, and evapotranspiration.

Interestingly, natural vegetation classes display weak to moderate positive correlations with minimum discharge. For instance, tropical forests ($r = 0.78$) and wetlands ($r = 0.58$) are positively associated with baseflows, suggesting that they help sustain low-flow conditions during dry periods. However, built-up and farmland areas are negatively correlated with minimum discharge, reflecting their limited capacity to store and slowly release water into the river system.

A compound bar graph below visualises the correlation coefficients between each LULC class and discharge variables by presenting the direction and strength of each relationship.

In relation to Figure 4.11, built-up and farmland classes show strong positive correlations with both mean and maximum discharge. This suggests that built-up and farmland expansions amplify surface runoff and increase peak flow conditions. However, forest, woodland, and wetland areas show strong negative correlations with these discharge parameters, indicating their hydrological importance in mitigating or preventing flow extremes. For minimum discharge, the trend is reversed, with natural vegetation maintaining a positive relationship, highlighting its role in regulating subsurface flow and maintaining hydrological equilibrium.

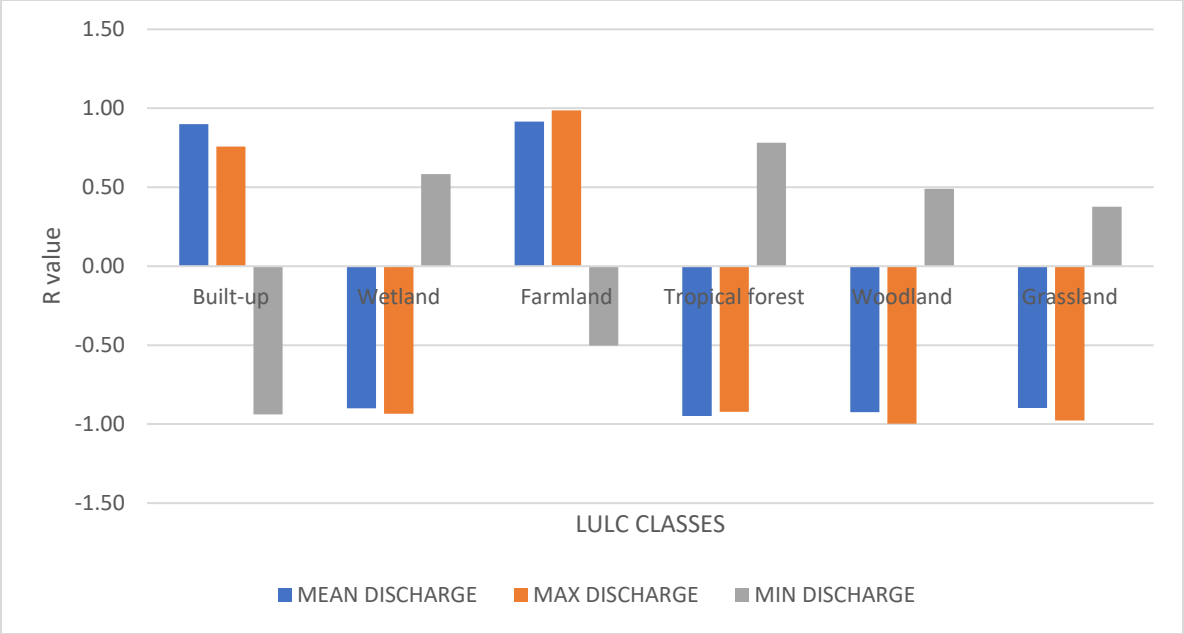

Figure 4. 11: Pearson's correlation

This graphical representation reinforces the statistical findings, providing a more precise visual interpretation of how different land cover types influence the flow regime of the Manafwa River Basin.

CHAPTER FIVE: DISCUSSION OF RESULTS

5.1 Introduction

This chapter discusses the findings of the study by interpreting the results presented in Chapter Four in relation to the study objectives and existing literature. The discussion examines the spatial and temporal patterns of land use/land cover (LULC) change, and the individual influence of climate and land use/land cover change scenarios on discharge variations in the Manafwa River Basin. By examining the results, this study aims to contribute to the knowledge and practical applications of the SWAT model, GCMs, and LULC variations in watershed management and disaster risk preparedness and adaptation.

5.2 Land Use/Land Cover Change

The results indicate that land use/land cover in the Manafwa River Basin underwent significant transformations between 2000 and 2040, with clear trends of natural vegetation loss and rapid expansion of farmland and built-up areas. Across all temporal intervals, the wetland class experienced the highest reduction, mainly due to encroachment by farmland and, to a lesser extent, built-up areas.

During the period from 2000 to 2010, 9.95% of the total area covered by wetlands was converted solely to farmland. This occurred mainly in the middle and lower sections of the basin, as these zones are characterised by gentle slopes that favour agriculture. This increase is likely driven by the expansion of the Doho rice scheme, which aims to increase agricultural output by incorporating outside farmers to meet rising demand. Similarly, woodland declined steadily, with 2.34% of its total area lost to farmland and built-up areas between 2000 and 2010, and 18.05% lost over the subsequent three decades. Such conversion patterns highlight the continued encroachment targeting the basin's natural vegetation, especially in the lower and middle subbasins. Woodland and grassland also declined, especially in the mid and high elevation areas of the basin; the reduction was mainly from woodland to farmland. The area covered by farmland increased from 263.6 km^2 in 2000 to 533.8 km^2 by 2040, which is three times the area coverage in 2000. These findings therefore conform with those of Erima et al. (2022) in the

manafwa basin for years 1995, 2008 and 2018, who found a similar pattern of LULC changes in the Manafwa river basin.

In contrast, farmland and built-up areas consistently expanded; farmland remained the dominant land use class, growing from 262.69 km^2 in 2000 to 533.8 km^2 in 2040, while built-up areas increased from 0.3 km^2 to 40.9 km^2 over the same period. The above shifts highlight persistent changes, particularly in natural vegetation classes, primarily driven by agricultural expansion and population growth. This trend further confirms the findings of recent land-use studies in tropical Africa (Erima et al., 2022; Kayitesi et al., 2022; Turyahabwe, 2019).

Percentage analysis of land cover revealed that farmland rose from 40.05% in 2000 to 70.38% by 2020, while wetland cover declined from 19.6% to 7.53% by 2020, indicating an overall 18 % loss in the wetland alone. The above pattern explains the government's intensified efforts to protect wetlands by reinforcing strict regulations to safeguard them. Tropical forests, grasslands, and woodlands similarly decreased by 3.57%, 6.35%, and 2.07%, respectively, at the expense of farmland and built-up areas, confirming an overall shift away from natural vegetation to human-induced landscapes. To a large extent, these findings are in agreement with those of Admas et al. (2024), Aigner et al. (2023), Mukasa et al. (2020), and Turyahabwe. (2019). During their studies, they emphasised the need to control agricultural expansion due to weak enforcement of land regulations specifically against wetlands. Besides that, the rising population creates high demand for food, which has consequently altered land cover change in East African catchments. Population growth in the Manafwa Basin is estimated at 3.4% annually since the 2024 population census (Uganda Bureau of Statistics, 2024), intensifying land pressure.

Furthermore, the presence and continued expansion of the Doho Rice Scheme, which has more than 10,000 outside local farmers, accelerated natural land cover conversion for agricultural use. Therefore, the spatial analysis shows that wetland degradation is concentrated in river floodplains, while forest loss is more evident in the upper catchment, particularly along gentle slopes, which favour agriculture. In woodland and grassland, the transition pattern reveals gradual conversion in mid-zone subbasins, leading to farmland or Built-up areas. Such zones are among those that are favourable to agriculture and human settlement.

The findings under Objective One confirm that the basin is undergoing rapid transformation, characterized by a decline in natural vegetation, driven by increased agricultural practices due to

high population growth and weak policy enforcement to protect the green belts. The above patterns are not in isolation but align with findings from a recent regional study by Noel & Heil (2024), who highlighted declining ecosystem services and altered hydrological responses in tropical watersheds.

5.3 Impact of Land Use/Land Cover Change on River Discharge

The influence of land use/land cover (LULC) change on river discharge within the Manafwa River Basin was assessed by utilizing land cover across four-time horizons: 2000, 2010, 2020, 2030, and 2040, while holding climate conditions constant (1983-2022). This enabled quantification of the hydrological response to LULC changes alone, thereby providing clarity on how current and projected LULC transformations are affecting stream flow behaviour over time. The results show a progressive increase in mean discharge from 12.70 m^3/s during the baseline period to 12.79, 12.996, 13.04, and 13.275 m^3/s for LULC in 2010, 2020, 2030, and 2040, respectively, reflecting a 4.48% increase over four decades. This rise is attributed to the conversion of natural vegetation namely wetlands, forests, and grasslands into farmland and built-up areas. It should be noted that clearing natural vegetation to replace it with crops affects several hydrological processes in the watershed, including rainfall interception.

According to Zhong et al., (2022), planted crops are characterized with less interception of rainfall, so in seasons where there is heavy rainfall, much of the rainfall will not be intercepted, thus falling directly on ground, when the ground becomes saturated, runoff will take place thereby contributing to increment in stream flow, this finding is supported by the findings of researchers Cooper, (2010) & Lin et al., (2020), who found out that the interception fraction falls with increasing event size/intensity, this therefore means that heavy rainfall is directly proportionally to more through fall.

Besides that, farming activities, such as ploughing, especially in the lower subbasins where the doho irrigation scheme is located, lead to soil compaction and reduced infiltration, making soils more prone to saturation. During rainfall, most of it does not infiltrate into the soil but flows as runoff, thereby contributing to incremental stream flow over time. Therefore, as natural vegetation, characterized by higher infiltration and evapotranspiration capacities, is replaced with modified cover and built-up areas, which are known for low infiltration, reduced evaporation,

and reduced evapotranspiration, an increase in surface runoff is inevitable and becomes the dominant hydrological pathway (Guzha et al., 2018). Consequently, not only did average flow increase, but peak discharges also do, from 19.48 m^3/s in 2000 to 19.68, 20.34, 20.56 and 20.66 m^3/s in 2010, 2020, 2030 and 2040. This points towards an escalating risk of hydrological extremes, specifically floods in the catchment, based on the findings of recent regional studies by Guzha et al. (2018) and Okoth et al. (2024), which link LULC change to increased floods in tropical highland watersheds.

Minimum monthly discharge showed a declining trend, with discharge reducing from 6.235 m3/s in the baseline year to 6.229, 6.261, 6.227 and 6.162 m3/s by 2040. This decline highlights deterioration in baseflow conditions, increased evapotranspiration rates, and changes in soil moisture depletion and storage. All resulting from reduced groundwater recharge due to soil sealing, wetland loss, and forest reduction (Atharinafi & Wijaya, 2021; Taye et al., 2019; Turyahabwe, 2019). The declining baseflow conditions also reflect an increasing dominance of surface conditions, pointing to low discharge and water availability during dry seasons, an outcome with profound implications for downstream agriculture and ecosystems. The timing of the maximum and minimum monthly discharges remained unchanged relative to Uganda's seasonal climate distribution across all LULC scenarios. Peak flows occurred in November, corresponding to the second rainy season (SON). On the other hand, the lowest flows were observed in August, which aligns with the second dry season (JJA)**.** This seasonal consistency was not a surprise, as LULC mainly influences the magnitude and partitioning of flow rather than seasonal timing, which is strongly governed by climate.

The spatial pattern of land cover conversion within the basin was directly proportional to changes in discharge. Lower subbasins, which were initially dominated by wetlands and grasslands, underwent extensive transformation into farmland and built up. This transformation has altered runoff generation zones, leading to faster and more concentrated flow. Similarly, for the upper subbasins, the conversion of forests and woodlands to farmland reduced infiltration and increased surface runoff, exacerbating peak flows downstream. Therefore, LULC change in the Manafwa River Basin significantly alters stream flow behaviour, increasing both average and peak discharges while reducing minimum flow. Given that farmland dominates the basin, hydrological simulation results confirm that land-use/land-cover changes, particularly farmland

and built-up areas play a crucial role in amplifying hydrological extremes. Therefore, if current trends continue, future LULC distributions may further destabilize the basin's water regime, affecting both ecological stability and water security. As such, integrated watershed planning that balances development with ecosystem conservation, especially wetlands, is essential to safeguarding the hydrological integrity of the Manafwa Basin and other similar tropical watersheds.

5.4 Impact of Climate Change on River Discharge

The hydrological response of the Manafwa River Basin to projected climate changes was analyzed by simulating discharge under two shared socioeconomic pathways: SSP2-4.5 and SSP5-8.5. This analysis covered the periods from 1983 to 2030 and from 1983 to 2040, while keeping land use and land cover constant at the calibrated state from 2000. This approach helped isolate the effects of climatic factors, allowing for a direct attribution of stream flow variability to future climate change. The results indicate a consistent increase in discharge under both scenarios, with the mean discharge rising from 12.70 m^3/s during the baseline period to 14.01 m^3/s in 2030 and 14.45 m^3/s in 2040. A similar pattern was observed under the SSP5-8.5 scenario, demonstrating that climate change alone can significantly intensify discharge from the basin. This finding aligns with recent research by Kayitesi et al. (2022), which noted climate-driven discharge amplification in tropical highland basins across East Africa.

Beyond the average discharge, the simulations also revealed an upward trend in peak monthly discharge, with maximum monthly discharge increasing from 19.48 m^3/s in November 1994 during the baseline period to 19.78 m^3/s in October 2027 and 20.122 m^3/s in October 2038 under SSP2-4.5. A similar trend was still observed under SSP5-8.5, where the highest discharge occurs slightly later, reaching 20.01 m^3/s in November 2030 and 24.86 m^3/s in September 2038, respectively. The above is consistent with the findings of Alfieri et al. (2016), who found that maximum discharges were increasing under climate change. These increases in peak discharge are a clear signal of elevated flood risks, particularly under high-emissions scenarios, and clearly show the need for enhanced flood preparedness across the basin.

On the other hand, minimum monthly flows show a steady increase across future climate scenarios, with discharge increasing from 6.235 m^3/s during the baseline to 6.64 m^3/s and 6.87 m^3/s under SSP2-4.5, and further to 6.31 m^3/s and 6.507 m^3/s under SSP5-8.5 in the years

2028 and 2030, respectively. Notably, the lowest flows observed under SSP5-8.5 indicate climatic scenarios with high temperatures; this results in higher evaporation and evapotranspiration rates, which, in turn, reduce the amount of water flowing out of the basin. These findings align with Onyutha's (2024) conclusions, which emphasize that rising temperatures and intensified evapotranspiration under high-emission pathways suppress baseflow generation and groundwater recharge, particularly during dry months.

Collectively, these findings confirm that climate change, particularly under high-emission scenarios, significantly alters the basin's discharge regime more than LULC change. However the above is contrary with findings of a study by Han et al. (2024) which was carried out on the upper basin of the Tarim River in Northwest China, in his study, Land cover change was the dominant driver to discharge in the river, this however differs from the direction of our research as he specifically looked at the upper reaches on the river while our study looked at the whole watershed of the Manafwa river, this is most likely what brought about the difference. Therefore, according to the findings, the maximum and minimum flows will increase existing vulnerabilities in the Manafwa Basin, thereby calling for integrated water resources management that anticipates hydrological instability under future climate trajectories.

5.5 Relationship Between Land Use/Land Cover Change and River Discharge

The results revealed that human made land use land cover classes, particularly farmland and built-up, exhibit strong positive correlations with mean and maximum discharge, and negative correlations with minimum discharge. In contrast, natural vegetation classes such as forest, woodland, wetland, and grassland display strong negative correlations with mean and peak flows but moderate positive correlations with minimum flows. These relationships are consistent with the hydrological theory, which explains that converting vegetated land surfaces to agricultural or built environments reduces infiltration capacity, increases overland flow, and accelerates rainfall–runoff response times (Huang, 2022). In contrast, intact vegetation enhances infiltration, evapotranspiration, and soil water storage, thereby supporting sustained baseflows even during dry periods (Brookfield et al., 2023).

The SWAT-simulated water balance ratios further confirm these patterns. As land use and cover changed from 2000 to 2040, the surface runoff component increased markedly from

approximately 0.02 to 0.11 while the baseflow ratio declined from 0.98 to 0.89. This shift indicates a progressive transition toward a "flashier" catchment, where a larger proportion of rainfall contributes directly to stream flow rather than percolating into groundwater or being lost through evapotranspiration. The strong positive correlation ($r \geq 0.90$) between farmland coverage and both mean and maximum discharge can thus be interpreted as a hydrological consequence of intensified runoff generation driven by the expansion of cultivated land.

However, the negative correlation between built-up and farmland classes and minimum discharge suggests that these land uses reduce the basin's ability to sustain groundwater baseflows, a finding consistent with earlier observations that vegetation removal leads to lower dry-season flows (Alger et al., 2021).

These findings align closely with studies conducted in other tropical and subtropical catchments. For example, a review about East African basins reported that forest loss was associated with a ~16 ± 5.5% increase in annual stream flow and a ~45 ± 14% increase in surface runoff (Alger et al., 2021). Similarly, in the Upper Paraná Basin of Brazil, conversion of forest to agriculture increased annual discharge by approximately 28% under comparable climatic conditions (Zeferino et al., 2021). In China, H. Liu et al. (2025) found that land-use change specifically urbanisation strongly modified hydrological regimes such as peak flows and flow duration, with topography acting as a moderating factor. These studies collectively support the finding that land-cover change often exerts a stronger control on hydrological alteration than short-term climate variability.

Within the Manafwa River Basin, SWAT-simulated water balance ratios under future climate scenarios (with constant LULC) showed relatively minor changes compared with LULC-only scenarios. This outcome reinforces the argument that climate change remains the dominant driver of hydrological change in the near to mid-term future. However, the basin's evolving land use/ land cover changes, marked by agricultural expansion and urban growth, appear to have a more immediate impact on stream flow magnitude and variability than projected climate shifts. Consequently, effective catchment management should integrate land-use planning, vegetation restoration, and conservation strategies as complementary measures to climate adaptation initiatives.

5.6 Implications of the Findings, and Future Research

The results of this study provide valuable insights into the changing hydrological behaviour of the Manafwa River Basin and highlight broader implications for the following: watershed management, regional hydrological modelling, and scientific knowledge in the tropics. According to the findings, there is a clear indication that both land use/land cover (LULC) and climate change influence river discharge, thereby highlighting the need to adopt integrated modelling frameworks in watershed management. The observed increase in mean, maximum and minimum discharge suggests a transition towards a chaotic hydrological regime, characterized by increased magnitudes of flood and drought risk. This is consistent with climate projections across East African watersheds (Gelete et al., 2020; Onyutha, 2024; Regasa & Nones, 2023).

From a watershed management perspective, the deterioration of wetlands, forests and grasslands highlights the need for targeted conservation and restoration efforts, particularly in the middle and lower subbasins since natural vegetation cover plays a critical role in flow regulation, sediment retention, and baseflow maintenance. Therefore, continued loss will exacerbate hydrological extremes, increase sediment loads and threaten the long-term sustainability of the watershed's water supply. The findings therefore advocate mainstreaming land-use regulation and climate-resilient planning into local development policies, especially in areas undergoing rapid agricultural and urban expansion, such as Manafwa District.

In hydrological research, this study reinforces the use of process-based models such as SWAT to capture the complex interactions between land cover dynamics and climate variability. However, it also highlights the importance of high-resolution spatial data, calibrated inputs and the need for future studies to explore more temporal and spatial scenarios, including socioeconomic projections, groundwater surface water interactions, and feedback loops under extreme events. Furthermore, the application of NEX-GDDP-CMIP6, which is bias corrected, presents a replicable methodology for future climate impact research in data-scarce tropical basins; such contributions not only enrich the body of hydrology with knowledge but also serve as a model for similar studies all over the world, where land cover transformation and climate change are occurring concurrently and rapidly.

5.7 Strengths and limitations of the study

Investigating land use/land cover and climate change, using the separation method provides a straightforward approach to understanding both specific and combined impacts on river discharge. This approach addresses a significant gap in previous hydrological assessments, which often consider these drivers in isolation. Secondly, using a calibrated and validated SWAT model supported by statistically evaluated performance metrics (NSE > 0.75, R^2 > 0.76) ensures robust simulation of stream flow under historical and future scenarios. Third, the incorporation of NEX-GDDP-CMIP6 climate projections, which are already downscaled, reflects best practices in regional climate modelling and positions the study within the most current global climate research framework. Finally, the LULC projections up to 2040, derived using TerrSet software, add a valuable long-term planning dimension to the study and support scenario-based decision-making.

Although the study has several strengths, it also presents some limitations. First, the use of satellite imagery and observed stream flow data, which had many poses, posed a significant challenge. Since calibration and validation processes are critical for ensuring model accuracy, these gaps may have negatively impacted the model's reliability. Additionally, the SWAT model assumes homogeneous conditions within sub-basins in the projected future, which may not accurately reflect reality.

Furthermore, the study relies on an ensemble of three General Circulation Models (GCMs) from the NEX-GDDP-CMIP6 project for climate projections. However, incorporating an ensemble of more than three GCMs could offer a broader range of possible climate futures. Lastly, the study did not include socioeconomic factors, such as land tenure and policy enforcement, which play a significant role in land-use and land-cover (LULC) changes; this omission may affect the accuracy of future LULC projections.

CHAPTER SIX: CONCLUSION AND RECOMMENDATIONS

6.1 Introduction

This chapter provides an overview of the key findings derived from the investigation of land use/land cover and climate change impacts on river discharge in the Manafwa River Basin. It revisits the study objectives, summarizes significant results, and draws relevant conclusions. Finally, it contains recommendations to inform watershed management, climate resilience planning, and future hydrological research.

6.2 Conclusion

The Manafwa Basin experienced extensive natural vegetation reduction with wetland, forest, and grassland declining by 18.77%, 7.23%, and 3.36%, respectively over the 2000 to 2040 study time, while farmland and built-up areas increased by 41.23% and 6.19% respectively. These transformations were spatially concentrated in mid and low lying subbasins, where wetlands, woodland and grasslands were mainly located.

While holding climate constant, LULC change alone led to a 4.49% increase in mean discharge and a rise in maximum flow from 19.48 m^3/s to 20.66 m^3/s, which accounts for 6.06% between 2000 and 2040, while minimum flows generally declined by 1.17%, reaching as low as 6.162 m^3/s using the 2040 LULC. These trends highlight reduced infiltration and increased surface runoff due to natural vegetation loss.

Under SSP2-4.5 and SSP5-8.5 scenarios, climate change alone increased mean discharge to 14.45 m^3/s by 2040, which translates into 13.78%. Maximum flow increased from 19.48 m^3/s to 20.122 m^3/s, which accounts for 3.29% between 2000 and 2040 under SSP2, and 10.18% for minimum monthly discharge under SSP2. Under SSP5, maximum flow increased from 19.48 m^3/s to 24.86 m^3/s by 2040, translating into 27.62%, while minimum monthly discharge increased from 6.235m^3/s to 6.507 m^3/s, translating into an increase of 4.36%, particularly under the high emission scenario. The above, point towards amplified hydrological extremes under future climatic conditions. It should be noted that both LULC and climate change contribute to increased discharge variability, reduced baseflow, and greater flood risk.

6.3 Recommendations

Based on the findings of this study, the following recommendations are proposed to support watershed management and disaster preparedness in the Manafwa River Basin and similar tropical catchments:

The study recommends that future flood vulnerability and risk assessments integrate both projected land use/land cover (LULC) and climate change scenarios to improve the accuracy of hydrological forecasts and guide adaptive planning. Strengthening this integration will enhance the design of climate resilient infrastructure, support proactive disaster mitigation strategies, and improve decision-making in watershed management.

Given the observed rise in surface runoff and discharge variability primarily driven by wetland degradation and loss of natural vegetation, there is an urgent need for ecosystem restoration. Priority should be placed on promoting agroforestry, reforestation in upland catchments, and targeted wetland rehabilitation to enhance infiltration, stabilize baseflows, and minimize flood severity.

Furthermore, climate resilience should be mainstreamed within district, sub-county, and watershed-level planning frameworks through both structural interventions (such as retention basins and embankments) and non-structural measures, including flood early warning systems, risk-sensitive land-use zoning, and community preparedness programs. Finally, improved hydrological modelling requires long-term, high-resolution spatial and climatic datasets; therefore, investment in localized monitoring infrastructure particularly rainfall stations, stream flow gauges, and real-time data is strongly recommended. Strengthening data collection systems will significantly improve model calibration and validation, thereby increasing the reliability and scientific credibility of future hydrological projections and flood risk assessments.

6.4 Directions for Future Research

Future research should aim to extend the modelling period to the end of the century. This will provide deeper insights into long-term hydrological shifts and offer a more strategic planning basis for infrastructure and ecosystem management. Given that agriculture is the dominant LULC in the study area, future research should examine how specific crop types influence evapotranspiration and runoff dynamics under projected climatic conditions.

The study focused on investigating the impacts on Stream flow alone; however, other components, such as water quality, sedimentation, and nitrogen levels in the basin, should also be investigated. This will offer a more comprehensive perspective on the watershed. Basing on the results, an assessment of the spatial extent and functional integrity of the existing buffers along rivers and lakes under projected environmental changes should be conducted. It will help inform adaptive land-use policies and conservation zoning, and increase individuals' resilience and adaptive capacity to extreme hydrological events. Future research can also explore advanced techniques, such as the Modified Empirical Budyko Method, which allows for nonlinear attribution of climate and land-use effects, compared to the separation method, which assumes linearity, this may yield more insights.

Employing multiple hydrological models, such as MIKE SHE, TOPMODEL, GR4J, and others, is necessary to improve the robustness of results and reduce model uncertainty when assessing the impacts of land use/land cover and climate change on river discharge. Since the Manafwa river basin is medium-sized, further research should be carried out on large basin watersheds, where more complex socio-ecological systems influence land-use dynamics and hydrological responses.

References

2023-global-natural-disaster-assessment-report.pdf. (2023).

Abbas, M., Atangana Njock, P. G., & Wang, Y. (2022). Influence of Climate Change and Land-Use Alteration on Water Resources in Multan, Pakistan. *Applied Sciences (Switzerland)*, *12*(10). https://doi.org/10.3390/app12105210

Abbas, T., Nabi, G., Hussain, F., & Faisal, M. (2015). Impacts of Landuse Changes on Runoff Generation in Simly Impacts of Landuse Changes on Runoff Generation in Simly. *ResearchGate*, *January*, 1–9.

Admas, M., Melesse, A. M., & Tegegne, G. (2024). Predicting the Impacts of Land Use/Cover and Climate Changes on Water and Sediment Flows in the Megech Watershed, Upper Blue Nile Basin. *Remote Sensing*, *16*(13). https://doi.org/10.3390/rs16132385

Ahmad, Z., Hafeez, M., & Ahmad, I. (2012). Hydrology of mountainous areas in the upper Indus Basin, Northern Pakistan with the perspective of climate change. *Environmental Monitoring and Assessment*, *184*(9), 5255–5274. https://doi.org/10.1007/s10661-011-2337-7

Aigner, E., Görg, C., Krisch, A., Madner, V., Muhar, A., Novy, A., Posch, A., Steininger, K. W., Bohunovsky, L., Essletzbichler, J., Fischer, K., Frey, H., Haas, W., Haderer, M., Hofbauer, J., Hollaus, B., Jany, A., Keller, L., Kubeczko, K., … Wieser, H. (2023). Technical Summary. *APCC Special Report: Strukturen Für Ein Klimafreundliches Leben*, 105–170. https://doi.org/10.1007/978-3-662-66497-1_4

Akpoti, K., Velpuri, N. M., Mizukami, N., Kagone, S., Leh, M., Mekonnen, K., Owusu, A., Tinonetsana, P., Phiri, M., Madushanka, L., Perera, T., Prabhath, P. T., Parrish, G. E. L., Senay, G. B., & Seid, A. (2024). Advancing water security in Africa with new high-resolution discharge data. *Scientific Data*, *11*(1), 1195. https://doi.org/10.1038/s41597-024-04034-0

Alfieri, L., Feyen, L., & Di Baldassarre, G. (2016). Increasing flood risk under climate change: a pan-European assessment of the benefits of four adaptation strategies. *Climatic Change*, *136*(3), 507–521. https://doi.org/10.1007/s10584-016-1641-1

Alger, M., Lane, B. A., & Neilson, B. T. (2021). Combined influences of irrigation diversions and associated subsurface return flows on river temperature in a semi-arid region. *Hydrological Processes*, *35*(8), e14283. https://doi.org/https://doi.org/10.1002/hyp.14283

Alshari, E. A., Abdulkareem, M. B., & Gawali, B. W. (2023). Classification of land use/land

cover using artificial intelligence (ANN-RF). *Frontiers in Artificial Intelligence*, *Volume 5*-. https://doi.org/10.3389/frai.2022.964279

Anand, V., & Oinam, B. (2020). *Future climate change impact on hydrological regime of river basin using SWAT model*. *5*(4), 471–484. https://doi.org/10.22034/gjesm.2019.04.07

Anderson, B. J., Brunner, M. I., Slater, L. J., & Dadson, S. J. (2024). Elasticity curves describe stream flow sensitivity to precipitation across the entire flow distribution. *Hydrology and Earth System Sciences*, *28*(7), 1567–1583. https://doi.org/10.5194/hess-28-1567-2024

Anderson, E., Hill, S., Nixon, R., Abbott, B., Lee, R., Wood, R., Carling, G., Hopkins, B., Corson-Dosch, H., Nell, C., & Bailey, E. (2024). Water cycle processes [poster]. *General Information Product*, *March*, 3531. https://scispace.com/papers/water-cycle-processes-poster-12opyvhl6b

Arnell, N. (n.d.).

Arnell, N. W., & Gosling, S. N. (2013). The impacts of climate change on river flow regimes at the global scale. *Journal of Hydrology*, *486*, 351–364. https://doi.org/10.1016/j.jhydrol.2013.02.010

Arnold, J. G., Srinivasan, R., Muttiah, R. S., & Williams, J. R. (1998). Large area hydrologic modeling and assessment part I: Model development. In *Journal of the American Water Resources Association* (Vol. 34, Issue 1, pp. 73–89). https://doi.org/10.1111/j.1752-1688.1998.tb05961.x

Assessing the Effects of Land Use Changes on Floods in the Meuse and Oder Catchment. (n.d.).

Atharinafi, Z., & Wijaya, N. (2021). Land use change and its impacts on surface runoff in rural areas of the upper citarum watershed (case study: Cirasea subwatershed). *Journal of Regional and City Planning*, *32*(1), 36–55. https://doi.org/10.5614/jpwk.2021.32.1.3

Atkinson, H. D. E., Johal, P., Falworth, M. S., Ranawat, V. S., Dala-Ali, B., & Martin, D. K. (2010). Adductor tenotomy: Its role in the management of sports-related chronic groin pain. *Archives of Orthopaedic and Trauma Surgery*, *130*(8), 965–970. https://doi.org/10.1007/s00402-009-1032-4

Attique, R., Rientjes, T., & Booij, M. (2023). Comparison between statistical and dynamical downscaling of rainfall over the Gwadar-Ormara basin, Pakistan. *Meteorological Applications*, *30*(5), 1–19. https://doi.org/10.1002/met.2151

Awasthi, C., Vogel, R. M., & Sankarasubramanian, A. (2024). Regionalization of Climate

Elasticity Preserves Dooge's Complementary Relationship. *Water Resources Research*, *60*(10), e2023WR036606. https://doi.org/https://doi.org/10.1029/2023WR036606

Ayele, H. S., Li, M.-H., Tung, C.-P., & Liu, T.-M. (2016). Impact of Climate Change on Runoff in the Gilgel Abbay Watershed, the Upper Blue Nile Basin, Ethiopia. *Water*, *8*(9). https://doi.org/10.3390/w8090380

Ayugi, B., Dike, V., Ngoma, H., Babaousmail, H., Mumo, R., & Ongoma, V. (2021). Future Changes in Precipitation Extremes over East Africa Based on CMIP6 Models. *Water*, *13*(17). https://doi.org/10.3390/w13172358

Babaremu, K., Taiwo, O., & Ajayi, D. (2024). *Impacts of Land Use and Land Cover Changes on Hydrological Response: A Review of Current Understanding and Implications for Watershed and Water Resources Management*. *19*, 256–267. https://doi.org/10.5281/zenodo.10049652#89

Balasubramanian, A. (2017). *PROF . A . BALASUBRAMANIAN Centre for Advanced Studies in Earth Science*. *April*.

Banda, V. D., Dzwairo, R. B., Singh, S. K., & Kanyerere, T. (2022). Hydrological Modelling and Climate Adaptation under Changing Climate: A Review with a Focus in Sub-Saharan Africa. *Water (Switzerland)*, *14*(24), 1–26. https://doi.org/10.3390/w14244031

Bati, H. G., Agumassie, T. A., Tegaye, T. A., & Belete, M. D. (2023). Effects of landscape attributes and climate variables on catchment hydrology. *Environmental Systems Research*, *12*(1), 9. https://doi.org/10.1186/s40068-023-00290-y

Belay, T., Melese, T., & Senamaw, A. (2022). Impacts of land use and land cover change on ecosystem service values in the Afroalpine area of Guna Mountain, Northwest Ethiopia. *Heliyon*, *8*(12). https://doi.org/10.1016/j.heliyon.2022.e12246

Belgiu, M., & Drăguţ, L. (2016). Random forest in remote sensing: A review of applications and future directions. *ISPRS Journal of Photogrammetry and Remote Sensing*, *114*, 24–31. https://doi.org/https://doi.org/10.1016/j.isprsjprs.2016.01.011

Berihun, M. L., Tsunekawa, A., Haregeweyn, N., Tsubo, M., Fenta, A. A., Ebabu, K., Sultan, D., & Dile, Y. T. (2022). Reduced runoff and sediment loss under alternative land capability-based land use and management options in a sub-humid watershed of Ethiopia. *Journal of Hydrology: Regional Studies*, *40*, 100998. https://doi.org/https://doi.org/10.1016/j.ejrh.2022.100998

Bihonegn, B. G., & Awoke, A. G. (2023). Evaluating the impact of land use and land cover changes on sediment yield dynamics in the upper Awash basin, Ethiopia the case of Koka reservoir. *Heliyon*, *9*(12), e23049. https://doi.org/10.1016/j.heliyon.2023.e23049

Bjarke, N. R., Livneh, B., Barsugli, J. J., Pendergrass, A. G., & Small, E. E. (2024). Evaluating Large-Storm Dominance in High-Resolution GCMs and Observations Across the Western Contiguous United States. *Earth's Future*, *12*(6), e2023EF004289. https://doi.org/https://doi.org/10.1029/2023EF004289

Borzì, I. (2025). Modeling Groundwater Resources in Data-Scarce Regions for Sustainable Management: Methodologies and Limits. *Hydrology*, *12*, 11. https://doi.org/10.3390/hydrology12010011

Boursiac, Y., Protto, V., Rishmawi, L., & Maurel, C. (2022). Experimental and conceptual approaches to root water transport. *Plant and Soil*, *478*(1), 349–370. https://doi.org/10.1007/s11104-022-05427-z

Brighenti, T. M., Gassman, P. W., Gutowski, W. J., & Thompson, J. R. (2023). Assessing the Influence of a Bias Correction Method on Future Climate Scenarios Using SWAT as an Impact Model Indicator. *Water*, *15*(4). https://doi.org/10.3390/w15040750

Brookfield, A. E., Ajami, H., Carroll, R. W. H., Tague, C., Sullivan, P. L., & Condon, L. E. (2023). Recent advances in integrated hydrologic models: Integration of new domains. *Journal of Hydrology*, *620*, 129515. https://doi.org/https://doi.org/10.1016/j.jhydrol.2023.129515

Cantoni, E., Tramblay, Y., Grimaldi, S., Salamon, P., Dakhlaoui, H., Dezetter, A., & Thiemig, V. (2022). Hydrological performance of the ERA5 reanalysis for flood modeling in Tunisia with the LISFLOOD and GR4J models. *Journal of Hydrology: Regional Studies*, *42*. https://doi.org/10.1016/j.ejrh.2022.101169

Castino, F., Bookhagen, B., & Strecker, M. R. (2017). Oscillations and trends of river discharge in the southern Central Andes and linkages with climate variability. *Journal of Hydrology*, *555*, 108–124. https://doi.org/https://doi.org/10.1016/j.jhydrol.2017.10.001

Change_ Adaptation of Water Resources Management to Climate Change - Gerardus Johannus Jacobus Bergkamp, Brett Orlando, Ian Burton - Google Books. (n.d.).

Change, I. C. (2021). *The Physical Science Basis Summary for Policymakers Working Group I Contribution to the Sixth Assessment Report of the Intergovernmental Panel on Climate*

Change. IPCC Geneva.

Chawanda, C. J., Nkwasa, A., Thiery, W., & Van Griensven, A. (2024). Combined impacts of climate and land-use change on future water resources in Africa. *Hydrology and Earth System Sciences*, *28*(1), 117–138. https://doi.org/10.5194/hess-28-117-2024

Chen, J., & Chang, H. (2021). Relative impacts of climate change and land cover change on stream flow using swat in the clackamas river Watershed, USA. *Journal of Water and Climate Change*, *12*(5), 1454–1470. https://doi.org/10.2166/wcc.2020.123

Chuenchum, P., Xu, M., & Tang, W. (2020). Predicted trends of soil erosion and sediment yield from future land use and climate change scenarios in the Lancang–Mekong River by using the modified RUSLE model. *International Soil and Water Conservation Research*, *8*(3), 213–227. https://doi.org/https://doi.org/10.1016/j.iswcr.2020.06.006

Cohen, S., Kettner, A. J., & Syvitski, J. P. M. (2014). Global suspended sediment and water discharge dynamics between 1960 and 2010: Continental trends and intra-basin sensitivity. *Global and Planetary Change*, *115*, 44–58. https://doi.org/https://doi.org/10.1016/j.gloplacha.2014.01.011

Cooper, M. (2010). Advanced Bash-Scripting Guide An in-depth exploration of the art of shell scripting Table of Contents. *Okt 2005 Abrufbar Uber Httpwww Tldp OrgLDPabsabsguide Pdf Zugriff 1112 2005*, *2274*(November 2008), 2267–2274. https://doi.org/10.1002/hyp

Costa, M. H., Botta, A., & Cardille, J. A. (2003). Effects of large-scale changes in land cover on the discharge of the Tocantins River, Southeastern Amazonia. *Journal of Hydrology*, *283*(1–4), 206–217. https://doi.org/10.1016/S0022-1694(03)00267-1

Cuxart, J., & Boone, A. A. (2020). Evapotranspiration over Land from a Boundary-Layer Meteorology Perspective. *Boundary-Layer Meteorology*, *177*(2–3), 427–459. https://doi.org/10.1007/s10546-020-00550-9

D. N. Moriasi, J. G. Arnold, M. W. Van Liew, R. L. Bingner, R. D. Harmel, & T. L. Veith. (2007). Model Evaluation Guidelines for Systematic Quantification of Accuracy in Watershed Simulations. *Transactions of the ASABE*, *50*(3), 885–900. https://doi.org/10.13031/2013.23153

Déry, S. J., Stadnyk, T. A., MacDonald, M. K., & Gauli-Sharma, B. (2016). Recent trends and variability in river discharge across \hack{\newline}northern Canada. *Hydrology and Earth System Sciences*, *20*(12), 4801–4818. https://doi.org/10.5194/hess-20-4801-2016

Dibaba, W. T., Demissie, T. A., & Miegel, K. (2020). Watershed Hydrological Response to Combined Land Use/Land Cover and Climate Change in Highland Ethiopia: Finchaa Catchment. In *Water* (Vol. 12, Issue 6). https://doi.org/10.3390/w12061801

Dinku, T., Funk, C., Peterson, P., Maidment, R., Tadesse, T., Gadain, H., & Ceccato, P. (2018). Validation of the CHIRPS satellite rainfall estimates over eastern Africa. *Quarterly Journal of the Royal Meteorological Society*, *144*, 292–312. https://doi.org/10.1002/qj.3244

Easton Z, & Bock E. (2015). *Publication BSE-191P Hydrology Basics and the Hydrologic Cycle*. 1–2. www.ext.vt.edu

Engdaw, F., Fetahi, T., & Kifle, D. (2024). Land use/land cover dynamics in the northern watershed of lake Tana: implications for water quality. *Frontiers in Environmental Science*, *Volume 12*. https://doi.org/10.3389/fenvs.2024.1426789

Erima, G., Gidudu, A., Bamutaze, Y., Egeru, A., & Kabenge, I. (2024). Spatiotemporal Analysis of the Hydrological Responses to Land-Use Land-Cover Changes in the Manafwa Catchment, Eastern Uganda. *Professional Geographer*, *76*(3), 259–276. https://doi.org/10.1080/00330124.2023.2275317

Erima, G., Kabenge, I., Gidudu, A., Bamutaze, Y., & Egeru, A. (2022). Differentiated Spatial-Temporal Flood Vulnerability and Risk Assessment in Lowland Plains in Eastern Uganda. *Hydrology*, *9*(11). https://doi.org/10.3390/hydrology9110201

Escobar, E., & Carvalho-Santos, C. (2022). Impacts of Future Climate on Water Ecosystem Services in the Watershed of the River Homem (Northwest Portugal). *Finisterra*, *57*(120), 125–148. https://doi.org/10.18055/Finis26254

Fernández-Castillo, P., Losada, T., Rodríguez-Fonseca, B., García-Maroto, D., Mohino, E., & Durán, L. (2025). Multidecadal variability of the ENSO early-winter teleconnection to Europe and implications for seasonal forecasting. *Npj Climate and Atmospheric Science*, *8*(1), 272. https://doi.org/10.1038/s41612-025-01160-3

G. Arnold, J., N. Moriasi, D., W. Gassman, P., C. Abbaspour, K., J. White, M., Srinivasan, R., Santhi, C., D. Harmel, R., van Griensven, A., W. Van Liew, M., Kannan, N., & K. Jha, M. (2012). SWAT: Model Use, Calibration, and Validation. *Transactions of the ASABE*, *55*(4), 1491–1508. https://doi.org/https://doi.org/10.13031/2013.42256

Gao, B., Davarzani, H., Helmig, R., & Smits, K. M. (2018). Experimental and Numerical Study of Evaporation From Wavy Surfaces by Coupling Free Flow and Porous Media Flow.

Water Resources Research, *54*(11), 9096–9117. https://doi.org/https://doi.org/10.1029/2018WR023423

Gao, D., Chen, A. S., Marthews, T. R., & Memon, F. A. (2024). *Evaluating future hydrological changes in China under climate change*. *June*, 1–34.

Gashaw, T., Tulu, T., Argaw, M., & Worqlul, A. W. (2018). Modeling the hydrological impacts of land use/land cover changes in the Andassa watershed, Blue Nile Basin, Ethiopia. *Science of the Total Environment*, *619–620*, 1394–1408. https://doi.org/10.1016/j.scitotenv.2017.11.191

Gasirabo, A., Xi, C., Kurban, A., Liu, T., Baligira, H. R., Umuhoza, J., Umugwaneza, A., & Dufatanye Edovia, U. (2023). SWAT model calibration for hydrological modeling using concurrent methods, a case of the Nile Nyabarongo River basin in Rwanda. *Frontiers in Water*, *5*. https://doi.org/10.3389/frwa.2023.1268593

Gebremichael, A., Gebremariam, E., & Desta, H. (2025). Assessment of soil erosion and sediment transport index in the Awash River Basin, Ethiopia: an application of the USLE model and GIS techniques. *Discover Sustainability*, *6*(1), 367. https://doi.org/10.1007/s43621-025-01018-x

Gedamu, G., Mitiku, K. W., Belay, M. A., Simegn, M. B., Chanie, S. D., Tilahun, W. M., Menber, Y., Wasihun, Y., Gebreegziabher, Z. A., Andualem, Z., Alemu, A. T., & Geddif, A. (2025). Barriers to the sustainability of rural water schemes in Sub-Saharan African countries: a systematic review. *Journal of Water, Sanitation and Hygiene for Development*, *15*(5), 427–442. https://doi.org/10.2166/washdev.2025.101

Gelete, G., Gokcekus, H., & Gichamo, T. (2020). Impact of climate change on the hydrology of Blue Nile basin, Ethiopia: A review. *Journal of Water and Climate Change*, *11*(4), 1539–1550. https://doi.org/10.2166/wcc.2019.014

Guerrero, J.-L., Westerberg, I. K., Halldin, S., Xu, C.-Y., & Lundin, L.-C. (2012). Temporal variability in stage–discharge relationships. *Journal of Hydrology*, *446–447*, 90–102. https://doi.org/https://doi.org/10.1016/j.jhydrol.2012.04.031

Guo, J., Su, X., Singh, V. P., & Jin, J. (2016). *Impacts of Climate and Land Use / Cover Change on Stream flow Using SWAT and a Separation Method for the Xiying River Basin in Northwestern China*. 9–13. https://doi.org/10.3390/w8050192

Guzha, A. C., Rufino, M. C., Okoth, S., Jacobs, S., & Nóbrega, R. L. B. (2018). Impacts of land

use and land cover change on surface runoff, discharge and low flows: Evidence from East Africa. *Journal of Hydrology: Regional Studies*, *15*, 49–67. https://doi.org/https://doi.org/10.1016/j.ejrh.2017.11.005

Haider, S., Masood, M. U., Rashid, M., Alshehri, F., Pande, C. B., Katipoğlu, O. M., & Costache, R. (2023). Simulation of the Potential Impacts of Projected Climate and Land Use Change on Runoff under CMIP6 Scenarios. *Water (Switzerland)*, *15*(19). https://doi.org/10.3390/w15193421

Han, Q., Xue, L., Qi, T., Liu, Y., Yang, M., Chu, X., & Liu, S. (2024). *Assessing the Impacts of Future Climate and Land-Use Changes on Stream flow under Multiple Scenarios : A Case Study of the Upper Reaches of the Tarim River in Northwest China*.

Hanks, R. J. (2015). Soil evaporation and transpiration. *Modeling Plant and Soil Systems*, 245–271. https://doi.org/10.2134/agronmonogr31.c11

Hansford, M. R., Plink-Björklund, P., & Jones, E. R. (2020). Global quantitative analyses of river discharge variability and hydrograph shape with respect to climate types. *Earth-Science Reviews*, *200*, 102977. https://doi.org/https://doi.org/10.1016/j.earscirev.2019.102977

Harrigan, S., Zsoter, E., Alfieri, L., Prudhomme, C., Salamon, P., Wetterhall, F., Barnard, C., Cloke, H., & Pappenberger, F. (2020). GloFAS-ERA5 operational global river discharge reanalysis 1979--present. *Earth System Science Data*, *12*(3), 2043–2060. https://doi.org/10.5194/essd-12-2043-2020

Hermassi, T., Jarray, F., Tlili, W., Achour, I., & Mechergui, M. (2025). Integrative hydrologic modelling of soil and water conservation strategies: a SWAT-based evaluation of environmental resilience in the Merguellil watershed, Tunisia. *Frontiers in Water*, *7*(February), 1–15. https://doi.org/10.3389/frwa.2025.1521812

Hodnebrog, Ø., Myhre, G., Samset, B. H., Alterskjær, K., Andrews, T., Boucher, O., Faluvegi, G., Fläschner, D., Forster, P. M., Kasoar, M., Kirkevåg, A., Lamarque, J.-F., Olivié, D., Richardson, T. B., Shawki, D., Shindell, D., Shine, K. P., Stier, P., Takemura, T., … Watson-Parris, D. (2019). Water vapour adjustments and responses differ between climate drivers. *Atmospheric Chemistry and Physics*, *19*(20), 12887–12899. https://doi.org/10.5194/acp-19-12887-2019

Huang, P.-C. (2022). An innovative partition method for predicting shallow landslides by

combining the slope stability analysis with a dynamic neural network model. *CATENA*, *217*, 106480. https://doi.org/https://doi.org/10.1016/j.catena.2022.106480

Hwang, S. N. (2017). The Effect of Land Cover Change on Flooding in Texas. *Journal of Geoscience and Environment Protection*, *05*(09), 123–137. https://doi.org/10.4236/gep.2017.59009

Ibrahim, S. (2023). Improving Land Use/Cover Classification Accuracy from Random Forest Feature Importance Selection Based on Synergistic Use of Sentinel Data and Digital Elevation Model in Agriculturally Dominated Landscape. *Agriculture*, *13*(1). https://doi.org/10.3390/agriculture13010098

Idowu, D., & Zhou, W. (2021). Land use and land cover change assessment in the context of flood hazard in Lagos State, Nigeria. *Water (Switzerland)*, *13*(8). https://doi.org/10.3390/w13081105

ipCC, A. R. (2021). *Climate change 2021*. The physical science Basis.

J. G. Arnold, Kiniry, J. R., Srinivasan, R., Williams, J. R., Haney, E. B., & Neitsch, S. L. (2013). Soil & Water Assessment Tool. Version 2012. *Input/Output Documentation Version 2012*, 654.

Jain, S. K., Mani, P., Jain, S. K., Prakash, P., Singh, V. P., Tullos, D., Kumar, S., Agarwal, S. P., & Dimri, A. P. (2018). A Brief review of flood forecasting techniques and their applications. *International Journal of River Basin Management*, *16*(3), 329–344. https://doi.org/10.1080/15715124.2017.1411920

Jasechko, S. (2019). Global Isotope Hydrogeology—Review. *Reviews of Geophysics*, *57*(3), 835–965. https://doi.org/https://doi.org/10.1029/2018RG000627

Jin, X., & Sridhar, V. (2012). Impacts of Climate Change on Hydrology and Water Resources in the Boise and Spokane River Basins. *JAWRA Journal of the American Water Resources Association*, *48*(2), 197–220. https://doi.org/https://doi.org/10.1111/j.1752-1688.2011.00605.x

Kamusoko, C. (2022). Land Cover Classification Accuracy Assessment. *Springer Geography*, *80*, 105–118. https://doi.org/10.1007/978-981-16-5149-6_6

Kayitesi, N. M., Guzha, A. C., & Mariethoz, G. (2022). Impacts of land use land cover change and climate change on river hydro-morphology- a review of research studies in tropical regions. *Journal of Hydrology*, *615*(PA), 128702.

https://doi.org/10.1016/j.jhydrol.2022.128702

Keller, A. A., Garner, K. L., Rao, N., Knipping, E., & Thomas, J. (2022). Downscaling approaches of climate change projections for watershed modeling: Review of theoretical and practical considerations. *PLOS Water*, *1*(9). https://doi.org/10.1371/journal.pwat.0000046

Khan, S., Bhardwaj, A., & Sakthivel, M. (2024). Accuracy Assessment of Land Use Land Cover Classification Using Machine Learning Classifiers in Google Earth Engine; A Case Study of Jammu District. *The International Archives of the Photogrammetry, Remote Sensing and Spatial Information Sciences*, *XLVIII-4–2024*, 263–268. https://doi.org/10.5194/isprs-archives-XLVIII-4-2024-263-2024

Kimbi, S. B., Onodera, S., Wang, K., Kaihotsu, I., & Shimizu, Y. (2024). Assessing the Impact of Urbanization and Climate Change on Hydrological Processes in a Suburban Catchment. *Environments*, *11*(10). https://doi.org/10.3390/environments11100225

Koch, H., Yangouliba, G. I., & Liersch, S. (2025). From Data Scarcity to Solutions: Hydrological and Water Management Modeling in a Highly Managed River Basin. *Water*, *17*(6). https://doi.org/10.3390/w17060823

Koehler, T., Wankmüller, F. J. P., Sadok, W., & Carminati, A. (2023). Transpiration response to soil drying versus increasing vapor pressure deficit in crops: physical and physiological mechanisms and key plant traits. *Journal of Experimental Botany*, *74*(16), 4789–4807. https://doi.org/10.1093/jxb/erad221

Koutsoyiannis, D. (2020). Revisiting the global hydrological cycle: is it intensifying? *Hydrology and Earth System Sciences*, *24*(8), 3899–3932. https://doi.org/10.5194/hess-24-3899-2020

Koutsoyiannis, D., & Mamassis, N. (2021). From mythology to science: the development of scientific hydrological concepts in Greek antiquity and its relevance to modern hydrology. *Hydrology and Earth System Sciences*, *25*(5), 2419–2444. https://doi.org/10.5194/hess-25-2419-2021

Krysanova, V., Vetter, T., Eisner, S., Huang, S., Pechlivanidis, I., Strauch, M., Gelfan, A., Kumar, R., Aich, V., Arheimer, B., Chamorro, A., Van Griensven, A., Kundu, D., Lobanova, A., Mishra, V., Plötner, S., Reinhardt, J., Seidou, O., Wang, X., … Hattermann, F. F. (2017). Intercomparison of regional-scale hydrological models and climate change impacts projected for 12 large river basins worldwide - A synthesis. *Environmental*

Research Letters, *12*(10). https://doi.org/10.1088/1748-9326/aa8359

Kucuk Matci, D., & Avdan, U. (2020). Optimization-based automated unsupervised classification method: A novel approach. *Expert Systems with Applications*, *160*, 113735. https://doi.org/https://doi.org/10.1016/j.eswa.2020.113735

Lamichhane, S., & Shakya, N. M. (2019). Integrated assessment of climate change and land use change impacts on hydrology in the Kathmandu Valley watershed, Central Nepal. *Water (Switzerland)*, *11*(10). https://doi.org/10.3390/w11102059

Langhammer, J., & Bernsteinová, J. (2025). Attributing the effects of climate change and forest disturbance on runoff using distributed modeling and indicators of hydrological alteration in Central European montane basins. *Journal of Hydrology: Regional Studies*, *57*, 102101. https://doi.org/https://doi.org/10.1016/j.ejrh.2024.102101

Legesse Gebre, S. (2015). Hydrological Response to Climate Change of the Upper Blue Nile River Basin: Based on IPCC Fifth Assessment Report (AR5). *Journal of Climatology & Weather Forecasting*, *03*(01), 1–15. https://doi.org/10.4172/2332-2594.1000121

Legesse Gebre, S., & Getahun, Y. S. (2016). Analysis of Climate Variability and Drought Frequency Events on Limpopo River Basin, South Africa. *Journal of Waste Water Treatment & Analysis*, *7*(3). https://doi.org/10.4172/2157-7587.1000249

Lehner, F., Nadeem, I., & Formayer, H. (2023). Evaluating skills and issues of quantile-based bias adjustment for climate change scenarios. *Advances in Statistical Climatology, Meteorology and Oceanography*, *9*(1), 29–44. https://doi.org/10.5194/ascmo-9-29-2023

Lei, W., Dong, H., Chen, P., Lv, H., Fan, L., & Mei, G. (2020). Study on Runoff and Infiltration for Expansive Soil Slopes in Simulated Rainfall. *Water*, *12*(1). https://doi.org/10.3390/w12010222

Lenderink, G., Buishand, A., & Van Deursen, W. (2007). Estimates of future discharges of the river Rhine using two scenario methodologies: Direct versus delta approach. *Hydrology and Earth System Sciences*, *11*(3), 1145–1159. https://doi.org/10.5194/hess-11-1145-2007

Leta, M. K., Demissie, T. A., & Tränckner, J. (2021). Modeling and prediction of land use land cover change dynamics based on land change modeler (Lcm) in nashe watershed, upper blue nile basin, Ethiopia. *Sustainability (Switzerland)*, *13*(7). https://doi.org/10.3390/su13073740

Li, K., Feng, M., Biswas, A., Su, H., Niu, Y., & Cao, J. (2020). Driving Factors and Future

Prediction of Land Use and Cover Change Based on Satellite Remote Sensing Data by the LCM Model: A Case Study from Gansu Province, China. *Sensors*, *20*(10). https://doi.org/10.3390/s20102757

Lin, M., Sadeghi, S. M. M., & Van Stan, J. T. (2020). Partitioning of Rainfall and Sprinkler-Irrigation by Crop Canopies: A Global Review and Evaluation of Available Research. *Hydrology*, *7*(4). https://doi.org/10.3390/hydrology7040076

Liu, H., Yan, H., & Guan, M. (2025). Evaluating the effects of topography and land use change on hydrological signatures: a comparative study of two adjacent watersheds. *Hydrology and Earth System Sciences*, *29*(8), 2109–2132. https://doi.org/10.5194/hess-29-2109-2025

Liu, Y., Wu, G., Fan, X., Gan, G., Wang, W., & Liu, Y. (2022). Hydrological impacts of land use/cover changes in the Lake Victoria basin. *Ecological Indicators*, *145*(October), 109580. https://doi.org/10.1016/j.ecolind.2022.109580

Lohani, A. K. (2018). Practicing Hydrology-An Overview National Institute of Hydrology. *Practicing Hydrology-An Overview National Institute of Hydrology*.

Londhe, D. S., Katpatal, Y. B., & Bokde, N. D. (2023). Performance Assessment of Bias Correction Methods for Precipitation and Temperature from CMIP5 Model Simulation. *Applied Sciences (Switzerland)*, *13*(16). https://doi.org/10.3390/app13169142

Lukas, P., Melesse, A. M., & Kenea, T. T. (2023). Prediction of Future Land Use/Land Cover Changes Using a Coupled CA-ANN Model in the Upper Omo–Gibe River Basin, Ethiopia. *Remote Sensing*, *15*(4). https://doi.org/10.3390/rs15041148

Mahmoud, S. H., & Alazba, A. A. (2015). Hydrological response to land cover changes and human activities in arid regions using a geographic information system and remote sensing. *PLoS ONE*, *10*(4). https://doi.org/10.1371/journal.pone.0125805

Mahmoud, S. H., Gan, T. Y., Allan, R. P., Li, J., & Funk, C. (2022). Worsening drought of Nile basin under shift in atmospheric circulation, stronger ENSO and Indian Ocean dipole. *Scientific Reports*, *12*(1), 8049. https://doi.org/10.1038/s41598-022-12008-8

Mango, L. M. (2010). *Modeling the Effect of Land Use and Climate Change Scenarios on the Water Flux of the Upper Mara River Flow , Kenya*. https://doi.org/10.25148/etd.FI10041632

Maraun, D., Wetterhall, F., Ireson, A. M., Chandler, R. E., Kendon, E. J., Widmann, M., Brienen, S., Rust, H. W., Sauter, T., Themel, M., Venema, V. K. C., Chun, K. P., Goodess,

C. M., Jones, R. G., Onof, C., Vrac, M., & Thiele-Eich, I. (2010). Precipitation downscaling under climate change: Recent developments to bridge the gap between dynamical models and the end user. *Reviews of Geophysics*, *48*(3), 1–34. https://doi.org/10.1029/2009RG000314

Martini, E., Bauckholt, M., Kögler, S., Kreck, M., Roth, K., Werban, U., Wollschläger, U., & Zacharias, S. (2021). STH-net: A soil monitoring network for process-based hydrological modelling from the pedon to the hillslope scale. *Earth System Science Data*, *13*(6), 2529–2539. https://doi.org/10.5194/essd-13-2529-2021

Matsa, M. M., Dzawanda, B., Mupepi, O., & Hove, J. (2023). Sustainability of donor-funded projects in developing remote minority Tonga communities of Zimbabwe. *Discover Sustainability*, *4*(1), 34. https://doi.org/10.1007/s43621-023-00152-8

Maxwell, A. E., Warner, T. A., & Fang, F. (2018). Implementation of machine-learning classification in remote sensing: an applied review. *International Journal of Remote Sensing*, *39*(9), 2784–2817. https://doi.org/10.1080/01431161.2018.1433343

Meles, M. B., Chen, L., Unkrich, C., Ajami, H., Bradford, S. A., Šimůnek, J., & Goodrich, D. C. (2024). Computationally efficient Watershed-Scale hydrological Modeling: Integrating HYDRUS-1D and KINEROS2 for coupled Surface-Subsurface analysis. *Journal of Hydrology*, *640*(July). https://doi.org/10.1016/j.jhydrol.2024.131621

Melese, S. M. (2016). Effect of Climate Change on Water Resources. *Journal of Water Resources and Ocean Science*, *5*(1), 14–21. https://doi.org/10.11648/j.wros.20160501.12

Mendonça, L. M. De. (2024). *Performance and projections of the NEX-GDDP-CMIP6 in simulating precipitation in the Brazilian Amazon and Cerrado biomes*. *May*, 3726–3741. https://doi.org/10.1002/joc.8547

Mendoza Paz, S., & Willems, P. (2023). The skill of statistical downscaling in future climate with high-resolution climate models as pseudo-reality. *Journal of Hydrology: Regional Studies*, *48*, 101477. https://doi.org/https://doi.org/10.1016/j.ejrh.2023.101477

Mengistu, A. G., van Rensburg, L. D., & Woyessa, Y. E. (2019). Techniques for calibration and validation of SWAT model in data scarce arid and semi-arid catchments in South Africa. *Journal of Hydrology: Regional Studies*, *25*, 100621. https://doi.org/https://doi.org/10.1016/j.ejrh.2019.100621

MIDRC Data Commons. (n.d.). https://data.midrc.org/

Milly, P. C. D., Dunne, K. A., & Vecchia, A. V. (2005). Global pattern of trends in stream flow and water availability in a changing climate. *Nature*, *438*(7066), 347–350. https://doi.org/10.1038/nature04312

Mishra, V., & Lilhare, R. (2016). Hydrologic sensitivity of Indian sub-continental river basins to climate change. *Global and Planetary Change*, *139*, 78–96. https://doi.org/https://doi.org/10.1016/j.gloplacha.2016.01.003

Mubialiwo, A., Onyutha, C., & Abebe, A. (2020). Historical Rainfall and Evapotranspiration Changes over Mpologoma Catchment in Uganda. *Advances in Meteorology*, *2020*(December 2019). https://doi.org/10.1155/2020/8870935

Mukasa, J., Olaka, L., & Said, M. Y. (2020). Drought and households' adaptive capacity to water scarcity in Kasali, Uganda. *Journal of Water and Climate Change*, *11*(S1), 217–232. https://doi.org/10.2166/wcc.2020.012

Mukrimaa, S. S., Nurdyansyah, Fahyuni, E. F., YULIA CITRA, A., Schulz, N. D., د ,غسان., Taniredja, T., Faridli, E. M., & Harmianto, S. (2016). No 主観的健康感を中心とした在宅高齢者における 健康関連指標に関する共分散構造分析Title. *Jurnal Penelitian Pendidikan Guru Sekolah Dasar*, *6*(August), 128.

Müller, L., & Döll, P. (2024). Quantifying and communicating uncertain climate change hazards in participatory climate change adaptation processes. *Geoscience Communication*, *7*(2), 121–144. https://doi.org/10.5194/gc-7-121-2024

Müller, O. V., McGuire, P. C., Vidale, P. L., & Hawkins, E. (2024). River flow in the near future: A global perspective in the context of a high-emission climate change scenario. *Hydrology and Earth System Sciences*, *28*(10), 2179–2201. https://doi.org/10.5194/hess-28-2179-2024

Mutale, B., Withanage, N. C., Mishra, P. K., Shen, J., Abdelrahman, K., & Fnais, M. S. (2024). A performance evaluation of random forest, artificial neural network, and support vector machine learning algorithms to predict spatio-temporal land use-land cover dynamics: a case from lusaka and colombo. *Frontiers in Environmental Science*, *Volume 12*. https://doi.org/10.3389/fenvs.2024.1431645

N. Moriasi, D., G. Arnold, J., W. Van Liew, M., L. Bingner, R., D. Harmel, R., & L. Veith, T. (2007). Model Evaluation Guidelines for Systematic Quantification of Accuracy in Watershed Simulations. *Transactions of the ASABE*, *50*(3), 885–900.

https://doi.org/https://doi.org/10.13031/2013.23153

Nahib, I., Ambarwulan, W., Rahadiati, A., Munajati, S. L., Prihanto, Y., Suryanta, J., Turmudi, T., & Nuswantoro, A. C. (2021). Assessment of the impacts of climate and LULC changes on the water yield in the citarum River Basin, West Java Province, Indonesia. *Sustainability (Switzerland)*, *13*(7). https://doi.org/10.3390/su13073919

Nakkazi, M. T., Sempewo, J. I., Tumutungire, M. D., & Byakatonda, J. (2022). Performance evaluation of CFSR, MERRA-2 and TRMM3B42 data sets in simulating river discharge of data-scarce tropical catchments: a case study of Manafwa, Uganda. *Journal of Water and Climate Change*, *13*(2), 522–541. https://doi.org/10.2166/wcc.2021.174

Nandi, A. (2018). Hydrology. In P. T. Bobrowsky & B. Marker (Eds.), *Encyclopedia of Engineering Geology* (pp. 500–501). Springer International Publishing. https://doi.org/10.1007/978-3-319-73568-9_311

Navarro-Racines, C., Tarapues, J., Thornton, P., Jarvis, A., & Ramirez-Villegas, J. (2020). High-resolution and bias-corrected CMIP5 projections for climate change impact assessments. *Scientific Data*, *7*(1), 1–14. https://doi.org/10.1038/s41597-019-0343-8

Ngoma, H., Wen, W., Ayugi, B., Karim, R., & Ongoma, V. (2021). *Evaluation of precipitation simulations in CMIP6 models over Uganda*. *November 2020*, 4743–4768. https://doi.org/10.1002/joc.7098

Noel, K., & Heil, B. (2024). Land-use land cover changes and their relationship with population and climate in Western Uganda. *Journal of Degraded and Mining Lands Management*, *11*, 6201–6212. https://doi.org/10.15243/jdmlm.2024.114.6201

Nsubuga, F. N. W., Namutebi, E. N., & Nsubuga-Ssenfuma, M. (2014). Water Resources of Uganda: An Assessment and Review. *Journal of Water Resource and Protection*, *06*(14), 1297–1315. https://doi.org/10.4236/jwarp.2014.614120

Okoth, J. M., Otim, D., & Kamalha, E. (2024). *East African Journal of Engineering Distribution of Floods Frequency of Manafwa River , Uganda*. *7*(1), 1–20. https://doi.org/10.37284/eaje.7.1.1670.IEEE

Omay, P. O., Muthama, N. J., Oludhe, C., Kinama, J. M., Artan, G., & Atheru, Z. (2023). Evaluation of CMIP6 historical simulations over IGAD region of Eastern Africa. *Discover Environment*. https://doi.org/10.1007/s44274-023-00012-2

Omay, P. O., Muthama, N. J., Oludhe, C., Kinama, J. M., Artan, G., & Atheru, Z. (2025).

Evaluation of satellite-based rainfall estimates over the IGAD region of Eastern Africa. *Meteorology and Atmospheric Physics*, *137*(2). https://doi.org/10.1007/s00703-025-01068-w

Omondi, B., & Angel, M. (2023). *Effects of climate change on stream flow and nitrate pollution in an agricultural Mediterranean watershed in Northern Spain*. *285*(May), 0–11. https://doi.org/10.1016/j.agwat.2023.108378

Ongoma, V., Chena, H., & Gaoa, C. (2018). Projected changes in mean rainfall and temperature over east Africa based on CMIP5 models. *International Journal of Climatology*, *38*(3), 1375–1392. https://doi.org/10.1002/joc.5252

Onyutha, C. (2024). Climate change impacts on hydrology and water resources in East Africa considering CMIP3, CMIP5, and CMIP6. *Frontiers in Climate*, *6*(October), 1–19. https://doi.org/10.3389/fclim.2024.1453726

Piani, C., Haerter, J. O., & Coppola, E. (2010). Statistical bias correction for daily precipitation in regional climate models over Europe. *Theoretical and Applied Climatology*, *99*(1–2), 187–192. https://doi.org/10.1007/s00704-009-0134-9

Piani, C., Weedon, G. P., Best, M., Gomes, S. M., Viterbo, P., Hagemann, S., & Haerter, J. O. (2010). Statistical bias correction of global simulated daily precipitation and temperature for the application of hydrological models. *Journal of Hydrology*, *395*(3), 199–215. https://doi.org/https://doi.org/10.1016/j.jhydrol.2010.10.024

Pouyan Nejadhashemi A, I. M. (2011). Evaluation of Swat Performance on a Mountainous Watershed in Tropical Africa. *Journal of Waste Water Treatment & Analysis*, *s3*, 1–7. https://doi.org/10.4172/2157-7587.s14-001

Questions, K. (n.d.). *Lecture 9: Evaporation*.

Rainfall, H., & Across, S. (2024). *Record Levels of Flooding in Africa Compounds Stress on Fragile Countries Record Levels of Flooding in Africa Compounds Stress on Fragile Countries*. *mm*, 1–12.

Rech, A., Pacheco, E., Caprario, J., Rech, J. C., & Finotti, A. R. (2022). Low-Impact Development (LID) in Coastal Watersheds: Infiltration Swale Pollutant Transfer in Transitional Tropical/Subtropical Climates. *Water*, *14*(2). https://doi.org/10.3390/w14020238

Reder, A., Fedele, G., Manco, I., & Mercogliano, P. (2025). Estimating pros and cons of

statistical downscaling based on EQM bias adjustment as a complementary method to dynamical downscaling. *Scientific Reports*, *15*(1), 1–22. https://doi.org/10.1038/s41598-024-84527-5

Regasa, M. S., & Nones, M. (2023). SWAT model-based quantification of the impact of land use land cover change on sediment yield in the Fincha watershed, Ethiopia. *Frontiers in Environmental Science*, *11*(September), 1–15. https://doi.org/10.3389/fenvs.2023.1146346

Rezaei, A. R., Ismail, Z. B., Niksokhan, M. H., Ramli, A. H., Sidek, L. M., & Dayarian, M. A. (2019). Investigating the effective factors influencing surface runoff generation in urbacatchments – a review. *Desalination and Water Treatment*, *164*, 276–292. https://doi.org/10.5004/dwt.2019.24359

Rhoads, B. L. (2020). Flow Dynamics in Rivers. *River Dynamics*, *May*, 72–96. https://doi.org/10.1017/9781108164108.004

Rica, C. (2020). 2020 MENDEZ - BIAS CORRECTION METHODS.pdf. *Mdpi*.

Robert, B., & Brown, E. B. (2004). *No 主観的健康感を中心とした在宅高齢者における 健康関連指標に関する共分散構造分析Title* (Issue 1).

Rocha, R., Dias Marinho -Especialista, J., & Ambiental -Fapan, G. (2024). *RCMOS-Revista Científica Multidisciplinar O Saber. ANÁLISE DA INFILTRAÇÃO DE ÁGUA NO SOLO EM DIFERENTES TIPOS DE USO E COBERTURA UTILIZANDO INFILTRÔMETRO DE DUPLO ANEL ANALYSIS OF WATER INFILTRATION IN SOIL UNDER DIFFERENT LAND USE AND COVER TYPES USING A*. *2*, 1–7.

Rodney, L., Fangmeier, D. D., & Elliot, W. J. (2013). Infiltration and Runoff. In *Soil and Water Conservation Engineering Seventh Edition*. https://doi.org/10.13031/swce.2013.5

Scafetta, N. (2024). Impacts and risks of "realistic" global warming projections for the 21st century. *Geoscience Frontiers*, *15*(2), 101774. https://doi.org/https://doi.org/10.1016/j.gsf.2023.101774

Sciuto, L., Vanella, D., Cirelli, G. L., Consoli, S., Licciardello, F., & Longo-Minnolo, G. (2025). Improving runoff estimation in hydrological models using remote sensing and climate data reanalysis in the Dittaino River Basin (Eastern Sicily, Italy). *Journal of Hydrology: Regional Studies*, *60*, 102569. https://doi.org/https://doi.org/10.1016/j.ejrh.2025.102569

Serdeczny, O., Adams, S., Baarsch, F., Coumou, D., Robinson, A., Hare, W., Schaeffer, M., Perrette, M., & Reinhardt, J. (2017). Climate change impacts in Sub-Saharan Africa: from

physical changes to their social repercussions. *Regional Environmental Change*, *17*(6), 1585–1600. https://doi.org/10.1007/s10113-015-0910-2

Sharma, A., Mehrotra, R., & Kusumastuti, C. (2023). Correcting systematic bias in derived hydrologic simulations – Implications for climate change assessments. *Journal of Water and Climate Change*, *14*(7), 2085–2102. https://doi.org/10.2166/wcc.2023.230

Sharma Banjade, S., Rai, N., & Subedi, B. (2024). Comparison of Supervised Classification Algorithms Using a Hyperspectral Image for Land Use/Land Cover Classification. *Environmental Sciences Proceedings*, *29*(1). https://doi.org/10.3390/ECRS2023-16702

Shrestha, B. B. (2019). Approach for analysis of land-cover changes and their impact on flooding regime. *Quaternary*, *2*(3). https://doi.org/10.3390/quat2030027

Simarmata, N., Wikantika, K., Tarigan, T. A., Aldyansyah, M., Tohir, R. K., Fauzi, A. I., & Fauzia, A. R. (2025). Comparison of random forest, gradient tree boosting, and classification and regression trees for mangrove cover change monitoring using Landsat imagery. *The Egyptian Journal of Remote Sensing and Space Sciences*, *28*(1), 138–150. https://doi.org/https://doi.org/10.1016/j.ejrs.2025.02.002

Song, S., & Yan, X. (2022). Evaluation of events of extreme temperature change between neighboring days in CMIP6 models over China. *Theoretical and Applied Climatology*, *150*(1), 53–72. https://doi.org/10.1007/s00704-022-04142-0

Sperna Weiland, F. C., van Beek, L. P. H., Kwadijk, J. C. J., & Bierkens, M. F. P. (2012). Global patterns of change in discharge regimes for 2100. *Hydrology and Earth System Sciences*, *16*(4), 1047–1062. https://doi.org/10.5194/hess-16-1047-2012

Stout, G. E. (1990). Climate and water. In *Eos, Transactions American Geophysical Union* (Vol. 71, Issue 12). https://doi.org/10.1029/90EO00112

Svoboda, J., Štych, P., Laštovička, J., Paluba, D., & Kobliuk, N. (2022). Random Forest Classification of Land Use, Land-Use Change and Forestry (LULUCF) Using Sentinel-2 Data—A Case Study of Czechia. *Remote Sensing*, *14*(5). https://doi.org/10.3390/rs14051189

Talukdar, S., Singha, P., Mahato, S., Shahfahad, Pal, S., Liou, Y.-A., & Rahman, A. (2020). Land-Use Land-Cover Classification by Machine Learning Classifiers for Satellite Observations—A Review. *Remote Sensing*, *12*(7). https://doi.org/10.3390/rs12071135

Tan, M. L., Gassman, P. W., Yang, X., & Haywood, J. (2020). A review of SWAT applications,

performance and future needs for simulation of hydro-climatic extremes. *Advances in Water Resources*, *143*, 103662. https://doi.org/https://doi.org/10.1016/j.advwatres.2020.103662

Tanksali, A., & Soraganvi, V. S. (2021). Assessment of impacts of land use/land cover changes upstream of a dam in a semi-arid watershed using QSWAT. *Modeling Earth Systems and Environment*, *7*(4), 2391–2406. https://doi.org/10.1007/s40808-020-00978-5

Taye, M., Simane, B., F. Zaitchik, B., G. Selassie, Y., & Setegn, S. (2019). Land Use Evaluation over the Jema Watershed, in the Upper Blue Nile River Basin, Northwestern Highlands of Ethiopia. *Land*, *8*(3). https://doi.org/10.3390/land8030050

Terink, W., Hurkmans, R. T. W. L., Torfs, P. J. J. F., & Uijlenhoet, R. (2010). Evaluation of a bias correction method applied to downscaled precipitation and temperature reanalysis data for the Rhine basin. *Hydrology and Earth System Sciences*, *14*(4), 687–703. https://doi.org/10.5194/hess-14-687-2010

Teutschbein, C., & Seibert, J. (2010a). Regional climate models for hydrological impact studies at the catchment scale: a review of recent modeling strategies. *Geography Compass*, *4*(7), 834–860. https://doi.org/10.1111/j.1749-8198.2010.00357.x

Teutschbein, C., & Seibert, J. (2010b). University of Zurich Zurich Open Repository and Archive Regional climate models for hydrological impact studies at the catchment scale : a review of recent modeling strategies Regional Climate Models for Hydrological Impact Studies at the Catchment-Scale. *Geography Compass*, *4*(7), 834–860.

Themeßl, M. J., Gobiet, A., & Heinrich, G. (2012). Empirical-statistical downscaling and error correction of regional climate models and its impact on the climate change signal. *Climatic Change*, *112*(2), 449–468. https://doi.org/10.1007/s10584-011-0224-4

Thiemig, V., de Roo, A., & Gadain, H. (2011). Current status on flood forecasting and early warning in Africa. *International Journal of River Basin Management*, *9*(1), 63–78. https://doi.org/10.1080/15715124.2011.555082

Trenberth, K. E. (2011). Changes in precipitation with climate change. *Climate Research*, *47*(1–2), 123–138. https://doi.org/10.3354/cr00953

Trenberth, K. E., Fasullo, J. T., & Shepherd, T. G. (2015). Attribution of climate extreme events. *Nature Climate Change*, *5*(8), 725–730. https://doi.org/10.1038/nclimate2657

Turco, M., Llasat, M. C., Herrera, S., & Gutiérrez, J. M. (2017). Bias correction and downscaling of future RCM precipitation projections using a MOS-Analog technique. *Journal of*

Geophysical Research: Atmospheres, *122*(5), 2631–2648. https://doi.org/https://doi.org/10.1002/2016JD025724

Turksezer, G. M., Alfieri, Z. I., Feyen, L., & Krausmann, L. (2017). *Climate change and critical infrastructure-floods*. https://doi.org/10.2760/007069

Turner, R. E. (2022). Variability in the discharge of the Mississippi River and tributaries from 1817 to 2020. *PLOS ONE*, *17*(12), 1–18. https://doi.org/10.1371/journal.pone.0276513

Turyahabwe. (2019). *Assessment of Impacts of Land Use Changes on Water Resources of River Mpanga Catchment*.

Uganda Bureau of Statistics. (2024). The National Population and Housing Census 2024 – Final Report - Volume 1 (Main), Kampala, Uganda. *Review of 3D Printing and Potential Red Meat Applications*, *1*(23 February 2021), 1–61. chrome-extension://efaidnbmnnnibpcajpcglclefindmkaj/https://www.ubos.org/wp-content/uploads/2024/12/National-Population-and-Housing-Census-2024-Final-Report-Volume-1-Main.pdf

United Nations Environment Programme. (2020). *Emissions Gap Emissions Gap Report 2020*. https://www.unenvironment.org/interactive/emissions-gap-report/2019/

Velasquez, P., Messmer, M., & Raible, C. C. (2020). A new bias-correction method for precipitation over complex terrain suitable for different climate states: a case study using WRF (version 3.8.1). *Geoscientific Model Development*, *13*(10), 5007–5027. https://doi.org/10.5194/gmd-13-5007-2020

Wamala, F., Gidudu, A., Wanyama, J., Nakawuka, P., Bwambale, E., & Chukalla, A. D. (2023). Assessment of irrigation water distribution using remotely sensed indicators: A case study of Doho Rice Irrigation Scheme, Uganda. *Smart Agricultural Technology*, *4*, 100184. https://doi.org/https://doi.org/10.1016/j.atech.2023.100184

Wang, X., Pang, G., & Yang, M. (2018). Precipitation over the Tibetan Plateau during recent decades: a review based on observations and simulations. *International Journal of Climatology*, *38*(3), 1116–1131. https://doi.org/https://doi.org/10.1002/joc.5246

Wang, Z., & Mountrakis, G. (2023). Accuracy Assessment of Eleven Medium Resolution Global and Regional Land Cover Land Use Products: A Case Study over the Conterminous United States. *Remote Sensing*, *15*(12). https://doi.org/10.3390/rs15123186

WBG. (2021). Climate Risk Country Profile: Uganda. *The World Bank Group*, 36.

www.worldbank.org

Willems, W., Kasper, G., Klotz, P., Stricker, K., & Zimmermann, A. (2016). Mean Daily Discharge and Discharge Variability. In W. Mauser & M. Prasch (Eds.), *Regional Assessment of Global Change Impacts: The Project GLOWA-Danube* (pp. 133–137). Springer International Publishing. https://doi.org/10.1007/978-3-319-16751-0_15

Williams, B. A., Venter, O., Allan, J. R., Atkinson, S. C., Rehbein, J. A., Ward, M., Di Marco, M., Grantham, H. S., Ervin, J., Goetz, S. J., Hansen, A. J., Jantz, P., Pillay, R., Rodríguez-Buriticá, S., Supples, C., Virnig, A. L. S., & Watson, J. E. M. (2020). Change in Terrestrial Human Footprint Drives Continued Loss of Intact Ecosystems. *One Earth*, *3*(3), 371–382. https://doi.org/10.1016/j.oneear.2020.08.009

Woldesenbet, T. A., Elagib, N. A., Ribbe, L., & Heinrich, J. (2017). Hydrological responses to land use/cover changes in the source region of the Upper Blue Nile Basin, Ethiopia. *Science of The Total Environment*, *575*, 724–741. https://doi.org/https://doi.org/10.1016/j.scitotenv.2016.09.124

Wudineh, F. A., Abebe, F., & Assistant, W. (2022). *Land Use and Land Cover Change and Its Impact on Flood Hazard Occurrence in Wabi Shebele River Basin of Ethiopia*. https://doi.org/10.21203/rs.3.rs-2128720/v1

Yang, D., Yang, Y., & Xia, J. (2021). Hydrological cycle and water resources in a changing world: A review. *Geography and Sustainability*, *2*(2), 115–122. https://doi.org/https://doi.org/10.1016/j.geosus.2021.05.003

Yang, Q., Tian, H., Friedrichs, M. A. M., Liu, M., Li, X., & Yang, J. (2015). Hydrological responses to climate and land-use changes along the north american east coast: A 110-Year historical reconstruction. *Journal of the American Water Resources Association*, *51*(1), 47–67. https://doi.org/10.1111/jawr.12232

Yang, Y., Roderick, M. L., Guo, H., Miralles, D. G., Zhang, L., Fatichi, S., Luo, X., Zhang, Y., McVicar, T. R., Tu, Z., Keenan, T. F., Fisher, J. B., Gan, R., Zhang, X., Piao, S., Zhang, B., & Yang, D. (2023). Evapotranspiration on a greening Earth. *Nature Reviews Earth & Environment*, *4*(9), 626–641. https://doi.org/10.1038/s43017-023-00464-3

Yun, X., Tang, Q., Wang, J., Liu, X., Zhang, Y., Lu, H., Wang, Y., Zhang, L., & Chen, D. (2020). Impacts of Climate Change and Reservoir Operation on Stream flow and Flood Characteristics in the Lancang-Mekong River Basin. *Journal of Hydrology*, *590*, 125472.

https://doi.org/10.1016/j.jhydrol.2020.125472

Zeferino, L. B., Gomes, L. C., Fernandes-Filho, E. I., & Oliveira, T. S. (2021). Environmental conservation policy can bend the trend of future forest losses in the oriental Amazon. *Regional Environmental Change*, *21*(2), 58. https://doi.org/10.1007/s10113-021-01787-x

Zhai, P., Pirani, A., Berger, S., Caud, N., Chen, Y., Goldfarb, L., Gomis, M. I., Huang, M., Leitzell, K., Lonnoy, E., Maycock, T. K., Waterfield, T., Yu, R., & Kingdom, U. (2021). *Citation of the IPCC Working Group I*. 33–144. https://doi.org/10.1017/9781009157896.Summary

Zhang, L., Cheng, L., & Brutsaert, W. (2017). Estimation of land surface evaporation using a generalized nonlinear complementary relationship. *Journal of Geophysical Research*, *122*(3), 1475–1487. https://doi.org/10.1002/2016JD025936

Zhong, F., Jiang, S., Van Dijk, A. I. J. M., Ren, L., Schellekens, J., & Miralles, D. G. (2022). Revisiting large-scale interception patterns constrained by a synthesis of global experimental data. *Hydrology and Earth System Sciences*, *26*(21), 5647–5667. https://doi.org/10.5194/hess-26-5647-2022

Zhou, M., Lu, L., Guo, H., Weng, Q., Cao, S., Zhang, S., & Li, Q. (2021). Urban Sprawl and Changes in Land-Use Efficiency in the Beijing–Tianjin–Hebei Region, China from 2000 to 2020: A Spatiotemporal Analysis Using Earth Observation Data. *Remote Sensing*, *13*(15). https://doi.org/10.3390/rs13152850

Zope, P. E., Eldho, T. I., & Jothiprakash, V. (2017). Hydrological impacts of land use–land cover change and detention basins on urban flood hazard: a case study of Poisar River basin, Mumbai, India. *Natural Hazards*, *87*(3), 1267–1283. https://doi.org/10.1007/s11069-017-2816-4

Appendix

Appendix 1: Code used on google earth engine to classify Landsat images

```
// 1. Define the study area
var manafwa = watershed;
Map.centerObject(manafwa, 11);
// 2. Load Landsat 7 ETM+ SR scenes for 2000 with low cloud cover
var l7sr = ee.ImageCollection('LANDSAT/LE07/C02/T1_L2')
  .filterBounds(manafwa)
  .filterDate('2000-01-01', '2000-12-30')
  .filter(ee.Filter.lt('CLOUD_COVER', 5))
  .map(function(image) {
    var optical = image.select(['SR_B1', 'SR_B2', 'SR_B3', 'SR_B4', 'SR_B5', 'SR_B7'])
                  .multiply(0.0000275).add(-0.2);
    return optical.copyProperties(image, image.propertyNames());
  });
// 3. Create median composite and clip to study area
var composite = l7sr.median().clip(manafwa);
// 4. Display composite
Map.addLayer(composite,
  {bands: ['SR_B3', 'SR_B2', 'SR_B1'], min: 0, max: 0.3},
  'Landsat 7 Composite 2000');
print('Number of images in collection:', l7sr.size());
// 5. Merge labeled training data (ensure 'landcover' is the class property)
var training = Built-up
  .merge(wetland)
  .merge(farmland)
  .merge(Tropicalforest)
  .merge(Grassland)
  .merge(woodland);
// 6. Sample training pixels
var sampled = composite.sampleRegions({
  collection: training,
  properties: ['landcover'],
  scale: 30
});
print('Sampled training data:', sampled.limit(5));
// 7. Split into train/test sets
var sampledRandom = sampled.randomColumn('random');
var trainSet = sampledRandom.filter(ee.Filter.lt('random', 0.8));
var testSet = sampledRandom.filter(ee.Filter.gte('random', 0.8));
// 8. Train the Random Forest classifier
var classifier = ee.Classifier.smileRandomForest(50).train({
  features: trainSet,
  classProperty: 'landcover',
  inputProperties: composite.bandNames()
});
// 9. Classify the composite image
var classified = composite.classify(classifier);
```

```
// 10. Display the classification map
Map.addLayer(classified.clip(manafwa),
  {min: 0, max: 5, palette: ['#bd2a00', '#1ad2fa', '#ff11eb', '#0c6038', '#d2a7b6', '#18fe11']},
  'LULC Classification 2000');
// 11. Calculate area per land cover class (in hectares)
var pixelArea = ee.Image.pixelArea().divide(10000); // hectares
var areaImage = pixelArea.addBands(classified).rename(['area', 'landcover']);
var stats = areaImage.reduceRegion({
  reducer: ee.Reducer.sum().group({
    groupField: 1,
    groupName: 'landcover'
  }),
  geometry: manafwa,
  scale: 30,
  maxPixels: 1e13
});
print('Area per land cover class (ha):', stats);
// 12. Convert stats to FeatureCollection
var classStats = ee.List(stats.get('groups'));
var areaFeatures = ee.FeatureCollection(classStats.map(function(item) {
  item = ee.Dictionary(item);
  return ee.Feature(null, {
    'landcover': item.get('landcover'),
    'area_ha': item.get('sum')
  });
}));
// 13. Accuracy assessment
var validated = testSet.classify(classifier);
var confusionMatrix = validated.errorMatrix('landcover', 'classification');

print('Confusion Matrix:', confusionMatrix);
print('Overall Accuracy:', confusionMatrix.accuracy());
print('Producers Accuracy:', confusionMatrix.producersAccuracy());
print('Consumers Accuracy:', confusionMatrix.consumersAccuracy());
// 14. Per-class accuracy export
var producers = confusionMatrix.producersAccuracy().toList();
var consumers = confusionMatrix.consumersAccuracy().toList();
var classCount = confusionMatrix.order().length();
var accuracyPerClass = ee.FeatureCollection(
  ee.List.sequence(0, classCount.subtract(1)).map(function(i) {
    return ee.Feature(null, {
      'class': confusionMatrix.order().get(i),
      'producers_accuracy': producers.get(i),
      'users_accuracy': consumers.get(i)
    });
  })
);

// Export per-class accuracy
Export.table.toDrive({
  collection: accuracyPerClass,
```

```
  description: 'Per_Class_Accuracy_2000',
  fileFormat: 'CSV'
});
// 15. Export area stats
Export.table.toDrive({
  collection: areaFeatures,
  description: 'LULC_Area_Stats_2000',
  fileFormat: 'CSV'
});
Export.image.toDrive({
  image: classified.clip(manafwa),
  description: 'Manafwa_LULC_Classification_2000_L7',
  folder: 'EarthEngine',
  fileNamePrefix: 'LULC_2000',
  region: manafwa.geometry(),
  scale: 30,
  maxPixels: 1e13
});
```

Appendix 2: Accuracy assessment

Classification Accuracy Assessment.

	2000		2010		2020	
land use/land cover	user's accuracy	producer's accuracy	user's accuracy	producer's accuracy	user's accuracy	producer's accuracy
Built-up	0.66	0.5	0.8	0.44	0.95	0.69
Wetland	0.77	0.87	0.82	0.85	0.83	0.78
Farmland	0.83	0.76	0.83	0.81	0.91	0.95
Tropical forest	0.97	0.97	0.90	0.93	0.91	0.89
Grassland	0.91	0.82	0.86	0.88	0.95	0.94
Woodland	0.70	0.66	0.83	0.76	0.76	0.69
overall accuracy	0.85		0.86		0.89	

Appendix 3: Watershed maps

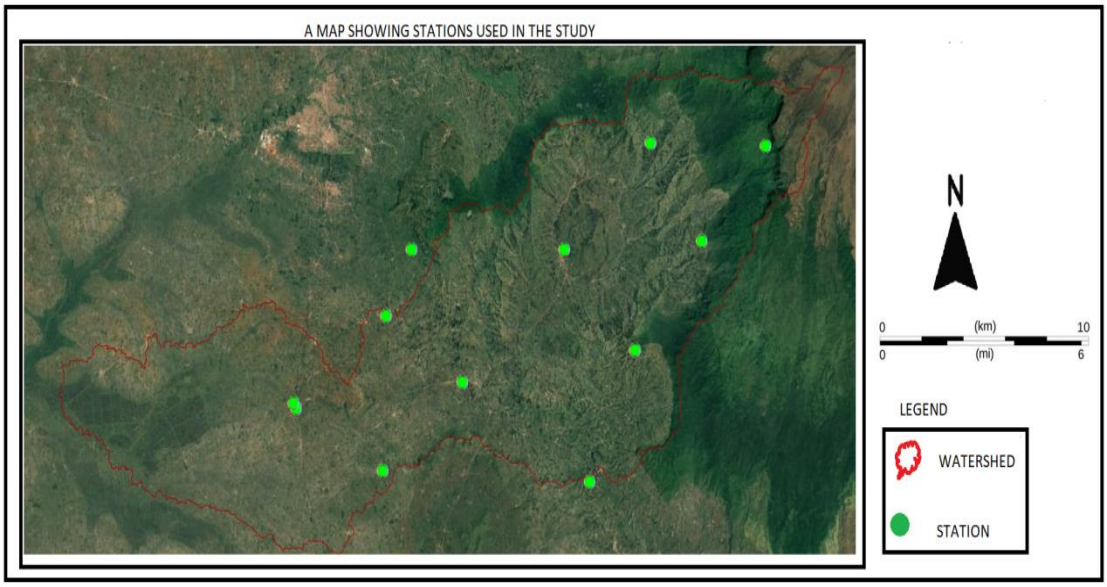

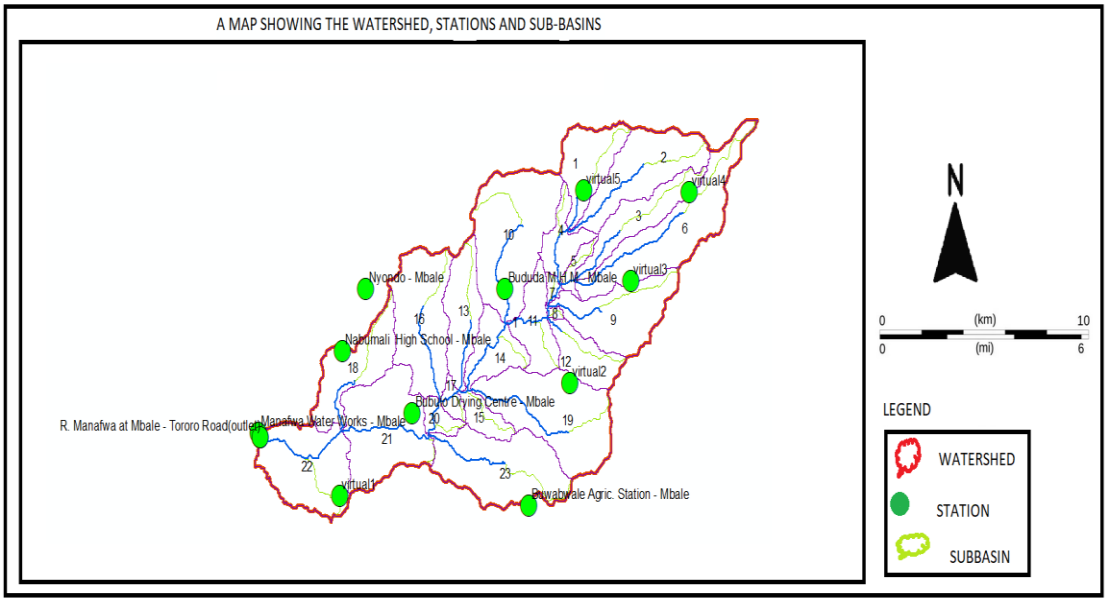

Appendix 4: Hydrology of Manafwa river basin

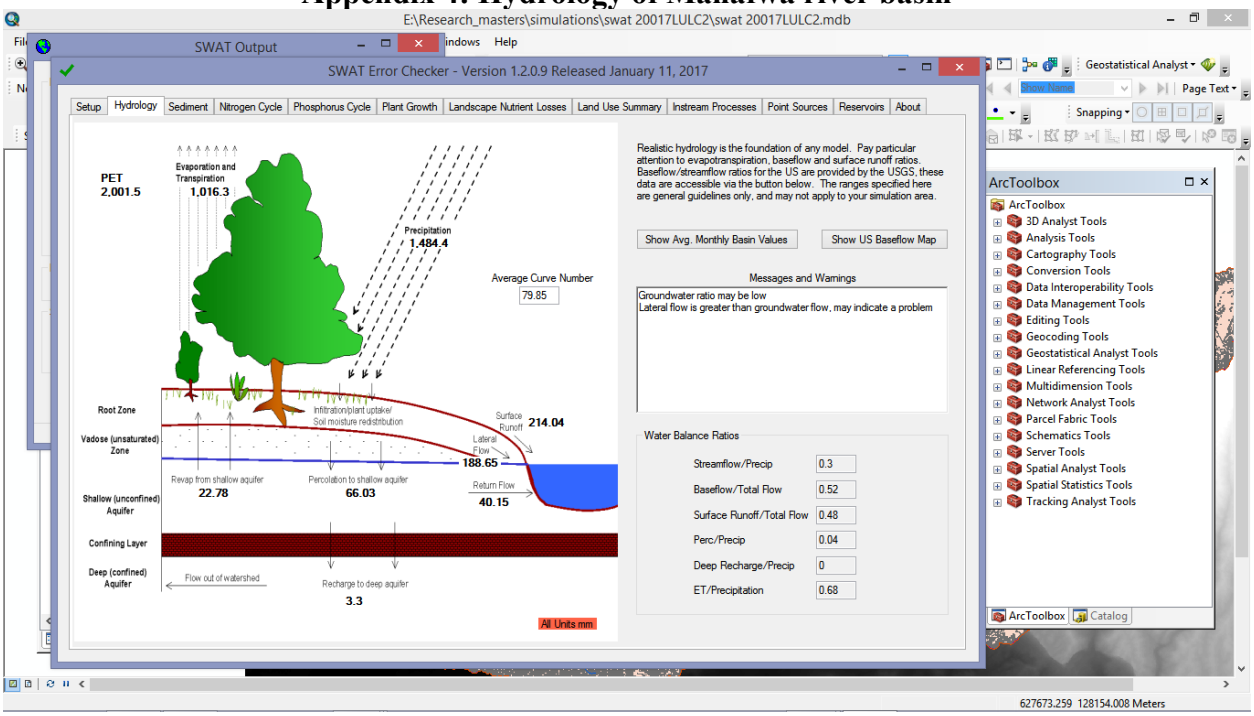

Appendix 5: Topographic report, land use/soil reports and HRU reports for the different scenarios

https://github.com/musokeisa/Hydrological-Reports-for-LULC20000.git

https://github.com/musokeisa/Hydrological-reports-for-LULC-2000-and-future-climate-spp2.git

https://github.com/musokeisa/future-climate-ssp5-vs-lulc-2000.git

https://github.com/musokeisa/hydrological-reports-for-LULC-2010-with-future-climate-ssp2.git

https://github.com/musokeisa/hydrological-reports-for-LULC-2010-with-future-climate-ssp5.git

https://github.com/musokeisa/hydrological-reports-for-LULC-2020-with-future-climate-ssp2.git

https://github.com/musokeisa/hydrological-reports-for-LULC-2020-with-future-climate-ssp5.git

https://github.com/musokeisa/hydrological-reports-for-LULC-2030-with-future-climate-ssp2.git

https://github.com/musokeisa/hydrological-reports-for-LULC-2030-with-future-climate-ssp5.git

https://github.com/musokeisa/hydrological-reports-for-LULC-2040-with-future-climate-ssp2.git

https://github.com/musokeisa/hydrological-reports-for-LULC-2040-with-future-climate-ssp5.git

Appendix 6: Discharge files for the different scenarios

https://github.com/musokeisa/Discharge-files